On Bidisperse Grain Size Distributions in High Density Turbidity Currents

Universiteit Utrecht

Menno Hofstra
Supervisor: Dr. J. T. Eggenhuisen
MSc-thesis V2
Faculty of Geosciences

Chapter 1: The effect of bidisperse grain size distributions on HDTC's : An experimental approach

1.0 Abstract 01

1.1 Introduction 02

1.1.1 Approaches in turbidity current research 02
1.1.2 Main research topic of this thesis 03

1.2 Background 04

1.2.1 General anatomy and flow structure of turbidity currents 05

1.3 Methods 08

1.3.1 Experimental setup 08
1.3.2 Dimensionless scaling 10
1.3.3 Velocity data analysis 11

1.4 Results 14

1.4.1 Summary of experiments 14
1.4.2 The Stability Field and depositional behaviour 15
1.4.3 Variations in Single Value Variables: U_{mean} and U_{max} 17
1.4.4 Velocity profiles of the experimental HDTC's 22
1.4.5 Shear-velocity approximations 27
1.4.6 Indications regarding dimensionless parameters 30
1.4.7 Additional visual observations 31

1.5 Discussion 32

1.5.1 Influence of fine-grained sediments on flow processes 32
1.5.2 Traction carpet model similarities 34
1.5.3 Approximating shear stress 36
1.5.4 Entrainment and dimensionless parameters 37
1.5.5 Recommendations for further research 37

1.6 Conclusions 39

1.7 Subchapter A : Sedimentary structures and depositional features of a flume deposit (Run#43) 40

A.1 Methods 40
A.2 Settling Rates 40
A.3 Results 41
A.4 Discussion 43

1.8 Acknowledgements 45

1.9 Nomenclature 45

1.10 Appendices 46

1.10.1 Additional validation of experimental approach 46
1.10.2 Appendix table 51
1.10.3 Full set of velocity profiles 53

1.11 References 60

Chapter 2: Simulating Bidisperse High Density Turbidity Currents in Massflow-3D™

2.0 Abstract 64

2.1 Introduction 65

2.2 Methods 66

2.2.1 Geometry & Mesh 66
2.2.2 Boundary conditions 67
2.2.3 Physics 68
2.2.4 Sensitivity Tests 70
2.2.5 Modelled runs 74

2.3 Results 75

2.3.1 Comparing velocity data 75
2.3.2 Dimensionless profiles 75
2.3.3 The effect of sediment fraction on velocity profiles 76
2.3.4 Observations regarding aggrading behaviour 76
2.3.5 Internal concentration/density structures 77
2.3.6 Turbulence kinetic energy and dynamic viscosity 78
2.3.7 Variations in initial volume concentration 80
2.3.8 Variations in slope/gradient 81

2.4 Discussion 83

2.4.1 Grain size distributions 83
2.4.2 Hindered settling 83
2.4.3 Similarities in velocity profiles 84
2.4.4 Explanations regarding velocity structures 84
2.4.5 Additional flow properties and comparison with previous work 85

2.5 Conclusions 89

2.6 Acknowledgements 90

2.7 Nomenclature 90

2.8 References 90

2.9 Appendices 91

Chapter 1

The Effect of Bidisperse Grain Size Distributions on HDTC's: An Experimental Approach

Menno Hofstra
University Utrecht

Universiteit Utrecht

Abstract

Physical experiments on high density turbidity current (HDTC) have been performed in a laboratory flume to investigate the effect of bidisperse grain size distributions on flow properties. In total three parameters are varied: slope (4-11.3 [deg]), sediment volume concentration (9-21v%) and grainsize fraction, with the latter being the ratio between two distinct sized clastic sediments (D50 = 144 & 50 µm). With high resolution U(D)VP (Ultasonic Doppler Velocimity Profiler) measurements, velocity profiles are constructed for each individual experiment, which are then compared.

The obtained data shows that the addition of a small portion of fine grained materials extensively enhances the carrying capacity and efficiency of turbidity currents. The influence of sediment fraction on the stability field (experimental conditions in which an equilibrium is reached) is substantial, but not as much on average velocities. The effect of sediment fraction on maximum (U_{max}) and average velocities (U_{mean}) is substantially smaller than what was found with varying gradient or initial concentrations.

The outer region velocity gradient decreases with higher proportions of fine materials. The more vertically uniform velocity structures must be attributed to more homogeneous suspended sediment distributions due to the addition of fines. This is explained by the fact that the fine fraction is more easily affected by the turbulence kinetic energy and therefore to entrainment with the ambient fluid.

As an addition shear stresses are approximated with the law of wall. This method can however not be applied to the aggrading runs, since the inner region profile deviates from a logarithmic function and shows more similarity with proposed 'traction carpet' model structures.

1) Introduction

In subaqueous environments the sediment flux from shallow water to deep marine is dominated by particle-laden density or gravity flows. The combination of the suspended sediment concentration and grain density determine the density contrast with the surrounding ambient fluid (water). This acts as the major driving force for sediment-loaded currents together with gravity. The gravity that is acting on this density difference is the driving force for these sediment-laden currents.

In turbidity currents fluid turbulence is largely responsible for the suspension of particles. These currents are known to be non-conservative, meaning that they can exchange sediments with the bedding plain (by erosion & deposition) and exchange mass and momentum with the ambient fluid above due to entrainment.

Generally the term turbidity current is applied to sediment-laden flows in ambient water. However strictly speaking it can also apply to other suspended solids in for example air (Middleton, 1993). Pyroclastic flows and snow avalanches show the same characteristic turbulent behavior as the sediment-loaded deep water currents. Detailed knowledge of the velocity structures and depositional character within sediment gravity currents is necessary to get a better understanding of the mechanism involved in sediment transport and deposition.

A better understanding of turbidite deposits is necessary, because they are one of the most common occurring sedimentary rocks. Since turbidites can form some of the most voluminous clastic sedimentary deposits they are of great interest for the petroleum geology. Furthermore, modern flows can act as severe threats for important seafloor structures, such as drilling structures and communication lines. In general it can be said they are of scientific, social and economic importance.

1.1) Approaches to turbidity research

There are four main approaches to study sediment gravity flows: in-situ measurements (Xu et al., 2004), describing ancient turbidite deposits, numerical modeling and physical flume experiments. The first two approaches are rather limited in the field of flow properties: in-situ measuring is very difficult to almost impossible due the catastrophic character of turbidity currents and the connection between the current and the deposit is lacking in ancient deposits. Therefore, numerical modeling and flume experiments are the best approaches to get a better understanding of flow properties and fluid mechanics regarding turbidity currents.

A lot of lock-exchange experimental work has been performed in the past to look at constant-volume turbidity currents in a simplified 2-D view (Amy et al., 2005, Altinakar, 1996;Choux et al.,2005, Felix ea., 2005). These experiments were mainly focused on obtaining basic knowledge on velocity, concentration and density structures. Recently more interest is also gained in properties as turbulence kinetic energy and stratification of the flow (Eggenhuisen & McCaffrey, 2011; Islam & Imran, 2010). A lot of debate has been going on about the existence of traction carpets (Sohn, 1997; Hand, 1997).

The influence of sediment properties on basic flow behaviour in especially high density turbidity currents is mostly still an enigmatic gap in our knowledge. Recently studies have started to focus on the influence of mixture properties: grainsize (Gladstone et al., 1998) and grain density (Hodson et al., 2010). Gladstone et al. (1998) showed by lock-gate flume experiments that bidisperse grain-size distributions in constant-volume gravity currents have great effect on the propagation and settling behaviour of the current. Since there is only basic knowledge of the effect of multidisperse grain-size distributions, the simplest advancement to test are bidisperse grainsize-distributions.

Before Gladstone et al. (1998), no systematic research had been performed on gravity currents with more than one single grainsize. Gladstone used two main sizes of silicon carbide particles (D50 = 25 & 69µm) in a 6m long flume and looked mainly at the sediment deposit density with different fractions of both particle sizes with distance from the lockgate. It was concluded that adding a small fraction of fine-grained sediments to

generally coarse-grained mixture has a relative large effect on flow behaviour in comparison to coarse sediments on a dominant fine-grained current. This was found both in the bidisperse as in a couple of polydisperse experiments. The general explanation of Gladstone et al. (1998) was that the fines, remaining much longer in suspension, maintain the excess current density more efficiently.

Hodson et al. (2010) looked at the effect of grain-density variation on turbidity currents, with a special interest for differences in behaviour of carbonate and siliciclastic-laden mixtures. With their lockgate experiments Hodson et al. (2010) also looked at time-distance measurements of the whole current as with Gladstone et al. (1998) . However, UVP data was obtained as well to construct vertical velocity profiles of the various mixtures with fractions of SiC and glass ballotini that were used in the experiments. Hodson found that if the initial bulk density increased, being dependent on sediment concentration and grain density, flow velocity was maintained longer. This was attributed for great part to the low settling velocity of the low-density particles in the mixture, when compared to similar initial sediment volume concentration flows with single-density particles.

Naturally, turbidity currents contain a wide range of grain sizes. This makes it necessary to look at its effect on flow behaviour. As was proven by Gladstone et al. (1998), it is important to know what influence grain size has on the transport capacity of the current. The leading work of Gladstone in the field of bidisperse distributions in experimental turbidity currents is very basic and is only based on observed distances achieved by each current. Therefore more detailed analysis in this field is necessary. Hodson et al.(2010) proved the importance of the modern UVP-equipment, it being essential to gain more detailed insight in how the flow structures are influenced by sediment properties.

The performed bidisperse HDTC experiments of this report can therefore help to get a more detailed insight in how more natural occurring sediment mixtures influence basic flow behaviour. This is of major importance if better and more sophisticated models are constructed for turbidity currents deposition in the nearby future.

1.2) Main research topic of this thesis

The aim of this thesis is to get a better understanding of the effect of bidisperse grain-size distributions on constant-discharge HDTC, with respect to basic flow properties. This includes getting a better understanding of the mechanisms involved which influence flow propagation and depositional behaviour. The main approach is the performance of Froude-scaled flume experiments in which high-resolution UVP-velocity data is obtained. For cross-checking and additional understanding of the fluid mechanics, identical experiments are performed by full 3-D numerical modeling with the commercial available software of Massflow-3D^{TM} (Chapter 2)

This combination has to give a better insight in the distinct behavior of more naturally sorted sediment mixtures relative to the simplified uni-modal mixtures that have mostly been used in flume and lock-gate experiments in the past.

2) Background

Classification of currents is mostly based on sediment concentrations, since it is relative easy to determine and all main flow properties are primarily related to flow concentration.

Until the beginning of the 21th century there has been a lot of improper and unclear use of terminology in the field of sediment gravity flows. Different terminology has been used for same processes as well as the same terminology for totally distinct processes. To clear things up multiple summary papers have been published recently to connect all published work. Mulder et al. (2001) constructed a diagram showing a wide range of used terminology and nomenclature for density flows in literature plotted against total volume concentration (Fig 2.1). The general range of high-density turbidity currents is set by Pierson & Scott (1985) to 5-45 v% with hyperconcentrated flows starting at approximately 25v%. At a level of more than 50v% these hyperconcentrated flows enter the field of the debris flows which acts as a Bingham plastic.

Lowe (1982), who was not incorporated by Mulder & Alexander (2001), was one of the first to state why a difference is made between natural occurring HDTC and LDTC (high/low density turbidity currents) with respect to suspension and transport mechanisms of sediments. In general a division can be made of three different ranges of particle grain-sizes which can be transported with the help of natural gravity flows.

1) Clay, silt and fine-/medium-grained sand
2) Coarse sand to small pebbles
3) Pebble- and cobble-sized clasts

The mechanism by which the materials end up in suspension is distinct for every group (Lowe, 1982). The first group is influenced by turbulence alone. Because this process is largely independent of concentration, it is possible to maintain fine materials in low density gravity flows. The second group can not be totally suspended and will be transported with the help of a combination of turbulence, hindered settling (due to high concentrations) and buoyant lift, which is provided by the interstitial mixture of water and fine-grained material (Lowe, 1982). When the last group occurs in concentrations greater than 10-15v% it can be supported by a combination of fluid turbulence, hindered settling, matrix buoyant lift, and dispersive pressure due to grain collision. Dispersive pressure will be less important in more fine grained mixtures.

The last two types of sediments, being dependent on high concentrations, can only be transported by HDTC.

Due to the large difference in influence of concentration between group 1 and group 2&3, there are significant differences in fluid mechanics and deposit characteristics between HDTC and LDTC.

According to Mulder & Alexander (2001) the additional fact making HDTC different from LDTC is that high concentrations prevent grain-size segregation. As a consequence no normal grading will develop in HDTC deposits such as is known from Bouma-A. Due to the complexity of the additional flow processes occurring in HDTC there is still a lot unknown about their interaction and the influence on general flow properties. This makes it interesting for further research.

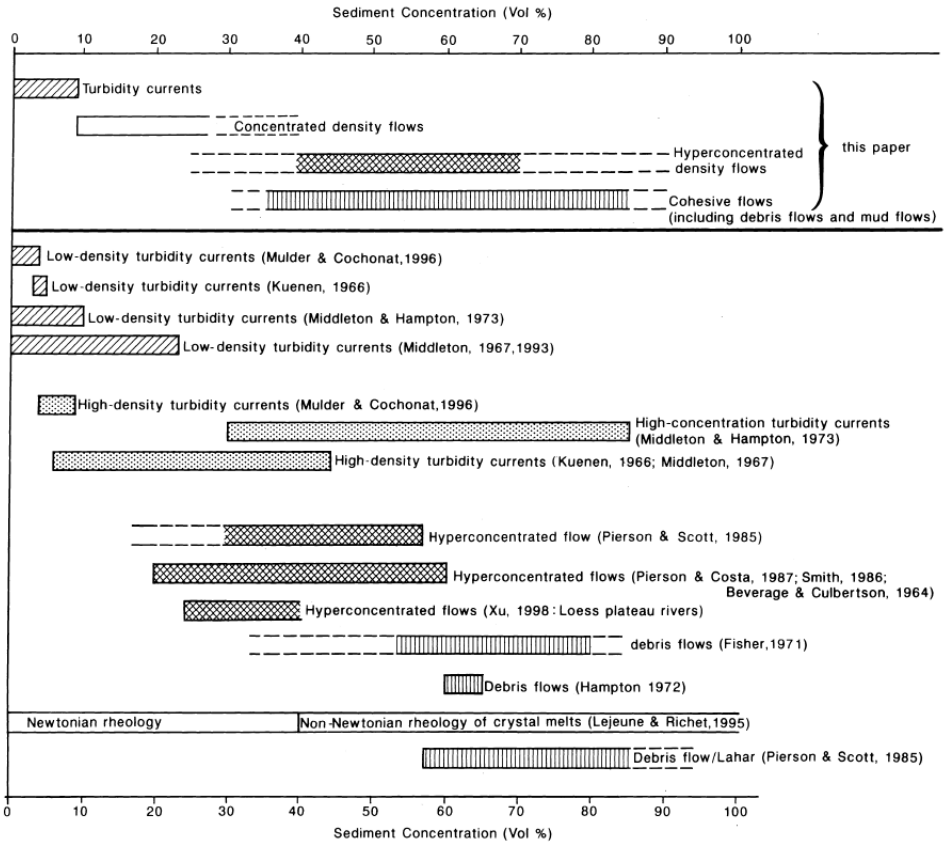

Fig 2.1: *Various terminology and nomenclature for sediment-laden gravity flows plotted against total volume concentration. The dashed lines represent possible conditions for boundaries, since the boundary can be dependent on other factors such as clay content (grainsize) (Mulder & Alexander, 2001)*

2.1)General anatomy and flow structure of turbidity currents

The entity of a turbidity current can always be subdivided into a head (front region), body and tail (Middleton, 1966a,b & Simpson (1987) (Fig. 2.2). As an addition a neck can connect the head of the current with the body of the flow. The head and neck are considered to be generally unstable, characterised by fluctuating velocities and a high amount of turbulence. The body of the flow also shows significant fluctuations (turbulence), but over a sufficient long time interval the average conditions remain constant. Due to the large resistance of the ambient fluid against the head of the current, flow velocities are generally the highest in the body (Leeder,1999 ; Meiburg & Kneller, 2010). The head is therefore largely independent from the slope of the lower boundary (bedding plain), while the gradient plays a major role in the body of the current.

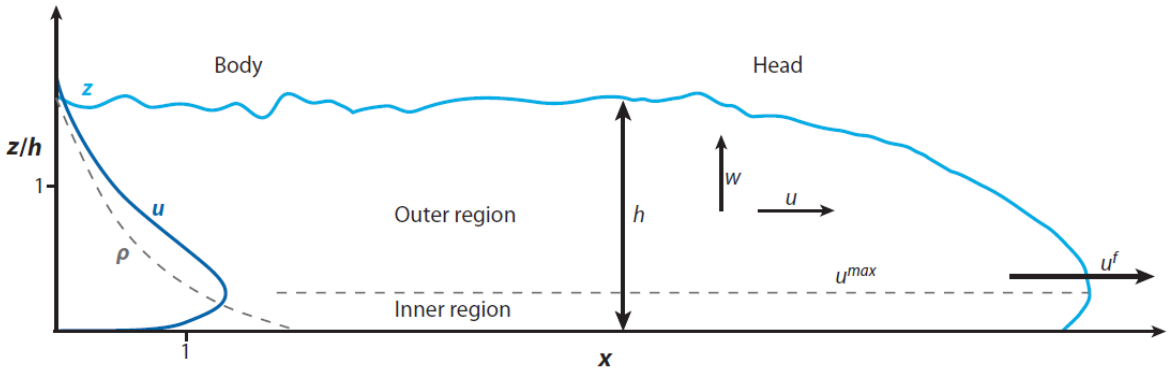

Fig 2.2 : *Simplified sketch of a turbidity current showing generalized sediment velocity and density profiles (Meiburg & Kneller, 2010)*

2.1.1 Velocity structure

An idealized dimensionless velocity profile (Fig. 2.2&2.3) of a turbidity current can be split up into two distinct regions which are the result of mechanical differences between the lower (Ulog) boundary and the upper (Udrag) boundary. The inner region consists of a positive velocity gradient, while the five to ten times thicker outer region has a negative velocity gradient (Meiburg & Kneller, 2010).

Altinakar et al. (1996) determined that both regions can simply be approximated with two basic functions: a logarithmic function for the inner (wall) region and a Gaussian fit for the outer (jet) region. Kneller et al. (1999) proposed an overlapping combination of both functions.

This creates (Eggenhuisen&McCaffrey, 2011):

$U(y) = U_{log} + U_{drag} - U_{logmax}$ *(Altinakar et al. , 1996 & Kneller et al., 1999)*

The two regions are connecting at the Umax which is located broadly at the lower quarter. A Gaussian fit for the outer region (shear layer) (Meiburg &Kneller, 2010) is however speculated by some (e.g. Kneller & Buckee, 2000), claiming that the outer region profile mostly deviates from any function. Instead, some constructed profiles of others show a much more linear fit (Ellison & Turner 1959, Xu et al. 2004). This could be possibly related to the resolution of the data.

The inner region is of special interest, since turbulence is created by bottom shear where sediment entrainment and deposition takes place. A simple logarithmic approximation ((Kneller et al.,1999; Sequeiros et al., 2010) can be used to make an estimate of shear velocities in this lower flow. This is a good method to get a direct measure for shear stresses out of experimental data.

2.1.2 Density structure

Because the density differences between the turbidity current and the ambient fluid is the main driving force, the internal density structure is of main influence for all flow properties. The distribution of the suspended sediment concentration determines the internal density structure and is by most (f.e. Altinaker, 1996) characterised by a concave shaped profile (Fig. 2.2) with the highest concentrated suspension in the inner region.

However many alternative (Fig. 2.4) profiles have been suggested, including stepped and multi-stepped structures. A lot is still unclear about what influences the concentration structure, which makes new research essential for further understanding internal flow properties.

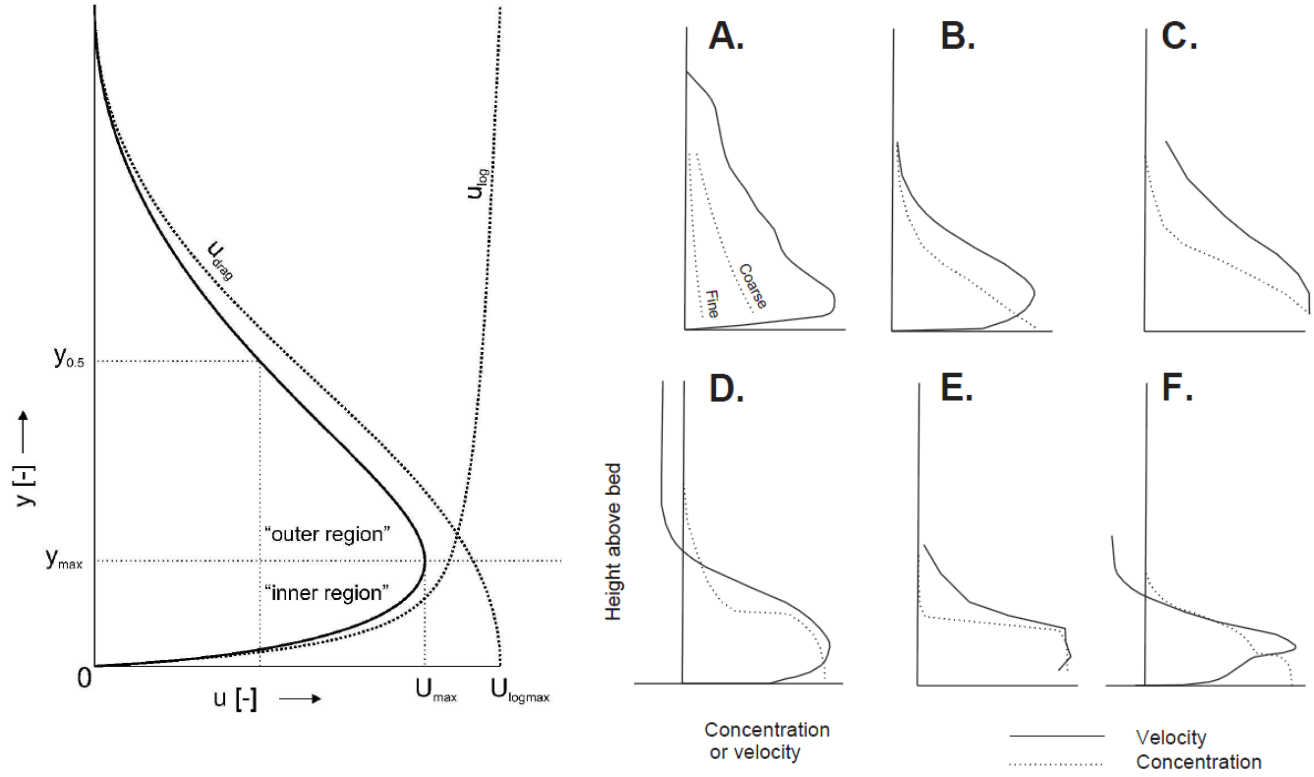

Fig. 2.3: (Left) *Idealised dimensionless velocity profile for experimental turbidity currents constructed with the help of a logarithmic function for the inner region and a Gaussian fit for the outer region crossing near Umax.* (Eggenhuisen & McCaffrey, 2011)

Fig. 2.4: (Right) *Constructed dimensionless velocity and concentration profiles from various experimental work (Amy et al. 2004). A = Continuous C-profiles for two fractions - strongly depositional subcritical current (Garcia, 1994) , B = Most common concave continuous profile with slight inflexion above Umax – weakly depositional subcritical current on low angle slope (Altinakar et al., 1996) C = Alternative continuous C-profile – low concentrated fluid mudflow (Van Kessel et al., 1996) D = Stepped C-profile above Umax – strongly depositional current (Middleton, 1966/1993) E = both stepped U and C-profile – high concentrated fluid mudflow (Van Kessel et al., 1996) F = Multi-stepped C-profile – high concentrated current (>35-40v%) (Postma et al., 1988)*

3) Methods

3.1) Experimental Setup

3.1.1 Flume Tank

The flume tank's main dimensions were 4m long and 0.07m wide. It had glass on one side and could be tilted at various angles (Fig. 3.1). The mixture was pumped from a mixing tank (1100 dm^3) containing the mixture of sediment and water, to the flume tank through a pipe in which the discharge could be measured and regulated. In every run the discharge was kept constant around 9.5m^3/h with an acceptable variance between 9.2 and 9.8 m^3/h.
At the moment of release in the flume tank the mixture gets in contact with the flume floor and is pushed out of the inlet. A tilted flat beam at the inlet prevents massive entrainment or instabilities of the flow due to abrupt transition into the tank.
On the flume floor a thin layer of sand was glued (D50= 144 µm) to simulate natural roughness while preventing erosion. An erodible bed would alter flow concentrations.
The main advantage of these 'pump' experiments relative to the more widely used lock-gate experiments is the possibility to manually determine the total timing of the experiment and therefore giving the current the possibility to become stable and retrieve a long range of data to partially average out the experimental defects.
Also return flow can be limited due to the constant flow movement and higher flow volumes can be reached in comparison with lock-exchange experiments.

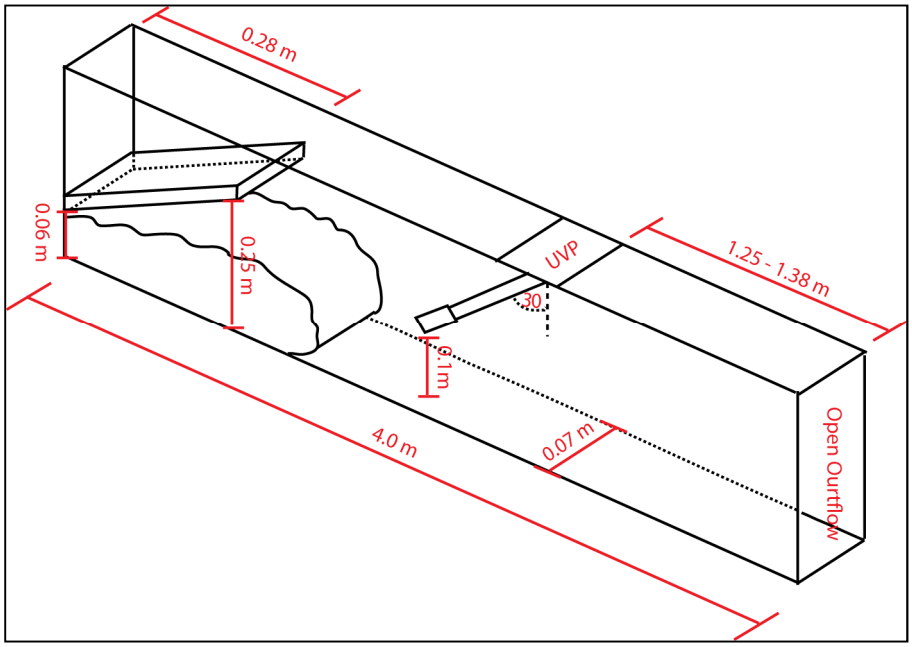

Fig. 3.1 *: Sketch of experimental setup with an example turbidity current. The mixing tank and outflow tank have not been included in this picture.*

3.1.2 Data Collection

In all runs U(D)VP (Ultrasonic Doppler Velocimity Profiler) and High-Speed video data were obtained. One single UVP probe (1Mhz) (Table 3.1) was located in the tank with an angle of 60° relative to the tank floor (Appendix 1) and a distance of 100mm above the bedding plain of the flume. The HD camera (210 fps) was orientated on the same section of the tank, focusing mainly on the inner region of the current.
The UVP data that was obtained consists of a combination of velocity data (over the whole measured distance and time) as well as the amplitudes of the received signals. With this data velocity profiles over certain time-intervals can be constructed. The amplitude data could be useful for locating the bedding plane (Appendix 1.10.1).
The HD imaging was used to look at depositional behavior (deposition rates), flow heights and general flow behavior. At a number of runs, red clay tracers were included to the mixture (max 1v%) to attempt to obtain additional information about flow behavior.
From one run (43) sedimentary cores were taken from the deposit for making thin sections and for performing laser diffraction grain size analysis (1.8 Subchapter A)

UVP Settings	
Number of probes	1-2
Probe height above bed (mm)	100 (95-107)
Probe angle relative to bed [deg]	60 (59.6-60.4)
Ultrasound frequency (MHz)	1
Sampling period (ms)	15
Channel distance (mm)	0,74
Channel width (mm)	3,7
Medium ultrasound speed (m/s)	1480
Velocity band width (mm/s)	3217,4
Pulse rep. freq. (kHz)	4,34783

Table 3.1: *UVP settings used during all experiments. The probe angle has been measured with a digital inclinometer and a standard deviation of 0.1 degrees has been incorporated*

2.1.1 Grain size distribution

In all experiments one silica sand and one silica silt were used to represent the fine (D50 = 50µm) and the coarse (D50 = 144µm) sediment which were varied in relative proportions and total volume concentration. The grain size distributions of both sediments contain a certain level of overlap (36.5v%) (Fig.3.2), mainly due to the wide distribution of the finer fraction.
The distribution of the coarser fraction is much narrower with a D90 and D10 of around 200 and 80 µm. An additional useful property of the fine sediment is its relatively light color compared to the coarse grained fraction, which makes it easier to see sedimentary structures when present in the deposits. Sediment concentrations have been determined by simple volume measurements done in the mixing tank.

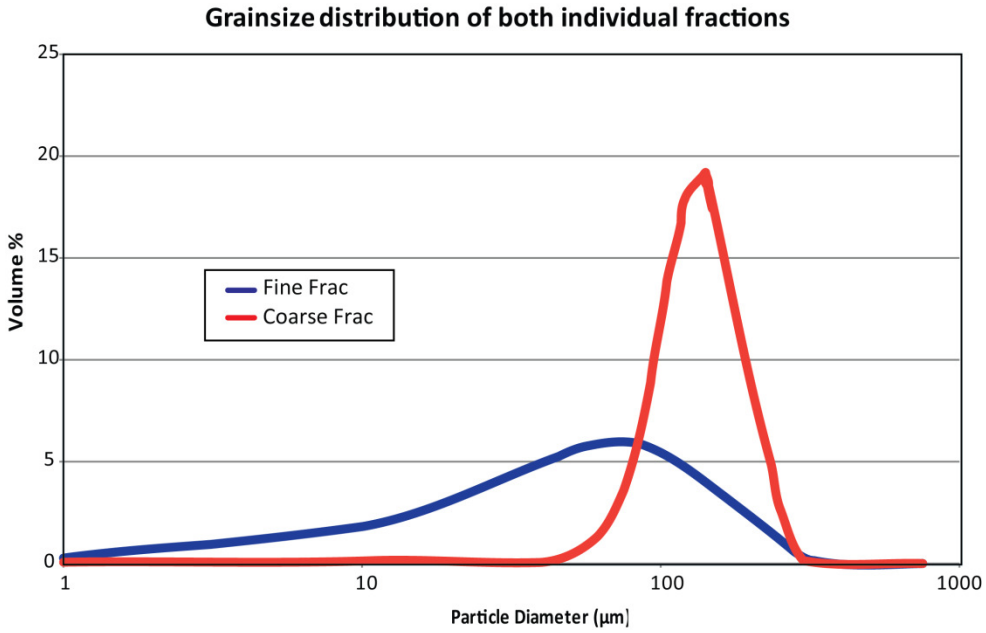

Fig. 3.2 : *Total distribution of both sediments (silica) measured individually (each is in total 100v%). There is a clear overlap in the middle due to the wide distribution of the fines relative to the coarse sands. Size classes are the same in both fractions, exponantionally increasing with size according to ($y=0{,}0071e^{0{,}1527x}$)*

3.2) Dimensionless scaling

All experiments are Froude scaled (Peakall et al., 1996), meaning that they can be compared with natural processes with the help of the general used dimensionless parameters (Re, Fr, Ri etc.). In turbidity currents this means that the densimetric Froude number must be supercritical (Fr'> 1) and Reynolds number high enough for turbulent conditions (Re > 2000) (Hodson & Alexander, 2010). Fr' can be determined by:

$$Fr' = \frac{U}{\sqrt{g' H}} \qquad (1)$$

The reduced gravity g' is a consequence of the density difference between the fluids ($\Delta\rho=\rho_c - \rho_a$):

$$g' = g.(\frac{\Delta\rho}{\rho_a}) \qquad (2)$$

Further, U stands for the mean velocity of the current and H for the flow height.
To make an estimate of the actual density in the current, the flume discharge at point of measurement has to be known (3). Here W_f stands for the width of the flume (0.07m). The difference between Q_f and $Q_i$is the consequence of entrainment occurring in the flume tank.

$$Q_f = H.w_f.U \qquad (3)$$

From this the 'expansion factor' (f_e) can be determined when comparing the initial discharge (Q_i) (measured during experiments) and the calculated discharge in the flume.

$$f_e = \frac{Q_f}{Q_i} \qquad (4)$$

The expansion factor can then be used as an estimate for the mean concentration in the current, using the known initial concentration (C_i). This approach neglects loss of concentration due to deposition.

$$C_f = \frac{C_i}{f_e} \qquad (5)$$

From the concentration the density of the current is determined:

$$\rho_c = (1 - C_f).\rho_a + C_f.\rho_s \qquad (6)$$

For calculating the ratio between the inertial and viscous forces in fluid mechanics, the Reynolds number is commonly applied (Peakall et al., 1996):

$$Re = \frac{\rho\, U\, H}{\mu_s} \qquad (7)$$

The density in (7) represents the total density of the current and μ stands for dynamic viscosity, which can be approximated (dependent of concentration) with the widely used relation of Roscoe (1953) for sediment suspensions:

$$\mu_s = \mu_a (1 - 1.35 C_f)^{-2.5} \qquad (8)$$

Finally, since entrainment into the body and vertical transport due to turbulence is important in HDTC's the bulk Richardson number is also well applicable (Meiburg & Kneller, 2010).

$$Ri = \frac{(\frac{\Delta\rho}{\rho_a}) g H \cos(\alpha)}{U^2} \qquad (9)$$

The fluid entrainment at the upper boundary in the turbidity current is dependent on the flow boundary instability, which can only be calculated from the gradient Ri-number. The entrainment rate is generally high when the flow is thin and fast, while the slope of the bedding plain is increased. High Richardson numbers should stimulate stratification of the flow, due to the reduction in vertical transport. This reduced mixing does not necessarily mean the lack of turbulence, but the presence of multiple turbulent systems which all need an external energy supply to sustain itself. (Kneller et al., 2000).
The approximation of these dimensionless values can give a good idea of the relative differences in flow behavior between individual experiments. However it has to be kept in mind that due to the large experimental error and determination of certain parameters, these values obtained with flume experiments are only approximations.

3.3) Velocity data analysis

Correcting the raw data

The velocity data that is obtained has to be corrected for the measuring angle of the probe. When making the assumption that the bulk of the turbidity current moves parallel to the bedding plane, this can be calculated with a simple angle correction. As is illustrated in Fig 3.3, the incoming velocity can be translated to the significantly larger x-direction velocity. When α (angle of probe) and V (incoming data) are known, velocity vector X can be easily calculated. It has to be assumed that the main direction of flow is parallel to the bed and that the vertical movement is only due to turbulence which results in no net movement.
To construct a vertical velocity profile or obtain any other velocity data the initial data needs to be averaged over a certain time interval, knowing that the average conditions in the body of HDTC's are assumed to be constant.

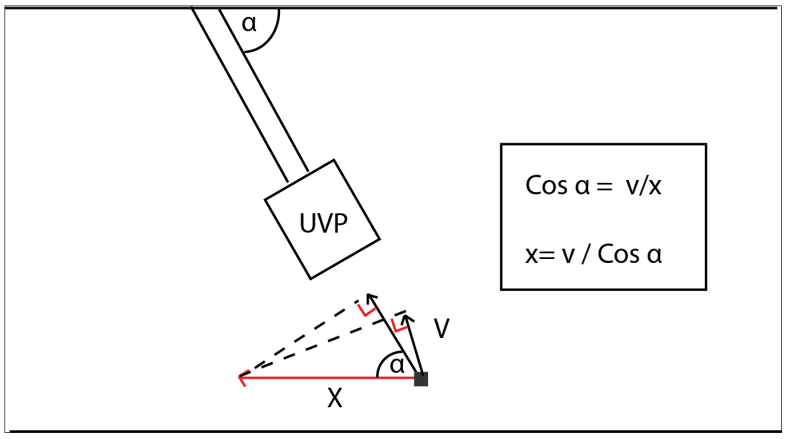

Fig. 3.3: *Sketch of probe configuration relative to the moving particles (square). The V-component is measured and had to be converted into the actual velocity vector (X). The various V-vectors indicate that a larger α, results in a bigger difference between the V-vector and the X-vector.*

3.3.1 Determining single value variables & velocity profiles from raw data

The advantage in the use of single values for describing flow behavior is that it greatly simplifies the analytic work and can be applied in calculating dimensionless parameters and other properties (Felix, 2009) From the basic velocity data at first the velocity maximum (U_{max}) and depth average velocity (U_{mean}) are determined. The way to calculate U_{max} is rather straight-forward. Since discharge can deviate during an experiment, the U_{max} is obtained from intervals of 1000 nodes (measurements), which is an average over 15 seconds. Most runs therefore result in 4-5 average U_{max} values, from which an optimum U_{max} is selected, dependent on the consistency of the discharge.

Determining U_{mean} is somewhat more challenging, but the basis is the same as with U_{max}. This is mainly due to the variation of the vertical position of the bedding plain and the limitations of the position of the UVP probe. Not all velocity data show a curve that perfectly reaches the point-zero-velocity when nearing the bed.
For depositional runs there are additional problems due to the shifting bedding plain, which also can cause the top outer region to reach distances above the probe.
The biggest difficulties have been encountered at recalculating the mean velocities of the earlier performed 100v% coarse runs. This is because of the difference in quality of the data below the velocity maximum (inner region), which in general resulted in much greater mean velocities than was expected. The maximum velocities of these previous experiments give conflicting results with the average velocities, giving much too high U_{mean}/U_{max} ratios. It is probably not sufficient to calculate the U_{mean} for these runs in the regular way (including the inner region).
An attempt is made to correct for this deviation, by looking only at the outer region of the velocity profile. A factor of ~1.04 has been determined, that represents the average difference between the U_{mean} of only the outer region (till U_{max}) and the total profile. With this factor, corrected average velocities have been calculated, which are substantially lower than the original values and are logically following a more similar course as the U_{max}.
For constructing vertical velocity profiles an interval of around 15s was chosen in the middle of the experiment, which showed a U_{max} and U_{mean} near the average values, as the best representative of the body of the flow.

3.3.2 Shear velocity of the inner region

For open channel equilibrium flows, bed shear stresses can be determined by (Sequeiros et al., 2010):

$$\tau_b = \rho U_*^{\,2} = \rho g h S \qquad (10)$$

However, this is not applicable for high density flows, since there is always active entrainment present with ambient water. Shear velocities of the inner region can be determined by the "law of the wall" from Kármán-Prandtl as is given in (11). (Kneller et al.,1999; Sequieros et al., 2010)
This includes the shear velocity (U*), the vertical position (Z), the von Kármán constant (k) and Z_0, which is the hydraulic (bed) roughness length (Julien, 1998; Carling, 1992).

Translating the formula to shear velocity, a simple linear function is created, which states that dividing the von Kármán constant with the logarithmic slope or coefficient A of the inner region gives the shear velocity divided by the actual velocity (13).

$$U(z) = \frac{U_*}{k} \cdot \ln\left(\frac{Z}{Z_0}\right) \quad (11)$$

$$\ln\left(\frac{Z}{Z_0}\right) = \ln(Z) - \ln(Z_0) = A \quad (12)$$

$$\frac{U_*}{U_{(z)}} = \frac{k}{A} \quad (13)$$

With the known value of 0.41 in clear-water for k, the shear velocity can easily be estimated by fitting a simple logarithmic function in the constructed velocity profiles of the inner region (12/13). The bottom shear stress can then be calculated with the first term of (10) (Fig.3.4).
It must be noted that (11) is somewhat simplified for stratified flows. Due to the vertical buoyancy flux this would normally include an extra term, however this is probably negligible (Kneller et al., 1999; Sequieros et al., 2010) Since overlap with the Gaussian "outer region" fit is expected near the velocity maximum, only the known velocities of the middle to lower 'inner region' can be used in the approximation. For each run shear velocities have been approximated, for which the element of interest in the section of each profile had to be re-determined at every calculation. This is because of the vertical shift of the profile, especially regarding the depositional runs. The same averaging intervals have been applied (+- 1000 nodes = 15s) as with the calculation of the U_{max}/U_{mean}.
Simple linear regression of the natural logarithm of the height versus velocity is expected to give a reasonable estimate of the shear velocity. A fit of 95-100% is considered to be valid enough for representing the correct fitting function.

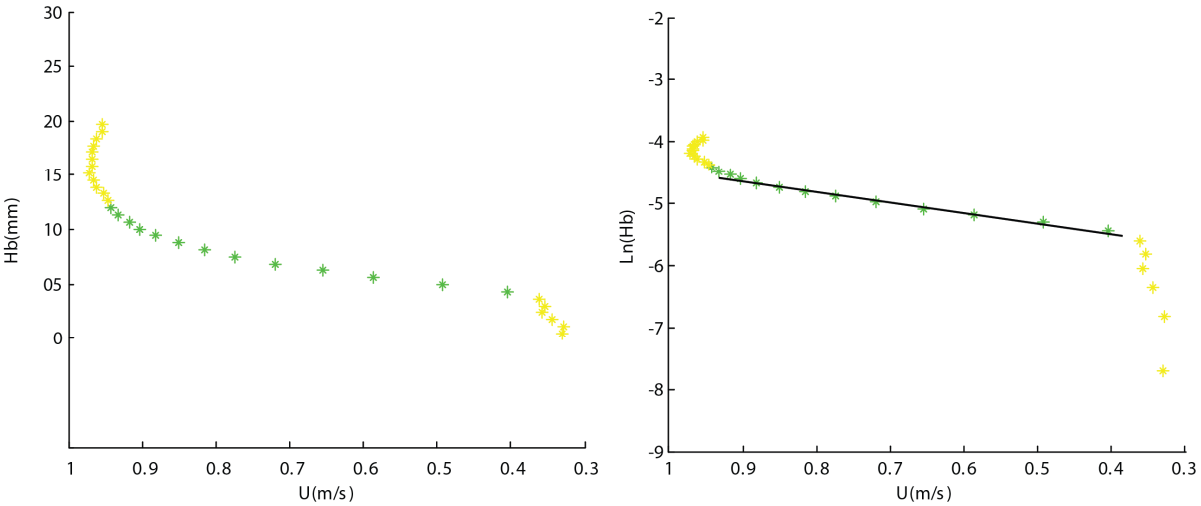

Fig. 3.4: *Example of shear velocity approximation by the 'law of wall' (13.5v%, 9.0 [deg], 00:100). The left figure shows the inner region of the actual velocity profile and at the right the same profile but with the natural logarithm of height. The green data points indicate the area that is proper for retrieving a good linear fit as can be seen in the figure on the right.*

4. Results

4.1 Summary of experiments

A total of 39 successful experiments (Table 4.1) were performed, all varying in slope, initial concentration and sediment fraction (coarse to fine ratio). The slope varied between 4 to 11.3 degrees, concentration was limited in 9-21v% and the sediment fraction (SF) has been classified to three main groups: 90:10, 50:50 & 75:25. One reference experiment with a 100v% coarse mixture was conducted for comparison with previous experiments. Also a total of six runs contained a 100v% fines mixture.

In every experiment-series it was attempted to find the first combination of conditions which gives deposition due to the reduction of the slope. When this point was reached, no further experiments were performed in this series (same v% and SF). As a consequence there is a variance in number of runs per series (Table 4.1).

This resulted in a total of 21 non-aggrading, 7 equilibrium and 11 aggrading runs. Distinction between non-aggrading and equilibrium conditions is based on the position in the flume and the fluctuating discharges. Since full velocities are not yet reached close to the inlet, deposition starts some distance before the point of measurement. This gives a good indication of how close the current is set towards an equilibrium.
The advantage of not totally stable discharges was that at equilibrium conditions an alternation between aggrading and erosion took place.

	Ratio C/F	100/00	90/10	75/25	50/50	00/100
Conc/slope						
9%/11.3			Run#16&Run#17	Run #25	Run#32	-
9%/9.0			Run#18	Run #26	Run#33	-
9%/7.0			-	-	Run#34	-
13-14%/11.3		Run#1	Run#2.1	Run#7	Run#19	Run#31,35 &36
13-14%/9.0			Run#2.2/Run#3	Run#8	Run#20	Run#37
13-14%/7.0			Run#4	Run#9	Run#21	Run#38
13-14%/5.5			-	-	-	Run#39
17%/9.0			Run#5	Run#10/Run#12	Run#22	
17%/7.0			Run#6	Run#11	Run#23	
17%/5.5			-	-	Run#24	
21%/9.0			Run#13	Run#40	Run#27	
21%/7.0			Run#14	Run#41	Run#28	
21%/5.5			Run#15	Run#42	Run#29	
21%/4.0			-	Run#43	Run#30	

Table 4.1: *Overview of all performed runs divided by sediment fraction (coarse/fine) and volume concentration-slope. Since there were a number of failed runs, the total number is 43.*

4.2 The Stability Field and depositional behaviour

From direct observations at all experiment, essential information is obtained about the depositional behaviour of the current. It is already known from previous results with identical setup and 100v% coarse mixtures (Clerx 2010) that the gradient and total volume concentration of the current have a direct effect on the depositional behaviour of the flow (Fig. 4.1). At certain experimental conditions the flow is said to be in equilibrium, maintaining a boundary between aggrading and non-aggrading. Equilibrium is defined as an average negligible net in deposition/erosion by the turbidity current.

The experimental flow is far from unaffected by fluctuations and the ideal experimental conditions are not always achieved. Therefore the runs that were recognised as being in equilibrium, showed mostly alternating moments of sedimentation and erosion, keeping the total sediment thickness to a very minimum or none.

Since all flume experiments do not incorporate erosion of the initial bed, the exact equilibrium conditions are mostly interpreted from the full matrix of data that has been obtained, as can be seen in Fig. 4.1.

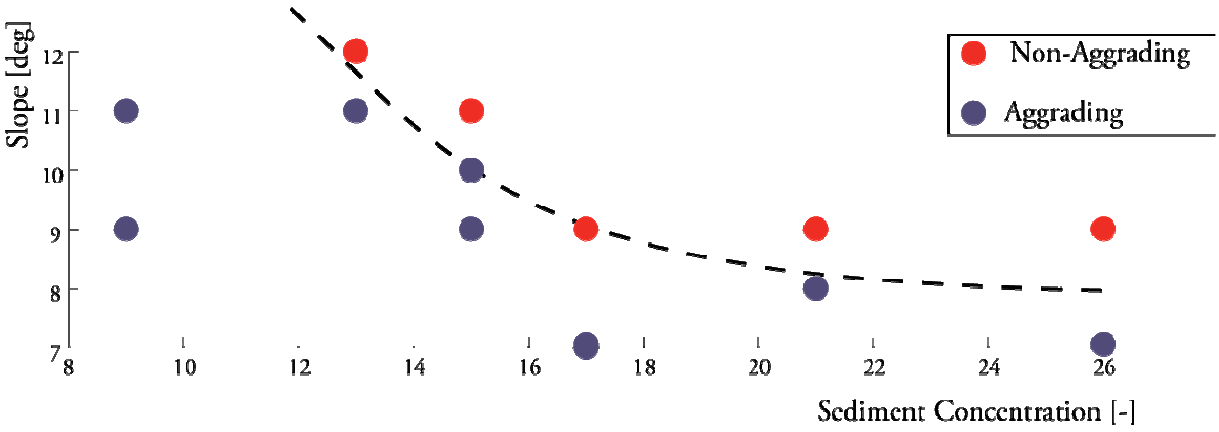

Fig 4.1: *Stability diagram of previous results with a loosely interpreted equilibrium line between aggrading and non-aggrading conditions.*

From the new experimental data of this report, identical graphs can be constructed as is shown in Fig.4.1 . All three parameters are combined when a third 'SF'-axis is joining all diagrams showing the full data-matrix on stability behaviour (Fig. 4.2). Aggradation rates which are obtained with the help of the video-data are added by color scale. Since higher sedimentation rates are expected further away from equilibrium conditions, it gives extra indications of the expected course of the equilibrium line.

In general it can be seen that these aggradation rates are in line with the expectations, keeping in mind that there is quite an error margin in these values (10-25%). Exponential fits are included giving indicating the predicted course of the equilibrium lines. These are then connected to create an equilibrium surface in the three-dimensional environment.

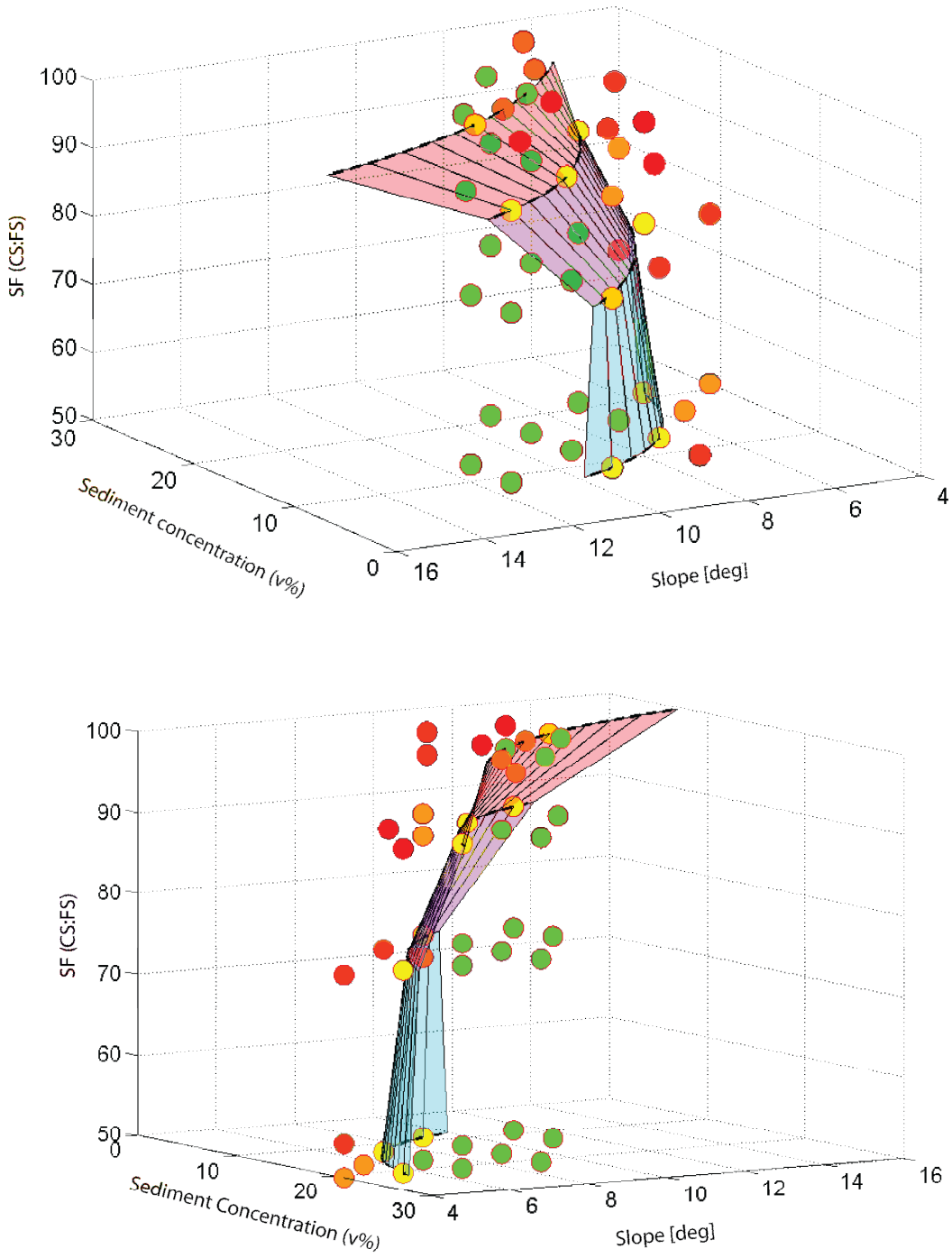

Fig. 4.2: *Full 3D Stabilitydiagram versus all three parameters: Sediment fraction, concentration and slope. The curved surface represents the interpreted equilibrium field with non-aggrading conditions on one side (green) and aggrading conditions on the other side (red). Settling rates are included with color scale (right)*

Fig. 4.3 shows all fitted equilibrium lines for every sediment ratio. It is clear that the addition of fine sediments in the mixture lowers the equilibrium conditions to smaller gradients. It also seems to slightly affect the position of the equilibrium line in the concentration axis. The distances between the equilibrium lines generally decline at higher total volume concentrations.
Further on, it shows that especially at the low-concentrated side, the distances between the curves becomes smaller with increasing fine sediments. The course of the 50:50 SF equilibrium line somewhat deviates from what follows from the others, which show relative less influence of concentration with higher proportions of fine sediments. At low concentrations and gradient the equilibrium lines of 75:25 and 50:50 are crossing each other, indicating possible loss of influence by SF at certain conditions.

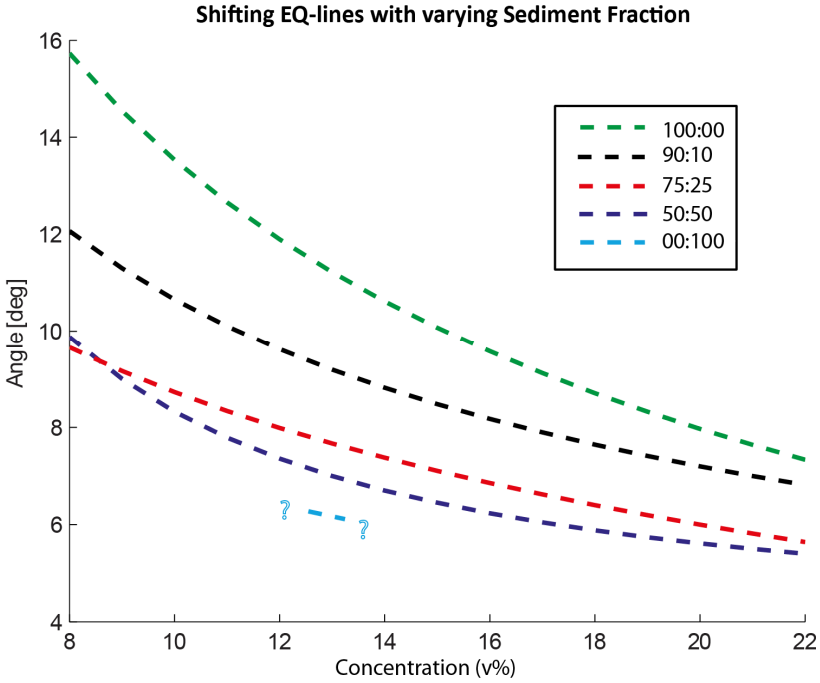

Fig.4.3: *Combination of all interpreted equilibrium lines with various sediment fractions (CS:FS). The line clearly lowers to smaller slopes with higher portions of fine sediments. For 00:100 only 13v% runs have been performed.*

4.3 Variations in single value variables: U_{mean} and U_{max}

One of the most basic velocity properties that can be studied is the average and the maximum velocity of the body of the current. In general U_{max} can be determined much more accurate than U_{mean}, due to additional problems in the analysis (Paragraph 2) . It is assumed that both act proportionally to each other (Felix, 2009) and therefore they are discussed together in the following paragraph.

4.3.1 $U_{max} - U_{mean}$

Variation in U_{max} was maintained in a range of 0.85-1.25 m/s, while variations in U_{mean} kept in a range of 0.4-0.7 m/s. The average Umean/Umax ratio of all runs is 0.55, which is close to the $U_{mean} \approx ½ U_{max}$ of Felix (2010). This ratio seems to have no clear relationship with variation in slope, volume concentration or sediment ratios.

First all variables are plotted versus slope. Because the experiments have been run in series with varying gradient (Fig. 4.4 & 4.5), experimental uncertainties are hereby limited. In an experiment series, all conditions except for slope should be identical, since they have not been altered.

Fig. 4.4 shows that on average there is a linear relationship between U_{max}-U_{mean} and slope, with a clear increase in velocity with increasing gradient. This is best visible in the U_{max} record which, after leaving out some extreme values, has an average increase of around 40 mm/s per degree, varying between 35-48 mm/s.

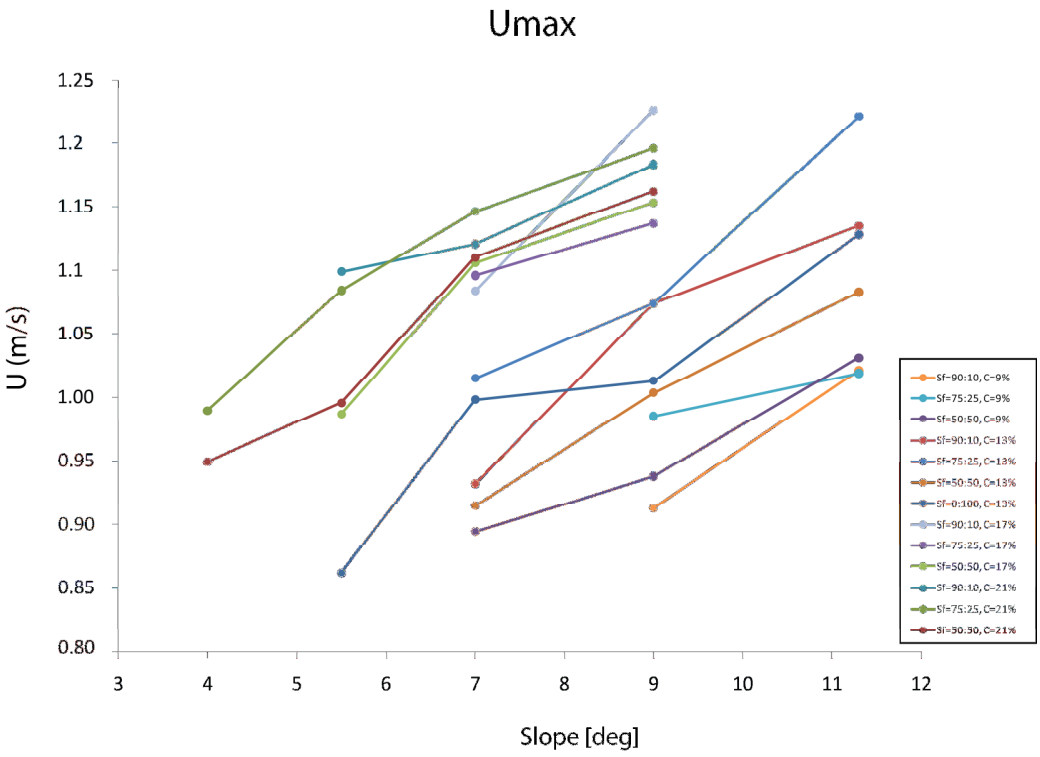

Fig 4.4: *Average Umax grouped/colored in slope-series versus slope. It shows on average a linear increase of ~ 0.04 m/s per degree.*

Further on, from the same figure it comes forward that U_{max} and U_{mean} are increasing with greater total volume concentrations, with the lower concentrated curves mainly at the lower side of the graph.

U_{max} and U_{mean} have also been plotted against sediment fraction (Fig 4.6 & 4.7). To complete the record, the 100% coarse runs from previous work are incorporated. The data has been split into four figures by distinct initial volume concentrations.
It is clear that the general differences along the curves are less than when looking at the other parameters (gradient and total volume concentration). But it shows that SF has still effect on the single velocity values.

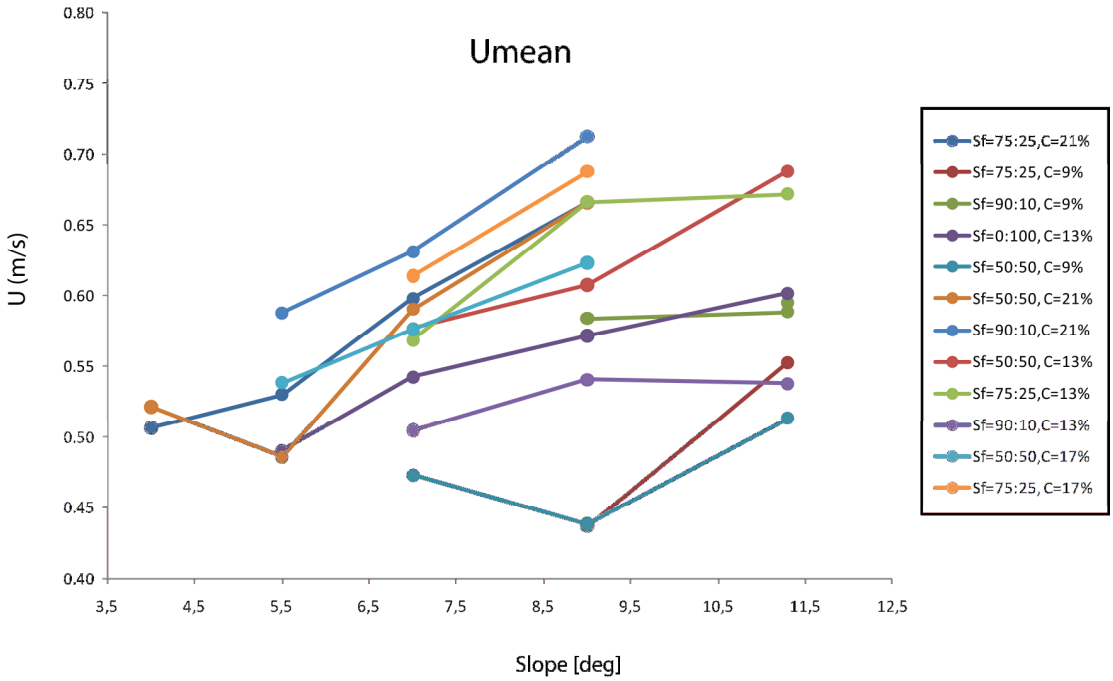

Fig 4.5: *U_{mean} grouped/colored by slope series versus slope. Even though less obvious as U_{max}, it shows an increase of average velocities with increased slope.*

In almost all U_{mean} and U_{max} curves a fast increase from the 100% coarse to 90:10 and 75:25 SF occurs. Only the low (9%) volume concentration runs seem to remain rather constant. After a certain 'maximum' has been reached mostly around 75:25 or 90:10 SF, the velocities decline or remain constant in the direction of 100% fines. The curves of 13% volume concentration (Fig. 3.6) show the most complete picture, since also information is known about the behavior of the current with 100% fines. U_{mean} and U_{max} contradict each other at high fine fractions, by an increasing U_{max} and a decreasing U_{mean}. This is also visible at the 17v% runs, but not at the 21v% runs. So far, the effect of deposition on current velocities has not been discussed. However since deposition has possibly a large effect on the structure of the flow, it cannot be neglected. In Fig 4.6 and 4.7 also the aggrading character of the runs has been included.

No direct relationship can be found between the aggrading character of the current and the SF-curves (Fig. 4.6 & 4.7). This is visible in the fact that there is no relation between the position of the maximum U_{mean} and U_{max} reached in the series or the general curvatures shown in the figures and the depositional behavior. It indicates that the velocities are probably independent of the depositional character of the current.

If there is a relationship between the position of the maximum U_{mean} & U_{max} and the other controlling factors is not quite clear. The high slope (9-11.3 [deg]) runs have a maximum U_{mean} & U_{max} more near the 90:10, while the lower slopes (4-7 [deg]) seem to have a maximum more near the 75:25. No direct relation is present between the maximum U_{mean} & U_{max} and the initial concentration.

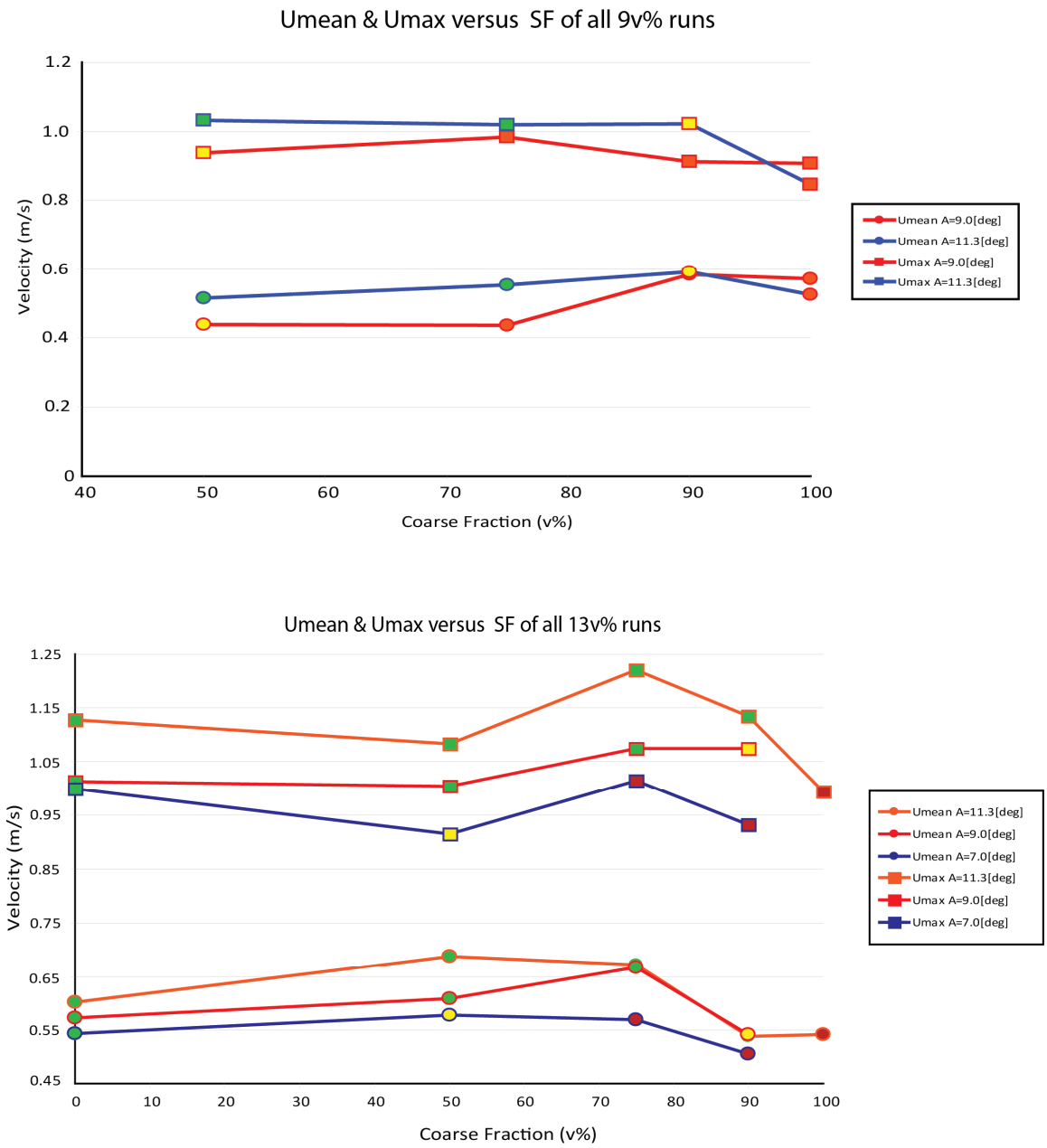

Fig 4.6: *Single velocity variables plotted with variance in sediment fraction for all 9v% runs (top) and 13.5v% (bottom). Aggrading behavior is indicated by: green – non aggrading, yellow – equilibrium, red – aggrading.*

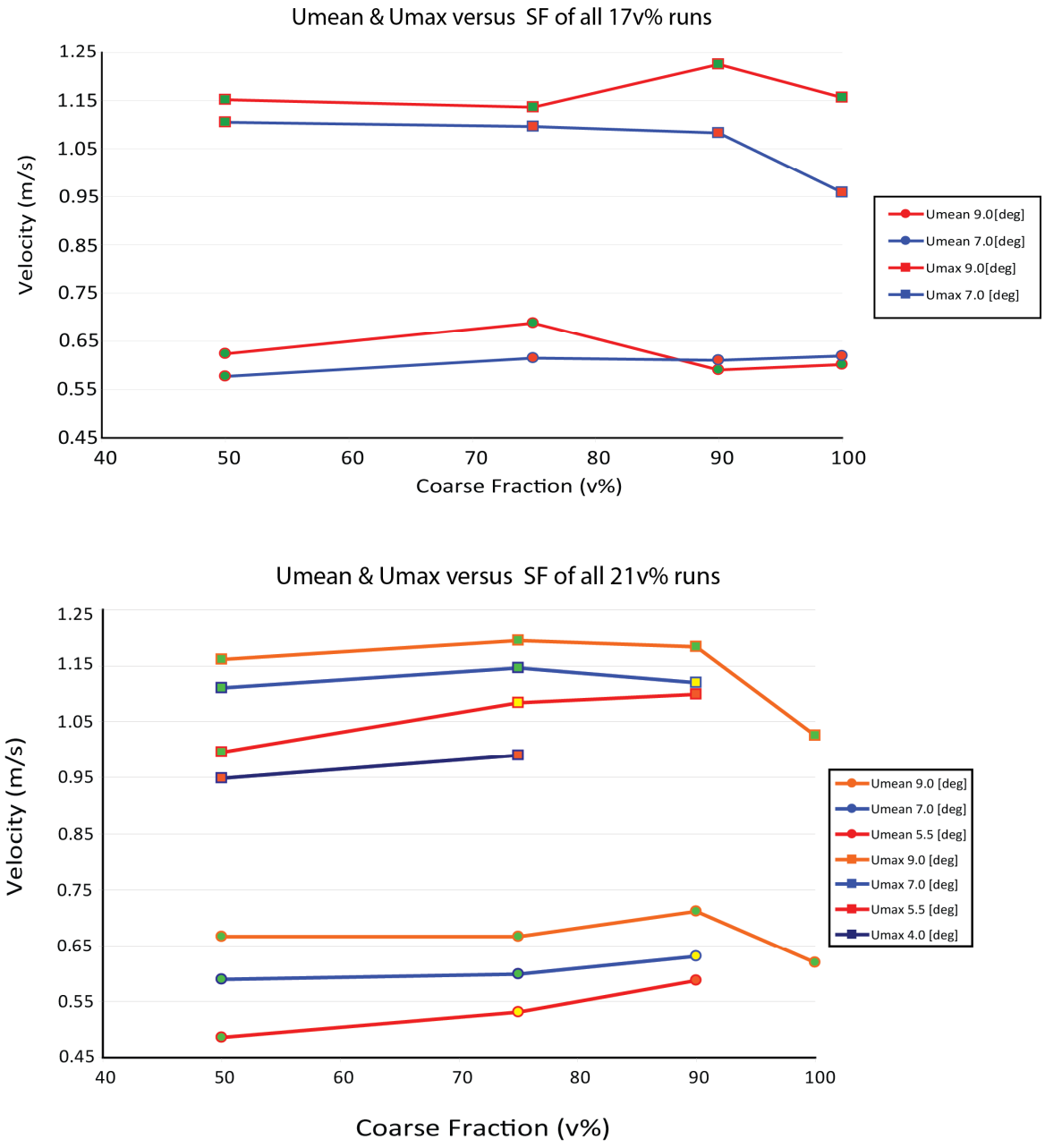

Fig 4.7: *Single velocity variables with variance in sediment fraction for all 17v% runs (top) and all 21v% runs (bottom) Aggrading behavior is indicated by: green – non aggrading, yellow – equilibrium, red – aggrading.*

3.3.2 Variations in single variables during individual runs

Additional information on current behaviour can be obtained from changes occurring during the individual experiments, when focusing on the body of the current. The start of the body of the current is at many cases still at relative high speed (high U_{mean} and U_{max}), due to complications with the inflow mechanism and therefore not a stable flow yet. It could be considered to be the neck of the current and therefore is mostly not taken into account for determining U_{max} and U_{mean}. The biggest influence on flow velocities, as was also proven by Clerx (2010) is the initial discharge. When the discharge fluctuates, it had a big effect on the mean velocity, logically increasing with higher discharge and decreasing with lower discharge. However results show that this does not directly yield for the maximum velocity as well. When discharge was considered constant, significant fluctuation in U_{max} can still be observed. This means that there is not always a linear relation between these two single variables and caution has to be taken when it is considered that there is a firm relation between U_{max} and U_{mean}. A second important observation is that U_{mean} often declines over time in near-equilibrium and depositional runs. This is probably relatable to deposition in front of the measuring probe.

3.4 Velocity profiles of the experimental HDTC's

3.4.1 General observations in dimensional vertical x-direction profiles

Because the velocity data that was obtained in the experiments is of great quality in both accuracy and resolution, it is of great use for direct profile comparison. Difficulty mainly remains in the precision in the determination of vertical distances (Paragraph 10) . As can be seen in Fig. 4.8, all constructed profiles show the main typical characteristics of an ideal velocity profile (Fig 4.3): velocity maximum close to the bedding plain, logarithmic profile close to the bed and a linear or Gaussian profile in the outer region. Most of the profiles go back to a zero-velocity point at the bedding plain, others are interpreted from the global structure of the curve and the course of the profile through time.
At first all series varying with gradient are compared. Fig. 4.8 only shows two experimental series, while the remaining can be found in the Appendices (1.10.3) The results give a logical decrease of velocity with declining slope (as was seen with the single variables), but also an increase of the distance between U_{max} and the bedding plain. Exceptions are however found in the near-equilibrium runs. Fig. 4.8 (and 1.10.3) also gives indications that an increase in slope, gives greater flow heights. The high angle runs are therefore probable to miss out part of the outer region.

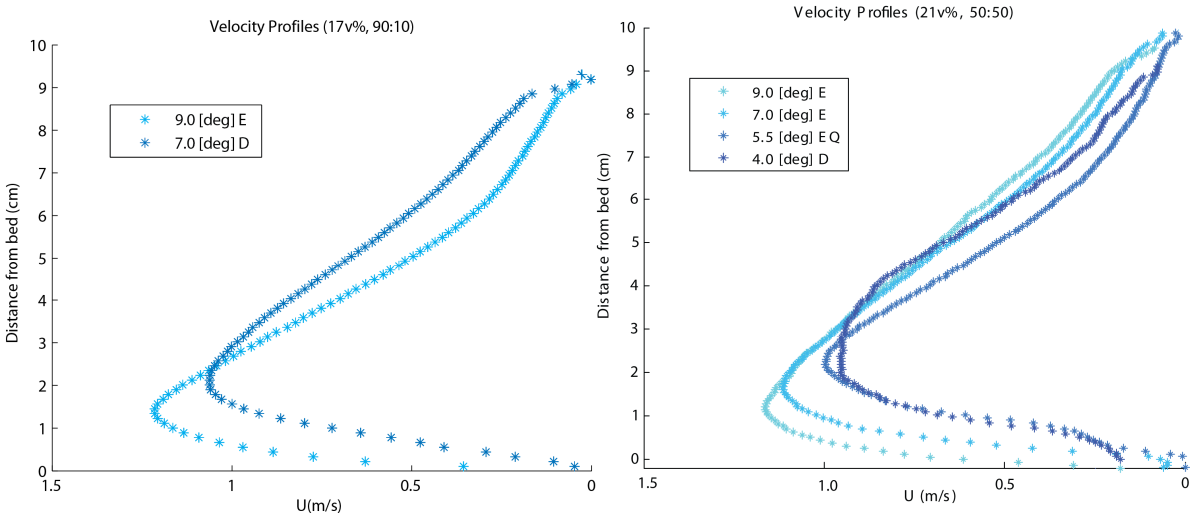

Fig.4.8: *Two experimental series showing average velocity profiles of 17v%, 90:10 and 21v%, 50:50 runs. The non-aggrading runs give the smoothest 'ideal' profiles, compared to some aggrading (21v%) profiles. All remaining graphs can be found in the appendices (1.11.3)*

Next, because the influence of bidisperse distributions on the flow structure is of main interest, all experimental data is compared by differences in coarse to fine ratios (SF) (Fig. 4.9). Because it is unknown what the influence of the depositional behavior of the current is on the velocity structure, it is assumed to be the best to only select the non-aggrading runs.
The combinations which are fully non-aggrading are: 21v%-9.0deg, 17%-9.0deg, 13.5v%-11.3deg. To include all concentrations also all 9.0v%-11.3deg runs are incorporated, which exists of one equilibrium run (90:10) and two non-aggrading runs (50:50, 75:25).
These figures show that the overall relationship between sediment fraction and the overall velocity structure is not very clear. The differences between profiles are significant less in the 9v%-11.3deg and 21v%-9.0deg runs relative to the others.

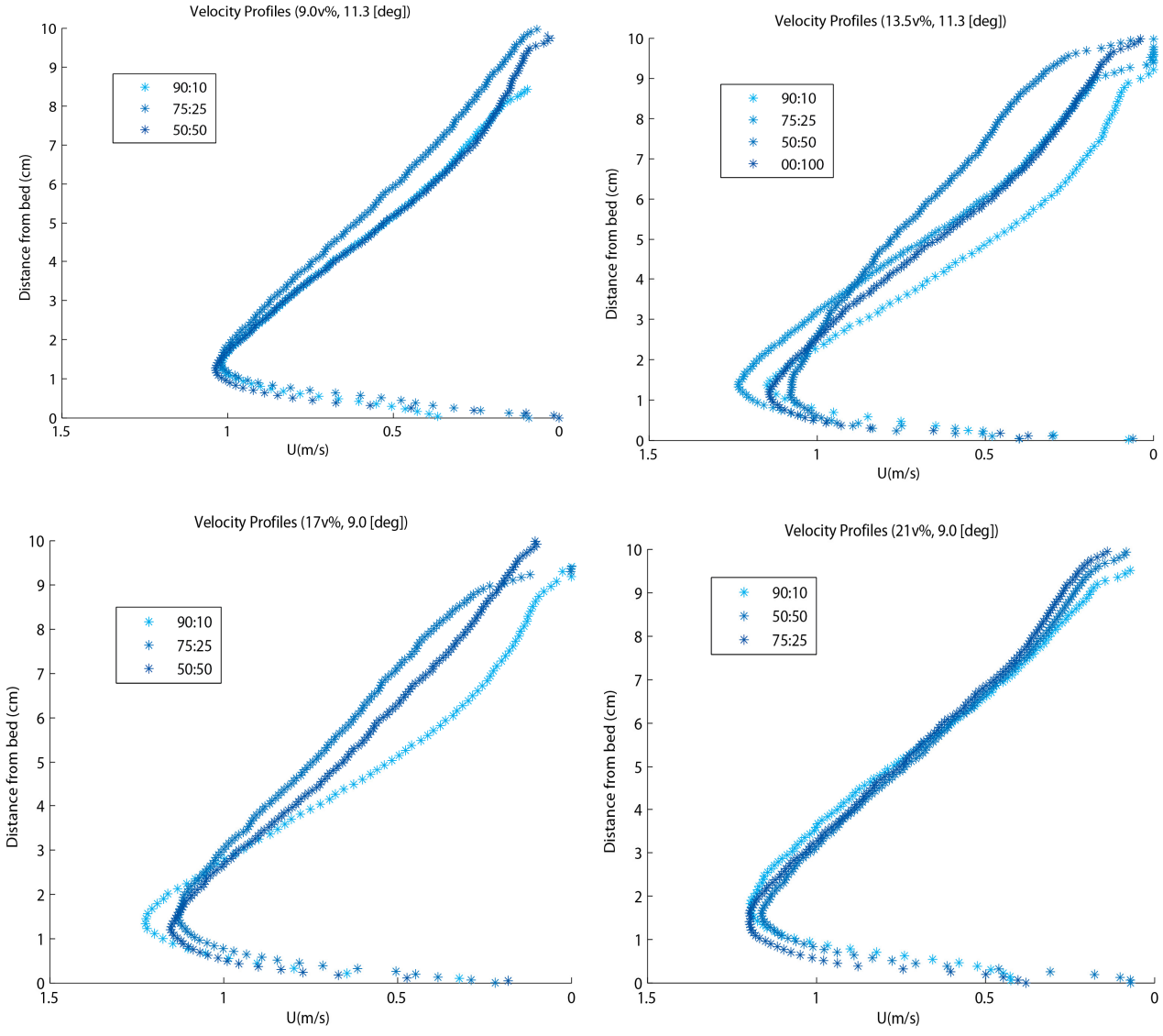

Fig. 4.9: (a-d) *Velocity profiles of only non-aggrading experiments (with exception of 9.0v%, 11.3 [deg], 90:10), grouped by sediment fraction.*

The biggest differences can be spotted in the outer region and it seems in e.g. in the 13.5v% series, that the velocity gradient above the maximum is less significant in the experiments with a high fines fraction. From the 17 and 21v% series it shows (somewhat unclear) that a higher relative portion of fines can result in more uniform velocities with lower maximum velocities and higher velocities at greater distance from the bedding plain.
Because it reveals that there is a lot of uncertainty accompanying these dimensional profiles, plotting the same profiles dimensionless as will be done next, can help to get a better understanding of the internal shape differences.

4.4.2 Dimensionless velocity profiles

In experimental turbidity research, velocity structures are commonly plotted dimensionless. This cancels out partially experimental errors (such as vertical scaling), gives the opportunity to compare runs on the basis of shape only and bridge scaling problems when looking at experimental work of others.
Dimensionless profile analysis makes it easy to compare the overall shape of the velocity structures. Especially differences in gradient in the outer and inner region can be better accentuated. Dimensionless profiles have been constructed from the obtained data by dividing all velocities by U_{max}, changing the vertical position of U_{max} to the origin of the x-axis and defining ½ U_{max} to be of value 1 in positive direction or negative direction.
Fig 4.10 show Fig 4.9c&d plotted dimensionless. The first graph has fixed points at U_{max} and at half this velocity in the outer region and therefore accentuates gradient differences in the inner region. Although differences are minor (following from all runs), from Fig 4.10a it follows that the runs with greater fine sediment content, show a more concave gradient. Further analysis that will be done on shear velocities, will give more proper inner region analysis
In Fig 4.10b the second fixated point is located in the inner region, giving more details of the outer region. It shows clearly a widening of the maximum velocity region and more homogeneous character with greater proportion of fines. The 50-50 profile is somewhat of an exception, probably relatable to experimental error.

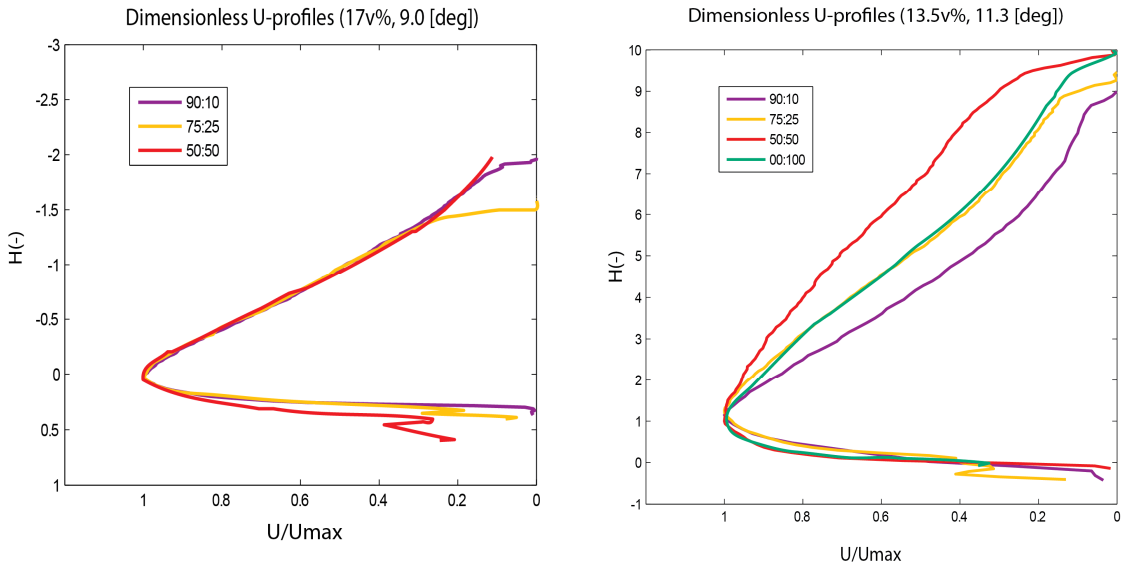

Fig. 4.10 (a-b): *Dimensionless velocity profiles of all 17v%/9.0 [deg] runs with fixation in outer region and all 13.5v%/11.3 [deg] runs with fixation in inner region*

4.4.3 Contrast in velocity structures of aggrading/non-aggrading currents

As an addition in use of the constructed dimensionless profiles, a better look can be given if clear differences can be made in the velocity structure of aggrading and non-aggrading currents.
Fig 4.11 illustrates variations in the dimensionless U-profiles (fixed in outer region) at average conditions with varying slope of the highest initial volume concentration runs (21v%).
As the gradient declines and equilibrium/depositional conditions are reached, the area around the Umax or the transition zone between the inner and outer region starts to widen. At the fully depositional runs this 'velocity nose' is at its maximum.
Further on it can be seen that an inflection point in the inner region of the velocity structure at EQ-D conditions is clearly present in the dimensionless profiles.
Fig 4.12 shows six runs with lower total volume concentrations. As with Fig 4.11 the difference in depositional character is obtained by distinct slopes. The 17 and 13v% runs agree with the 21v% results, although they are less obvious. The lowest 9v% runs however show the exact opposite of all others.
The effect of slope and depositional behavior on the shape of the profile is therefore probably also dependent on the initial used concentration.

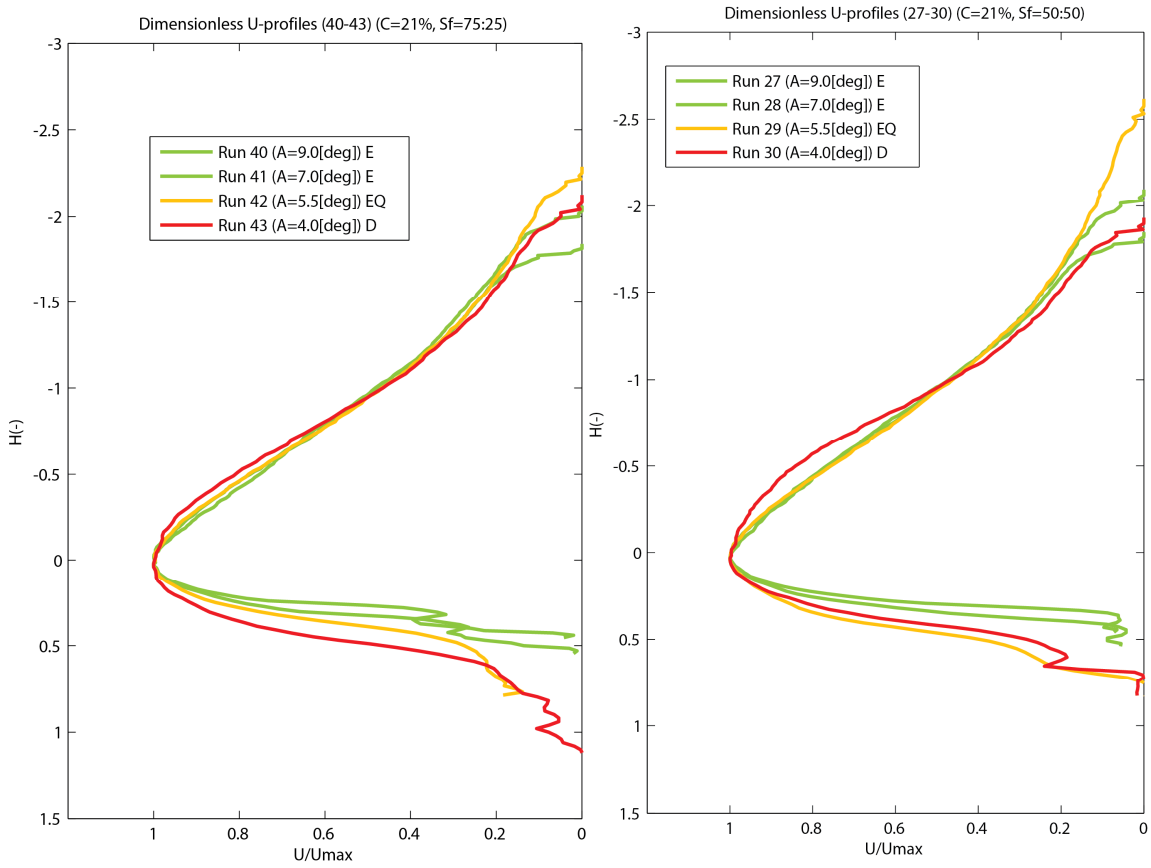

Fig 4.11*: Two series of experiments with 21v% showing shape differences in velocity structures between aggrading and non-aggrading runs. The high-velocity region is clearly affected.*

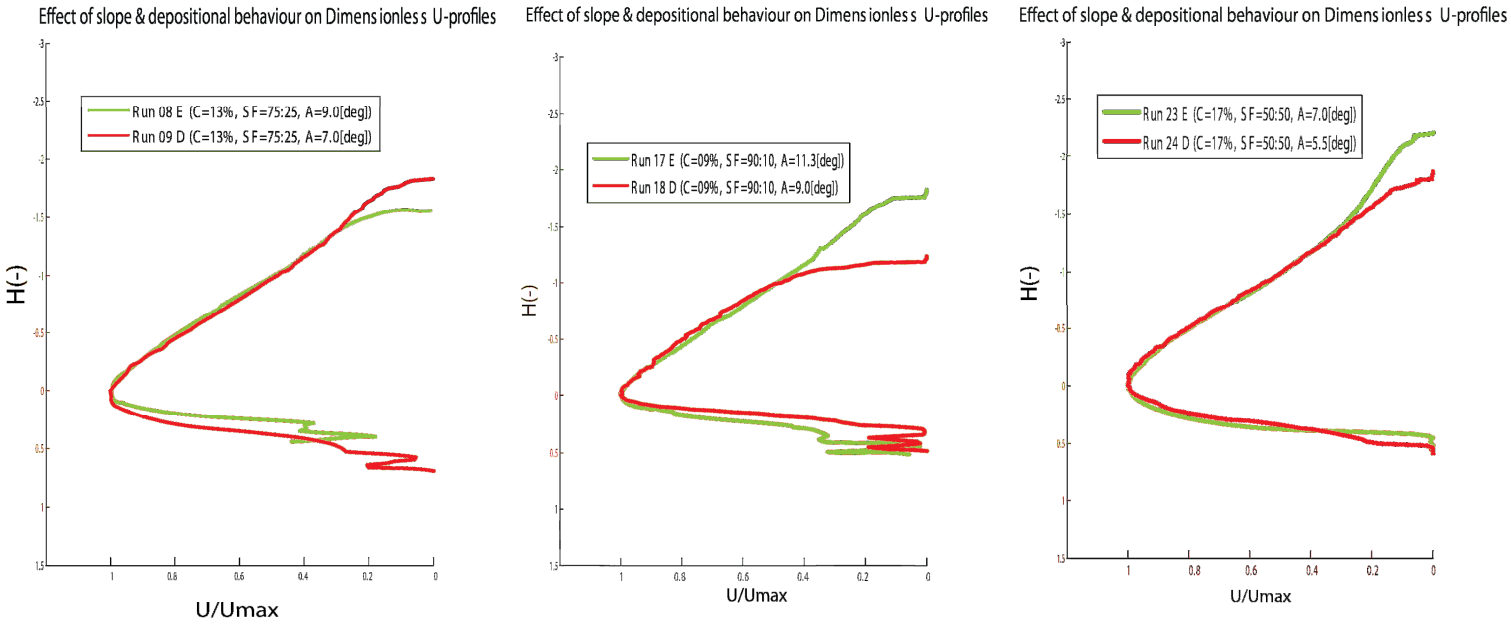

Fig 4.12: *Three examples of relative low-concentrated runs and the effect of aggrading behavior on velocity structures*

3.5 Velocity structure variation with time in aggrading runs

It is of great interest if distinctions in the velocity structure can also be recognized during the course of a depositional run. The non-rigid deposit will have its effect on the boundary conditions and on the velocity structures in the flow.

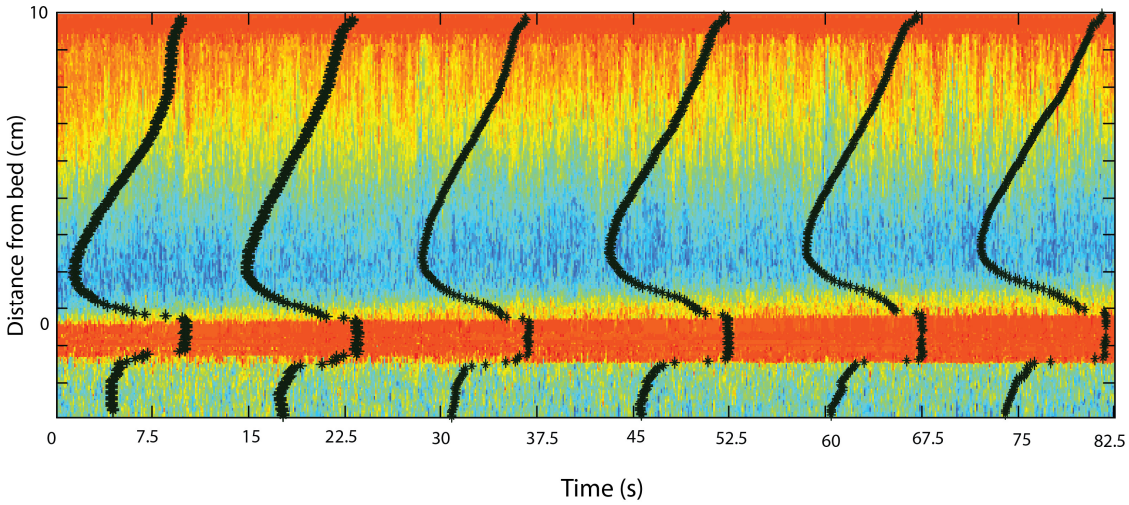

Fig 4.13: *Velocity map of Run#24 (17v%, 5.5 [deg], 50:50) including velocity profiles averaged over 15s, showing structure transformations occurring during the experiment*

As with Run #24 (17v%, 5.5 [deg], 50:50) the velocity map (Fig 4.13) illustrates due to deposition an increased bed height over time (thick red line).
The neck of current in the first 7.5 seconds is non-depositing and the U-profile is identical to most non-depositional runs showing a smooth logarithmic inner region.

But while the deposit increases in the aggrading body, the inner-regional profile starts to develop an inflection point at certain distance from the bedding plain. At a later stage this inflection point starts to lose its significance again, which straitens out the inner region velocity gradient.

4.5 Shear-velocity approximations

As previously described (Methods 3.0) , the shear velocities have been approximated with the help of the law of wall. Since this method is rather sensitive to experimental errors and depends a lot on the quality of the data, caution has to be taken in the interpretation of the results.

After leaving out the extreme and unrealistic values ($U_* > 0.2$m/s), it shows (Fig. 4.14) that the shear velocities are heavily related to the depositional behaviour of the current.

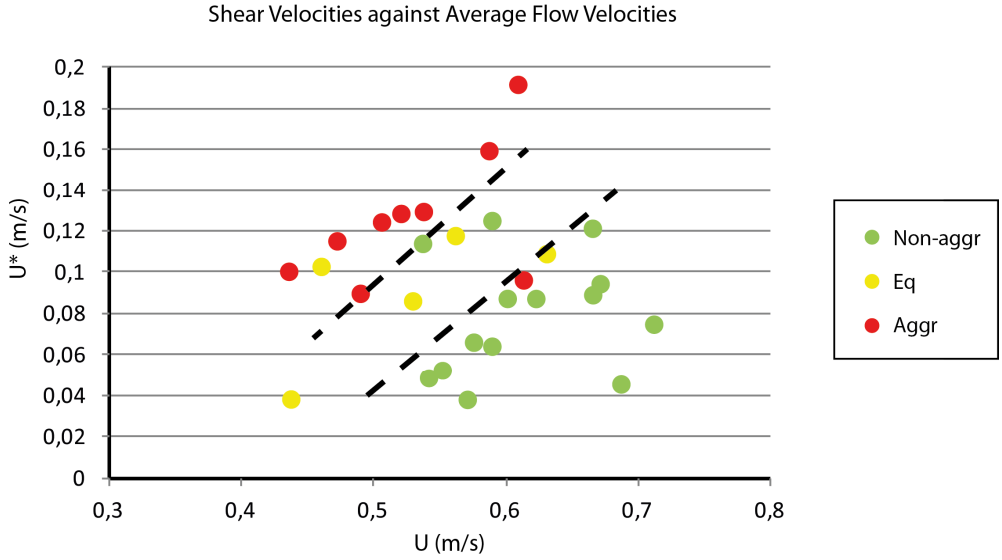

Fig. 4.14: *Approximated shear velocities versus U_{mean} + indication of aggrading behaviour. Aggrading currents give significantly higher shear velocities than non-aggrading currents. Dotted lines indicate possible transition zones.*

On average the aggrading runs have higher shear velocities than the non-aggrading.
This is somewhat strange when looking at the following relation (Sequieros et al., 2010) which is the critical velocity for the deposition of granular particles:

$$\frac{w_s}{U*} \approx 1 \qquad (4.1)$$

This means that settling velocity of particles (w_s) must be identical to the shear velocity (U*) at equilibrium conditions. When $w_s > U_*$, the current is releasing sediment (Kneller et al., 2003) and when $w_s \leq U_*$ everything is tended to be in suspension. Therefore it is unrealistic that the aggrading flows give higher shear velocities, since this would mean an even greater increase in particle settling velocities. Because sediment fraction does not show a logical relation with the approximated shear velocities, there must be reason.
As was shown in the previous paragraph, the inner region velocity profile changes over the course of an aggrading run. This obviously will affect the approximated 'law of wall' shear velocities and it can be questioned if they will be still valid at such aggrading conditions. Changes in shear velocities of these aggrading runs over time are plotted in Fig. 4.15 The region of inflection point until bed has been left out in these approximations.

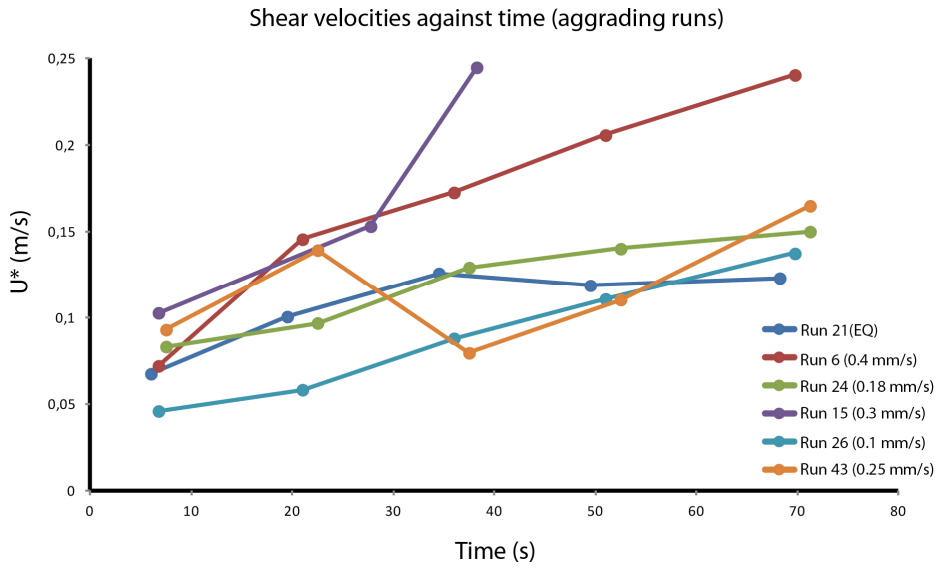

Fig 4.15: *The course of shear velocities in aggrading runs with time. Settling velocities are indicated in the legend, showing relative high shear velocities with higher settling rates.*

It shows a general trend of increased shear velocities over time. This seems to be connected to the settling rates or the height of the deposit. The aggrading runs with the highest settling rates show in general higher shear velocities; however there no clear relationship with increase over time. Only one equilibrium run with net non-deposition becomes stable after 30 seconds, which can be attributed to a change in discharge (too low at start). The increased discharge increases velocities and therefore prevents further aggrading conditions.
Remaining relations between any of the parameters and the approximated shear velocities are rather vague. There are however enough indications to assume shear velocity increases with greater volume concentration (Fig. 4.16), when leaving out the extremes (U*>0.25m/s).

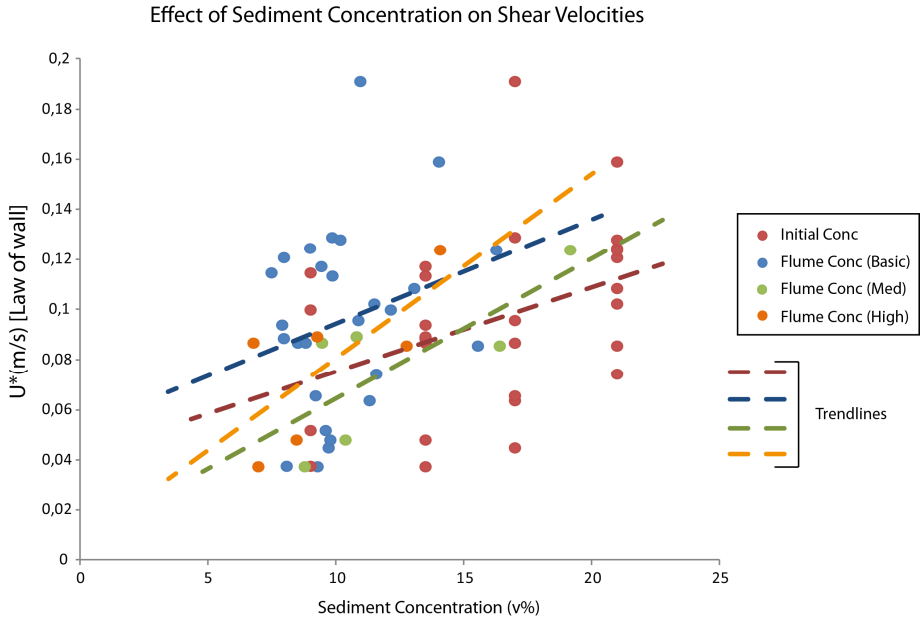

Fig. 4.16*: Shear velocities plotted against sediment concentration: Initial and three in-flume concentration approximations (1.10.2). Notice has to be given on the limited amount of data points in the High and Med series. Linear trendlines are indicated*

With all four concentration measures (Initial C and three flume approximations) there is a general linear increasing trend varying in slope between 3.4-7.4 mms^{-1}/v%. But the general range is too large to give a lot of certainty about these measures.

3.5.1 Chezy equation

Kneller (2003) constructed a simple modification of the Chezy equation for retrieving shear stresses in open channel flow (Middleton & Southard, 1984) which is mainly depended of the current density, flow height and slope of the channel (S).

$$U_* = \sqrt{g\frac{\Delta\rho}{\rho}hS} \qquad (4.2)$$

This relation was intended for open channel flows without horizontal divergence, but according to Kneller et al. (1999) this probably also can be well applied to the inner region. It only needs 'h' and 'Δρ' to be restricted to the vertical position of Umax. These relative measures in the flow structure have been incorporated in a new relation with a factor 'ξ' for the relative position of U_{max} to total flow height and 'ζ' is dependent of the shape of the density profile.

$$U_* = (g(\xi\frac{\Delta\rho_T}{\rho})\zeta h_T S)^{1/2} \qquad (4.3)$$

This modification of the Chezy equation can be compared with the results obtained from the 'law of wall' method for the runs where the position of U_{max} could be accurately be determined. The local density difference is somewhat more of a challenge, since no direct information is known about the internal density structure. Therefore an assumption has been made that the inner region is an area of high density and that the initial density difference between the ambient fluid and the mixture is quite similar. Due to entrainment flow density decreases during the experiment relative to the initial density of the mixture. However the inner region near the bed is generally higher concentrated, affecting the bed shear stresses. Because no direct concentration measurements have been taken the initial densities of the sediment mixtures are applied for the bed shear stress calculation.

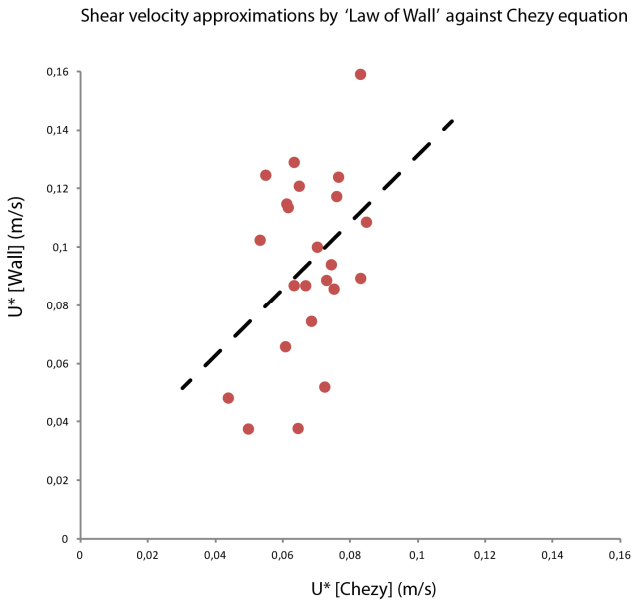

Fig. 4.17: T*wo methods for approximating shear velocities plotted against each other ('Law of wall' and Chezy equation by Kneller (2003)). Unrealistic 'law of wall' approximations have been left out. The dotted line indicates the general linear trendline.

The outcome of the Chezy approximations (Appendix Table 1.10.2) are significantly deviating from the 'law of wall'. On average the method of Kneller (2003) gives around 25% lower shear velocities. When extreme values (U*>0.25m/s) are left out in the 'law of wall' approximations, this difference is reduced to around 15%. But still there is a standard deviation from the U*(kneller)/U*(wall) ratio of around 40% (Fig. 4.17)

3.6 Indications regarding dimensionless parameters

From the total series of experiments the Fr,Re and Ri-numbers are approximated (1.10.2). Especially the exact height of the flow is uncertain and therefore a range of values is given. From the video data a maximum (including total lower concentrated region) and medium (partially including lower concentrated region) flow height were obtained for a large number of runs. These were used to calculate the medium and maximum dimensionless values. This was based on the speculation if the much lower concentrated upper flow can be seen independent or dependent of the highly concentrated underflow. Since the obtained video data was not always efficient to obtain total flow heights, only a limited amount of runs include medium and maximum values.
For the third basic-group a constant of 10cm was applied in all calculations. All applied mean velocities have been determined over 10cm as well, since this was the average distance between the probe and the bedding plain. Therefore the basic-group dimensionless parameters are internally more reliable than when using the actual flow height.

The biggest consequence of the range in flow heights is the uncertainty of the actual flow concentrations (1.10.2) and it shows that due to entrainment the volume concentrations can be sometimes reduced to almost half of its initial value. However this does not directly result in very major variations in Fr and Ri-numbers. Variations in Re are somewhat larger due to distinct use of flow height. However all flows are fully in the turbulent regime (Re>2000) with values between the 20 & 50e3.

Fr-numbers are all supercritical (Fr > 1) and generally low in currents which do not show a lot of entrainment or dilution. When the Fr-numbers (1.2-2.1) are plotted against the 'expansion' factor (or entrainment), it shows a more or less linear increase with expansion factor (Fig.4.18). It is however highly dependent on the flow height that has been chosen as can be seen on the wide range of values in the medium and high series.
When only the high-concentrated region is taken into account the increase in expansion factor is logically less with higher densimetric Froude numbers. There is no major difference between the basic and high series.

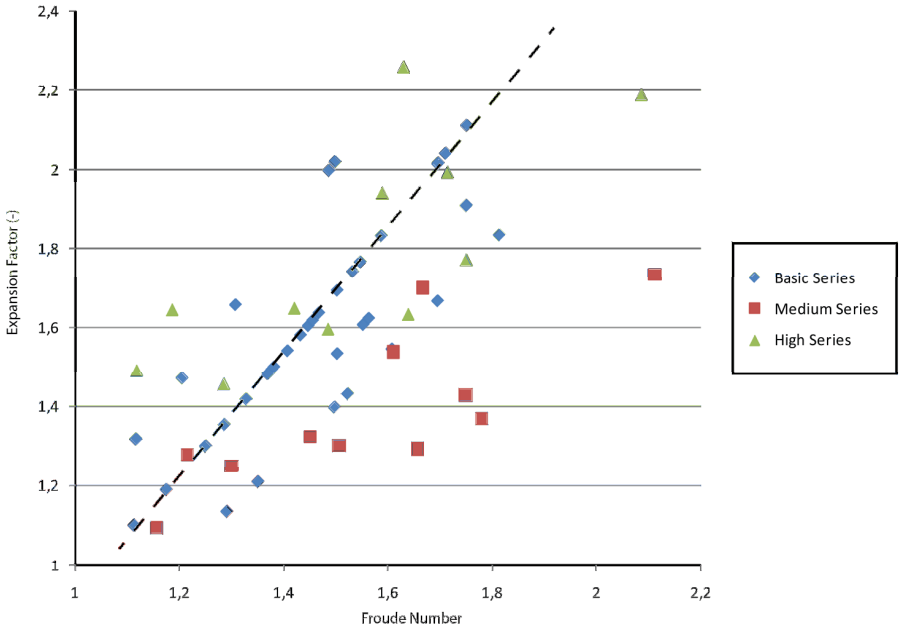

Fig 4.18: *Calculated densimetric Froude numbers against expansion factor (initial against flume volume). It shows its dependence on chosen flow heights. The basic series (H =0.1m) shows the best linear relation (indicated by trendline)*

This also yields for the average flow Ri-numbers (0.2-0.85) which are in almost all flows way above the proposed critical value of 0.25 (Meiburg & Kneller, 2003) making them subcritical. The importance of this critical value can however be speculated.

They are greatly influenced by the difference in slope, also indirectly by its effect on velocities. Because of the High Ri-numbers, it is expected that all runs should be characterized by some form of stratification of flow. The general character of the concentration structure (Kneller et al., 2000) can influence the stratification below the velocity maximum. If the profile is smooth the stratification and local Ri-number is generally stable, but when a stepped profile exists there can exist a region of unstable stratification at close distance from the bed.

Fig. 4.19 shows the combination of al bulk Ri-numbers (0,2-0,9) versus slope. Because relation 2.9 contains a slope factor, the Ri-number is linearly increasing with lower gradients. All three series show approximately the same results. The medium series give on average higher Richardson numbers compared to the high series, but in general the range between the distinct series is limited.

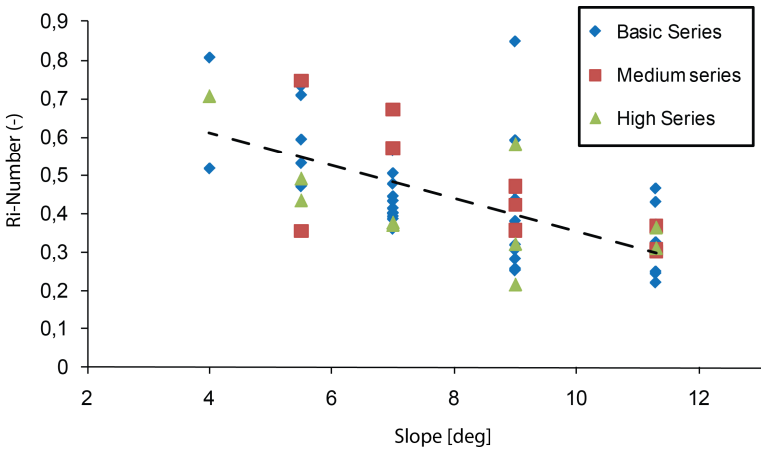

Fig.4.19*: Calculated Richardson numbers versus slope for every flow height series. The added trendline indicates the average course of the basic series*

3.7 Additional visual observations

The overall quality of the video data is not sufficient to give detailed information about internal structures of the current. This is for a substantial part the cause of the finest equally suspended particles, which blurs all structure in the flow.
In every runs where the (relative coarse grained) tracer particles were included, they were transported primarily very close to the bedding plain as bed load. Occasionally some particles could be carried higher up the flow due to vertical turbulence.

A somewhat unclear distinction in almost all flows could be made in a high-density and low-density area (which is the basis for the different flow height series). The high density lower region is characterized by relative constant high velocities, while the much slower low density region is dominated by inconsistently occurring vortexes.

5) Discussion

The large quantity of data acquired in this report can give a lot of new insights about internal flow properties of high density turbidity currents and especially in the field of bidisperse currents. Since the processes in high concentrated turbulent flows can be very complex, experimental study is needed to give insight in the grain-to-grain interactions in such flows.

The direct contribution of the fine sediments in the mixture has been studied with the proposed ability of the current to sustain its sediments in suspension more efficiently.

This is at first also a logical consequence of the lower settling rates (Stokes law) of the fine grained sediments. Since deposition of the fine fraction is prevented, the density difference is longer maintained which makes it more difficult for the coarse fraction to settle.

However this does not directly explain why the relationship between sediment fraction and aggrading behaviour is non-linear, shown by the curvature of the stability field (Fig 4.2). This also follows from all velocities values, which show that the differences between a 100v% coarse run and a 90v% coarse run are much more significant than between all 75:25 and 50:50 SF runs.

The effect of sediment fraction on the equilibrium line seems to slowly smooth out when the fine fraction is increased to the volume percentage of 50%. Or in another perspective: the addition of small portion of fine sand in a coarse-grained mixture has a larger effect on depositional conditions than the same addition in a mixture which already contains a portion of fines.

The direct effect of sediment fraction on velocities (Fig. 4.6 & 4.7) is minimal compared to the changes made in slope and total volume concentration (Fig. 4.4 & 45) in these experiments. But the variation in U_{max} and U_{mean} with changing sediment fraction is roughly the same fashion. Shape variations would be expected to be also visible in the ratio U_{max}/U_{mean}. The average value of ~1.85 ± 0.17 shows quite large deviations, but cannot be logically explained by any of the variables (gradient, concentration or sediment ratio). This value is somewhat higher than the 1.70 ± 0.12 of Felix's (2010) coarse grained experiments or the 1.64±0.17 of Buckee et al. (2001) and a lot larger than the 1.3 of Altinakar et al. (1996)

Differences in behaviour between U_{max} and U_{mean} could (partially) be a consequence of the limitations of the UVP probe. The standard set 10cm height can especially at the runs with high gradients miss out partially the outer region of the profile, which results in higher U_{mean} values than is actually present.

5.1) Influence of fine-grained sediments on flow processes

From the retrieved results (Fig. 4.2 & 4.3) it can be concluded that the supplementation of the finer-grained sediments is more important than the actual quantity. This is in agreement with the results retrieved by Gladstone et al. (1998).

As was said before, from Gladstone et al. (1998) it was concluded that in flowing mixtures containing a small portion of fines also the coarse-grained particles will travel larger distances before settling. When a small portion of coarse grains are added to a fine-grained current however, not much will happen. This is because the coarse grains will settle relatively fast, leaving the remaining current fully fine-grained. The finest fraction in the distribution, even though of small proportion, has the greatest effect on maintaining the flow energy and increasing travelling distances.

The data from Gladstone et al. (1998) is however not sufficient for getting better understanding of the exact process, due to the lack of any internal flow information. Further on, it is not clear if the behaviour of the very fine and sharp SiC-grains can be compared with natural sediments.

The constructed velocity profiles (1.10.3) and single variables (fig. 4.4 - 4.7) indicate that the internal processes are not so straight forward. The overall weight and density of the mixture must be the same in all runs at constant volume concentration, but the vertical distribution can be totally distinct. The shape variations in the constructed profiles are dominantly depended on the concentration distribution, since it is the main driving force for the current.

The addition of fine sediments is establishing the ability to better distribute the suspended sediments, due to the fine sediments being easier affected by turbulence. The fine particles need less turbulent kinetic energy to keep them into suspension, which allows the current to keep its momentum. A more uniform concentration distribution suppresses the internal shear and therefore energy loss by allowing more extensive mixing.

It is somewhat unclear in the single variables (Fig 4.6 & 4.7) if there is an optimum (around 75:25-90:10) or a certain velocity level which remains stable from this maximum till 100v% fines.

A velocity optimum would mean that a total fine mixture does not result in the best energy conservation. Another factor which is of importance is the entrainment. The flow heights of the previous performed 100v% coarse runs are on average a factor of 0.85 less than the experiments of this report when considering the full flow (1.10.2). The height of the highest internal concentration region in the flow of these bidisperse experiments is however identical to the flow height of 100v% coarse runs (~10cm). Internal concentration measurements are however not available, which makes it difficult to estimate the effect of entrainment between distinct conditions.

The easy turbulent movement of the fine particles does not only result in a better distribution but also in more entrainment with the ambient fluid. A mixture of dominantly coarse sands has therefore a higher overall concentration, but has a more uniform sediment distribution than a current with 100v% coarse.

The 9v% runs show the least to almost no velocity variations with sediment fraction (Fig. 4.6). This is logical since the actual flow concentration is even more reduced and grain-to-grain interactions in low-concentration turbidity currents are of no great importance, making flow processes dominated by turbulence.

With the basic flow height of 10cm the initial 9v% is s reduced to 6-8v% in the flow, dependent on flow velocities. These volume concentrations are more characteristic for LDTC (Middleton and Hampton, 1973; Middleton 1967/1993)

The higher concentrated (21v%) runs do not really show a velocity optimum (Fig. 4.7), but remain somewhat more constant in velocities after a certain addition of fines with changing SF. Caution has to be taken in the 100v% coarse runs, since these had to be corrected and therefore contain extra uncertainty.

Decrease in U_{mean} during equilibrium and aggrading runs could possibly be an effect of deposition in front of the probe. The loss of concentration due to deposition is minimal (Appendix 1.10.1), however it can also act as an obstruction; slowly increasing in size, it can result in a gradual decrease of velocities.

As said before, the experimental work earlier done on bidisperse distributions in HDTC is limited to the works of Gladstone et al. (1998) and more grain-density based work such as Hodson & Alexander (2010). However similar conclusions were drawn from numerical studies (Salaheldin, 2000) and other mathematical models (Harris et al. 2002). Simple one-dimensional numerical modeling of poorly-sorted mixtures had been performed by Salaheldin et al. (2000). Special interest was taken on the effect of the fine-grained fraction on flow dynamics and the resulting deposits. An adaption of the four-equation model of Parker et al. (1986) was constructed for heterogeneous suspended sediments. Steady and continuous depositional currents were run on a 50km long channel, resembling the bed profile of the Amazone Submarine Channel. It was found that an increase of the fine fraction in a bidisperse mixture resulted in a decrease of total flow height and increase in velocities and total sediment flux. This was explained by the more efficient transportation of sands in mud-rich

turbidity currents, by enhancement of the internal energy supplying process. The modeled runs with higher proportions of fines were capable of transporting higher sand volumes at greater distances, even though their initial sand volume was less. As an addition, the size of the finest fraction was altered to look at changes in effectiveness. Logically it was found that a decrease in size of the finer fraction increased the effectiveness of the current to sustain itself. Two runs were conducted with a more polydisperse distribution (four fractions), which showed similar behavior as the bidisperse currents.

In this report the main focus has been on bidisperse sediment distributions, while naturally polydisperse turbidity deposits are much more common. However, because the ability of the current to transport suspended materials is dependent on the finest fraction in polydisperse mixtures, the internal processes are assumed to be highly comparable to bidisperse mixtures. Therefore the performed experiments can be compared with polydisperse HDTC's which contain fine materials of the same order as the used fine fraction (D50=µm).

Gladstone et al. (1998) also suggested that the entrainment of muds by erosion of the head can increase the fine-fraction of the mixture and therefore increase maintenance of energy. It is implied that clean-sand turbidite bodies therefore should always be less extensive than bodies containing muds and clays. Grainsize analysis done on the deposit of one of the experiments (Run#43) in this report, shows results that contradict this statement (Subchapter A).

General classifications of turbidite systems are also based on the mud or sand richness (Reading & Richards, 1994). Reading & Richards created a wide classification system on the basis of grain size and feeder system. Mud-rich submarine fans are commonly enormous and said to be efficient, transporting large volume, far travelling relative low-density currents.

Mud/sand-rich submarine fans, which can be classified as bidisperse or polydisperse currents, have typical sand percentages of 30-70v%. They are still highly efficient and are moderate in size. When the volume percentage of sand exceeds the 70%, they are classified as sand-rich. A large number can be classified as being low-efficient, resulting in thick massive sands with small travel distances into the basin. The development of levees is significantly less than the more mud-rich variants and more low sinuousity to braided system develop. The addition of fine material therefore has not only a large consequence on the travelled distances of the current but also the eventual geometry and characteristics of the deposit.

The results of the performed experiments in this report show on average a maximum sediment carrying efficiency around 75v% sand, which would consequently give the most extensive turbidite body in an open environment. In the classifications of Reading & Richards (1994) a deposit with this sediment ratio would be classified sand-rich. On top of that, from the grain size analysis (Subchapter A) done, it follows that in the short distance of the flume tank fully coarse grained clean-sand deposits are deposited. This makes clear that it is possible to produce clean-sand turbidite bodies from bidisperse HDTC's. Therefore it is incorrect to state that clean-sand bodies should always be less extensive than bodies containing muds and clays. If this holds valid, it means that when a clean-sand turbidite body is found in the field, the chance exists that it makes out part of a bidisperse mixed system which can be more fine-grained distally or basin-inwards.

5.2) Traction carpet model similarities

The single value velocity variables (Fig. 4.6 & 4.7) seem not to be affected by the depositional character of the current. Settling rates have been minimal in all runs and the loss of density differences due to deposition is consequently minimal as well. This results in almost no effect on the overall current velocities.

However the internal velocity structure is clearly affected as was shown by the dimensionless profiles (Fig. 4.10), resulting in wider high-velocity region and an inflection point in the inner region. It can be argued if the widening nose can be a defect of the vertical migration of the profile due to sediment settling. However even on low resolution sampling (100 nodes = 1.5s), the same results are obtained. This shows that this is not a

defect of averaging, but an internal flow property. An explanation has to be found in the effect of deposition on internal density or sediment distribution. More evenly vertical distributed sediment concentrations will result in more blunt velocity maxima.

A fairly good explanation for better internal distribution could be the interaction with the bedding plain. There is continuous exchange of sediments with the deposits due to the turbulence energy, which could lead to more vertical homogeneous sediment distribution, resulting in a thick high velocity region.

The infliction point results in a low-velocity region close to the bedding plain. This must be a consequence of interaction between the new aggradable bedding plain and the current. The characteristics of this near bed low-velocity zone show great similarities with proposed 'traction carpet' models as f. e. Lowe (1982), Middleton (1980) and Hiscott (1994) .

Especially the findings of Sohn (1997) are of interest. According to Sohn the velocity structure of a traction carpet carrying flow is not characterized by the logarithmic or concave up structures known from the inner region of clear fluid flows. Instead it shows an exponential decay towards the bedding plain, resulting in a concave convex (S-shaped) velocity profile (Fig. 5.1).

Due to the local increase of the apparent viscosity in the traction carpet region (Wan & Wang, 1994), the flow starts to separate with a very viscous low-velocity zone defined as the traction carpet and the normal low-viscous high-velocity zone above.

Fig 5.1.shows the proposed velocity structure of Sohn (1997) and an overlapping velocity profile of Run#43 (21v%, 4.0 [deg] & 75:25). As can be seen the inner region (red) shows high similarities and is divided in a transition, collisional and frictional region. The inflection point represents a change in fluid rheology, where in the near-bed region dispersive shear stresses dominate and in the top region turbulent and viscous shear stresses dominate.

Further on Sohn (1997) suggests that the collisional region is mostly better developed in coarse-grained flows, while the frictional region is more extensive below high-concentrated fine-grained flows. This is due to the effect grain size has on the frictional region, by affecting the residence time of the individual grains. In general the thickness of the frictional region increases when the grain flux rate is increased and shear stress is lower. There is however no distinction between these two regions in the velocity structure, which makes it not possible to see if this indeed holds valid in the experiments of this report.

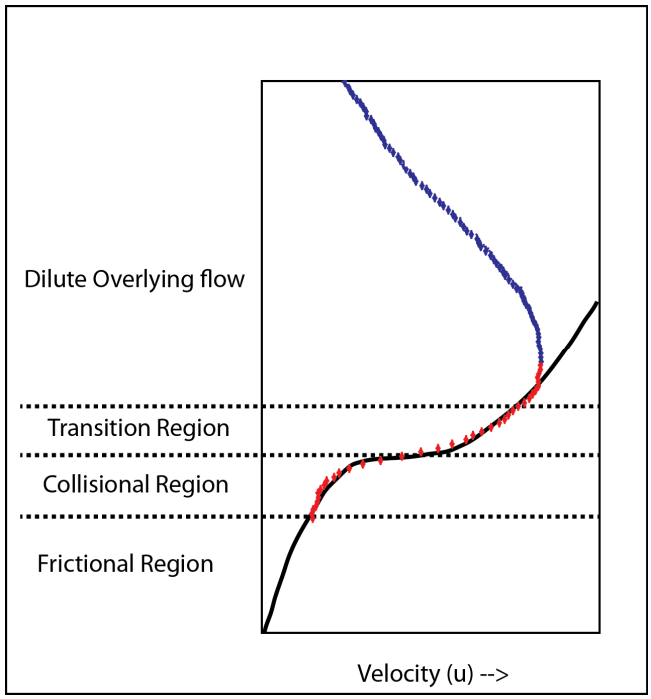

Fig. 5.1: *Altered figure of Sohn (1997), showing the suggested vertical velocity structure (black) of a traction carpet with its three distinct regions. On top the velocity profile of a 21v%,4.0 [deg], 75:25 run is plotted showing an identical shaped inner region (red), but more slow and dilute outer region (blue)*

5.3) Approximating Shear stresses

As was seen in the previous chapter, the approximated shear velocities from the 'law of wall' and the Chezy relation of Kneller (2003) show deviating results (Fig.4.16). Generally the 'Law of Wall'' shear velocities are 15-25% higher than with the Chezy approximations.

This can be partially explained by the fact that the relation of Kneller (2003) is quite simplified and is more specified for low concentrated flows. The differences must be explained by the lack of grain-to-grain interaction in the Chezy equation, which only includes the shear boundary effect.

With increasing slope, bottom friction becomes relatively unimportant relative to effects at the interface (turbulent entrainment). Therefore it is better that the Chezy equation is only applied to flows on very low slopes (Lüthi, 1988). In other relations with higher slopes bottom friction can be neglected such as was done by Turner (1973) which held true between 12-90 degree slopes.

The range of slope of the experiments in this report lies between 4 and 12 degrees, which therefore makes bottom friction and upper flow shear equally important. The Chezy relation is therefore not that sufficient for the intermediate gradients and high concentration currents in this report.

The conflicting results of Fig. 4.15, which shows increased shear velocities with aggrading currents, is a consequence of the altered profile structure of the equilibrium and aggrading runs. In the 'traction carpet' model the inner region can not be approximated by a logarithmic function. Because the boundary between the collisional and transition region includes a very sharp drop (Fig. 5.1) the resulting shear stresses are relatively high. Therefore 'the law of wall' only holds valid for the non-aggrading experimental runs. It seems to be only valid for fully turbulent boundaries.

The increase in shear velocities as was seen in Fig. 3.16 is the consequence of the slowly developing traction carpet during the course of the run. Due to the fact that most are still increasing at the end of the experiment, it can be concluded that most of the 'traction carpet systems' were still not fully developed.

Further on, as is proven by Thomson et al. (2005), caution has to be taken in the potential cohesive character of the fine sediments. Thompson et al. (2005) performed experimental work specified on bed shear stresses in turbulent flows. The direct effect of sediment volume concentration of clay suspensions on the bed drag coefficient in an annular flume was studied with the help of the law of wall. It was found that up to a concentration of 20g/l (~0.8v%) the coefficient could decline to almost 50% of its original value due to stratification of the flow or turbulence suppression. At higher concentrations the viscosity starts to influence shear stresses due to the cohesive properties of the sediments and at 200g/l (~7v%) the drag coefficient was similar to clear water conditions. When the concentration of suspended sediments increases, the viscous effects begin to outweigh drag reduction. As a consequence, this results in an overestimation of the law of wall in these high concentrated cohesive flows.

Due to the lack of shear stress data when only the non-extreme non-aggrading are selected in the data set of this report and due to the other varying parameters (SF & slope), no clear picture can be obtained of the exact relationship with sediment volume concentration. However the data that is present indicates an increase in shear forces with greater concentrations (Fig. 4.16). This is not logical when it is assumed that all mixtures are non-cohesive.

If there is a cohesive effect of the fine sediments this would change with sediment fraction. But the wide range of data, suggests instead a decrease in shear stress with increased fine fraction. Therefore it can be said that the unclear decline of shear stress with increased concentration is not an effect of slightly cohesive behaviour of the fine sediments.

The significant level of experimental error and the lack in data is mainly too large to give good constructed conclusions in this field.

5.4) Entrainment and dimensionless parameters

Previous lock-exchange experiments have tested the magnitude of dilution due to water entrainment in the moving current. McCaffrey et al. (2003) measured with a siphon tube close to the outlet that his mixture concentration had fallen to half of its initial value of 5v% over very short distance. This could not be attributed to deposition, which was insignificant. The rapid entrainment is a problem for the validation of HDTC being able to transport sediments at long-ranges. However dilution which is entrainment-related can be in most cases an artefact of the flow generation mechanism. In the example of McCaffrey et al. (2003), the flow enters the flume as a jet, incorporating an extensive amount of ambient water. The expansion factor of the currents in this report is however limited to 1.1-2.2, which is relatively low. This is probably the effect of the much more gentle release of the current inside the flume.

When only the high-concentrated region as the 'medium series' of the flow is taken into account and the much more dilute outer part of the outer region is neglected, the expansion factor does not become much greater than 1.5 (max 1.7). This can only be the case when the concentration loss due to the interaction with this dilute region is very minor.

In general it can be said that the entrainment in the short distance the currents travel in the experimental flume is limited, but still rather significant (Appendix 1.10.2). The initial concentrations can differ a couple of volume percent with the actual flume concentrations.

The lack of influence of flow height on the dimensionless parameters is a logical consequence of its effect on the expansion factor (f_e), since this will influence flow density. From (3.1), (3.7) and (3.9) it follows that variations in flow height will be compensated by changes in flow density.

From Fig. 4.17 and (Appendix 1.10.2) it follows that all runs are supercritical, but with an expansion of only 10% the critical value of Fr = 1 is nearly reached. When the current would have compacted instead of diluted, it would have become subcritical.

Limited entrainment is caused by a combination of relative low gradients (5.5-9 [deg]) and low concentrations (9-13.5v%). This is a logical consequence of the increased gravity factor with higher slope and increased density difference with higher concentrations. When the density differences with the ambient fluid above are greater, there is more tendency to entrain.

The bulk Ri-numbers, obtained from (3.9) show as in Fig.4.17 they are highly influenced by the chosen gradient. A higher Ri-number would mean a greater level of stratified flow, which is therefore in these experimental series for most part dependent on relative low gradients.

5.5) Recommendations for further research

Even though the dataset that was obtained for this report is quite substantial, at some fields it was insufficient to give vital proof for a number of assumptions, such as the relation between concentration and shear stress. Therefore a more complete database which includes additional non-aggrading runs could give more certainty.

This report was only specified on two distinct grainsizes (D50 = 50 & 144 µm). Variation in the chosen sediments would be of interest for further research. Also the addition of more than two fractions could help in a better understanding of flow processes. As was stated before, the effect of fines in polydisperse HDTC on the carrying capacity will not be substantially different as with bidisperse HDTC. However the possible influence on velocity structures is unknown.

The lack of actual inner-flume concentration measurements is a major disadvantage for getting understanding of the complex flow processes. The combination of concentration and velocity profile data could be much more valuable when cross-checking with numerical models. The addition of this data would be a very valuable medium for improving numerical models such as Massflow-3D^{TM}.

As comes forward from the general classification of Reading & Richards (1994), mud-rich turbidity currents do not only travel large distances but also show deviating deposit geometry. It is of interest to see how the geometry of the turbidity deposit will react on variations in sediment fraction.

The sub-research done on the deposit of one experimental run (Subchapter A), shows the possibility of recognizing important sedimentary features in the flume deposits when multiple grain sizes (variant in colour) are used. Since this work was only limited to one of the depositional currents, it could be extended to get a more sophisticated understanding. Eventually this could be an excellent method for connecting internal flow processes in HDTC's with actual turbidity deposits.

Conclusions

Point 1:

- **The curvature of the stability field tells that the addition of a small portion of fines to a coarse grained mixture has a much larger effect than the same addition in a mixture which already contains a portion of fine sediments. At certain conditions (low concentration & slope + high fine fraction), the effect seems totally diminished.**

- The stability field of the experimental HDTC is affected by changes in slope, initial volume concentration and sediment fraction. Increased fine fraction lowers the equilibrium line to smaller gradients, which means that the current can sustain more efficient on lower slopes.

- Changes in slope and initial concentration have the largest effect on U_{max} and U_{mean}, however also the sediment fraction is of influence. There is especially a fast increase in velocities between 100v% coarse mixtures and 90:10 or 75:25 (CS:FS) sediment fraction.

- The main differences in velocity profiles with sediment fraction, is the decrease in outer region velocity gradient with increased fine fraction. This is the consequence of better homogeneous suspended sediments due to the greater influence of turbulent kinetic energy on the fines.

- Entrainment and dilution is limited for these experiments with maximum loss of 50% of the initial sediment concentration.

- All runs are supercritical (Fr>1), highly turbulent (Re>>2000) and show relative high bulk Ri-numbers (0.2-0.9), indicating stratified flow.

Point 2:

- **The inner region structures of the equilibrium and aggrading runs in general deviate from the non-aggrading runs by showing an inflection point close to the bedding plain. This shows a lot of similarities with proposed 'traction carpet' models.**

- **Due to the deviating structure of the aggrading currents, the law of wall is not sufficient with aggrading conditions for approximating shear stress. This explains the unrealistic high values obtained.**

Point 3:

- **According to the grain size analysis done (Subchapter A) it is possible to deposit clean-sand turbidite deposits from bidisperse HDTC's. In these systems the coarse fraction settles close to the source, while the fine fraction continues to flow.**

7) Subchapter A: Sedimentary structures and depositional features of the deposit of Run#43

A1) Methods

The deposit of run# 43 (C=21%, SF=75:25, A=4.0[deg]) has been examined in further detail to see if sedimentary structures and differences in lateral and vertical grain-size distribution could be observed. Since the sediment mixture contains a bi-modal grain-size distribution, it is expected that if both the coarse and fine-grained sediments are deposited, this could result in observable characteristic sedimentary structures known for turbidity currents.

A total of 12 cores has been taken from the deposit (Fig. A2.1), of which thin sections have been made and laser-diffraction grainsize analysis (Mastersizer S long bed Ver 2.18) has been applied. Since there were major difficulties in obtaining the lowest part of the cores, these are mostly missing in the analysis.

Fig. A1: *Vertically exaggerated sketch of deposit (Run#43) indicating position of samples and D50 variance for the larger cores.*

A2.2) Settling rates

The average settling rate during the experiment that lasted around 100 seconds was 0.25mm/s and showed a fast decelerating-trend over time (table A1). Starting with rather high settling rates for the first 10 seconds, it slowly dropped down to 0.15mm/s at the end of the experiment.

Video T start (s)	Video T stop (s)	T interval (s)	Added Sed thickness (mm)	Sed rate (mm/s)
27.056	38.572	11.516	7.54	0.65474123
38.572	74.528	35.956	11.561	0.321531872
74.528	120.429	45.901	7.042	0.153417137
25.132	**130.544**	**105.412**	**26.141**	**0.247988844**

It is of importance that the discharge was too high at the beginning of the experiment (11.0m^3/h), but nicely 9.5m^3/h in the middle to end of the run. This could have been off influence on the course of the settling rate over the experiment.

A3) Results

The full deposit showed quite a lateral difference in thickness (2-12.5cm) over the flume (figure A2.1). This is mainly due to the low energy at close distance from the inlet, which causes early deposition.

Some general observations were done before further analysis:

- The whole deposit included an clearly observable 2mm-layer of very fine grained sediments on top.
- Closer to the inlet the fraction of (coarse-grained) tracers increases
- Laminae were observed over almost the whole deposit (Fig. A2) with thicknesses varying between 3mm and smaller than 0.1mm.
- The thicker section close to the inlet shows the clearest and thickest lamina over at least 2/3 of its whole vertical length

The results from the thin sections were not very much of interest and therefore are not discussed any further.

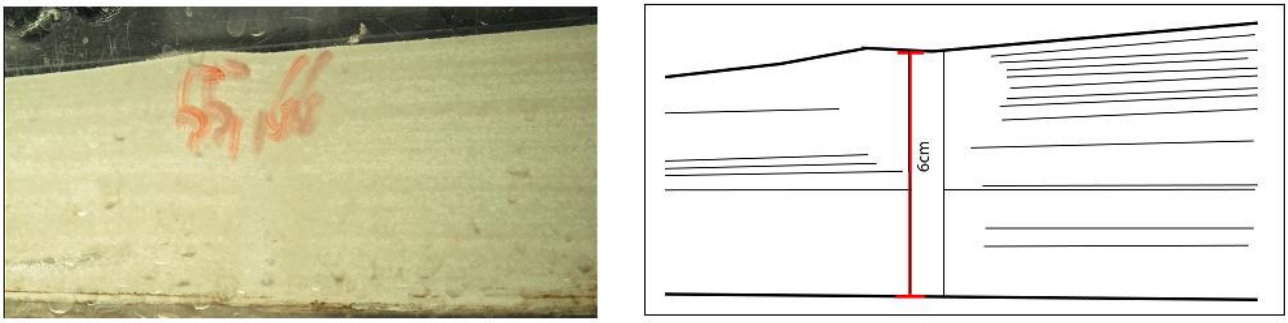

Fig. A2*: (left) picture of a zoomed-in section of the deposit at samples 5 &6, (right) Interpretation of this same section with various laminae*

Grain size analysis

The samples used for grain size analysis have been divided in varying depth intervals (due to restrictions in sampling use for the analyzer), to look at differences in vertical grain size distribution in a lateral and vertical sense. As can be seen in Fig. A3, the most characteristic feature in all samples is that the top section of the deposit shows a fast decrease in D50's . At most locations the fast decrease in grain size reaches depths of 1.5-2.0 cm. As is seen in the larger samples (S11-S12), vertical changes become much less significant at greater depths.

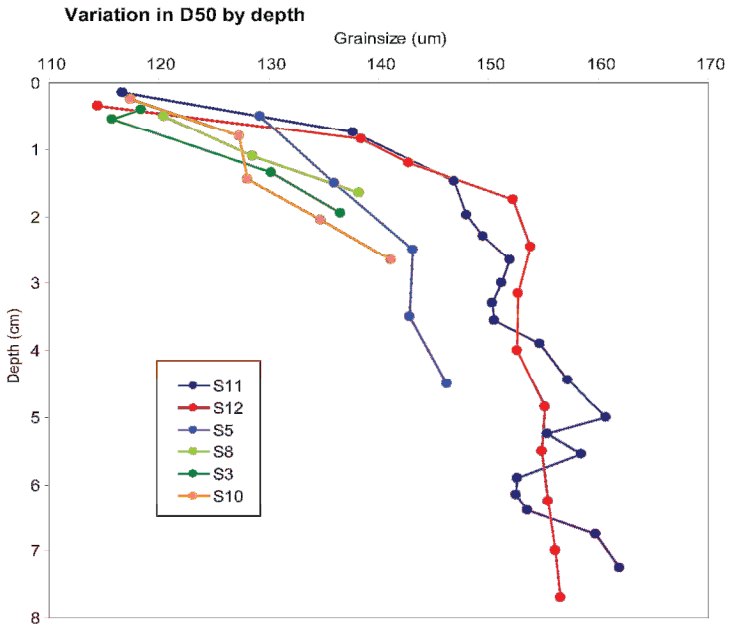

Fig. A3: *Variation of D50 in all cores versus depth. Since the deposit thickness varies, the different cores differ in length.*

At the utter top there seems to be no major lateral differences in D50, however it increases when going into depth. The samples located closer to the inlet (sample 5, 11, 12) show a greater increase in D50 than further away from the inlet (sample 3,8 & 10). This is further illustrated by figure A2.4, which shows average D50's at +/- 2cm depth. The samples close to the inlet show D50's above the actual D50 of the coarse sediment, while the samples at greater distance than 1.75m from the inlet show D50's below the D50 of the coarse fraction.

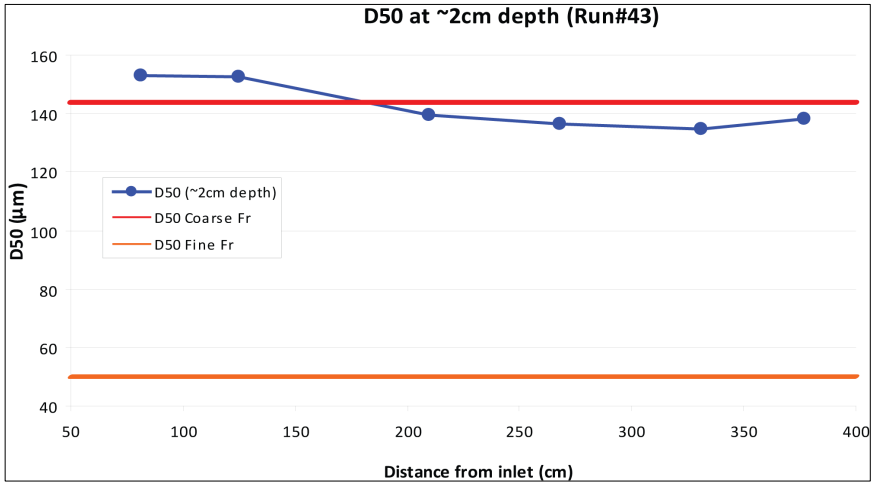

Fig.A4: *Lateral variation of D50 at approximately 2cm depth in the deposit. It shows that the fine fraction in the mixture (25v%) is not or almost not present in the deposit.*

In S11, S12 and S5 it seems that there still is a slight fining-upwards present at greater depth, however not very significant (<5% change from 7-2cm depth). The location of S3 (Fig. A1) is identical as at which the UVP measurements and the video-data have been obtained. Therefore it is known that from the eventual deposit of 3.8cm, the top 0.72cm should be at least attributed to the tail of the current. This corresponds to a shift to smaller grain sizes between 0.55 and 1.35cm depth towards the top. As can be seen this is mostly the cause of addition of much finer grains (D10 (Fig. A5a)), which logically leads into an increase of the skewness in the grain size distribution (Fig. A5b)

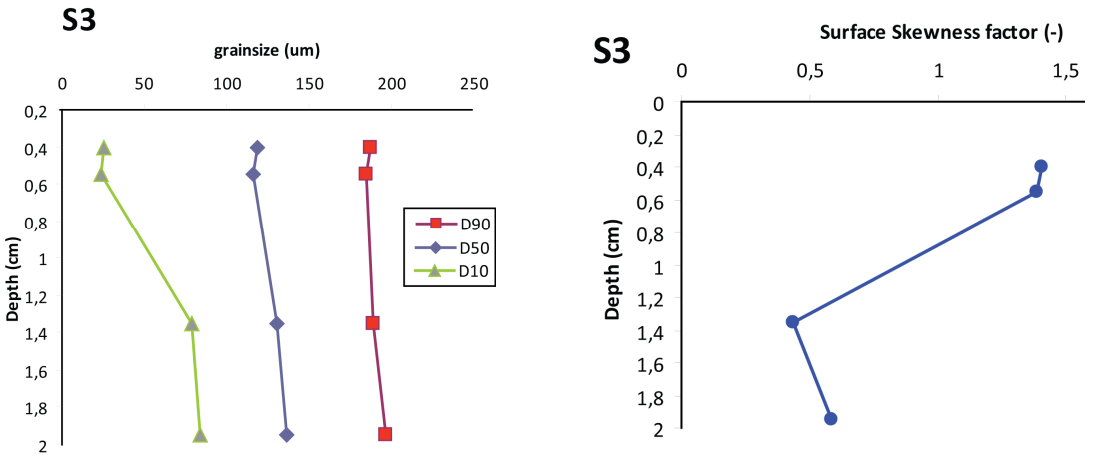

Fig.A5a&b: *Grainsize variation at Sample 3 with depth and the surface skewness factor, which shows an increase of the grainsize distribution skewness towards the top.*

S11 and S12 are the longest cores, since the deposits at these locations were the thickest. A major difference between the two however, is that S11 shows much more fluctuations at depth than S12 (Fig. A6). These are mainly fluctuations in the coarser field (D90) of the S11 distribution. Since there are no major differences in the amount of tracers in both samples, another explanation has to be found. Also in these samples the fining of the top layer is mainly influenced by the D10 of the distribution.

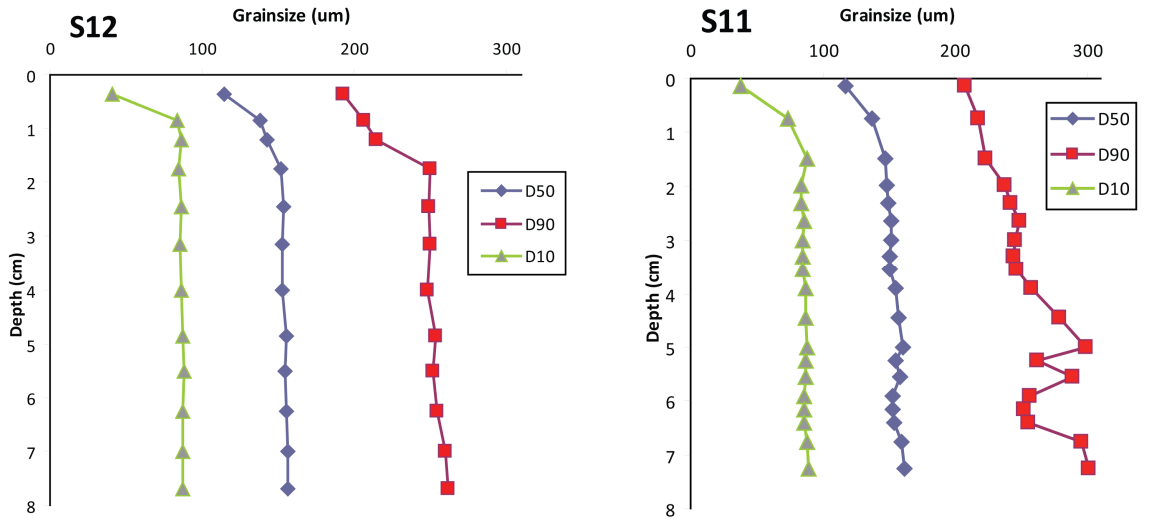

Fig.A6*: Grainsize variation at Sample 11 & 12 versus depth*

A2.4) Discussion

The retrieved results are explained by the following series of statements:

- The thin fines-layer on top can be explained by very late settling of more fine-grained materials that maintain in the water column long after the turbidity current has passed.

- The top shift to lower D50's can be attributed to the tail of the current. Due to the drop in discharge, energy decreases and sedimentation rates increase. This seems to be enough to substantially increase the fine fraction in the deposition, causing the sudden decrease in grainsize in the top layer.

- The thickness of the laminae increases with increase of the deposit height; therefore it is probably affected by the settling rate.

- Differences in S11 and S12 can be attributed to the fluctuating conditions at location S11, due to its position. Since the laminae thicken towards the inlet, it can be a defect of the sampling distances. S12 has a somewhat lower sampling resolution and thinner laminae, which could cause all laminae to be averaged out, showing no substantial variations.

- Sumner et al. (2008) showed the effect of laminae formation on the D50 with depth, which look rather similar to the results of S11(Fig. A7). Experiments of Sumner et al. (2008) showed that the settling rate of 0.44mm/s was a critical point in creating planar laminae (Bouma Tb). Above this value a structureless, poorly graded and sorted deposit was formed (Bouma Ta). Also identical is the fast decrease in settling rates over the course of the run.

- Since the D50 of the fine fraction is far below the D50 of the deposit at more than 2.0cm depth, it does not seem to compromise a significant part in the deposit and all lateral changes in grain size at this depth must be attributed to the distribution of the coarse fraction (Fig 3.2) itself.

- The minor fining upwards in the lower sections is hard to explain when the current conditions of the main body of the flow are constant. It could however also be a defect of late reworking by filtration inside the sample itself.

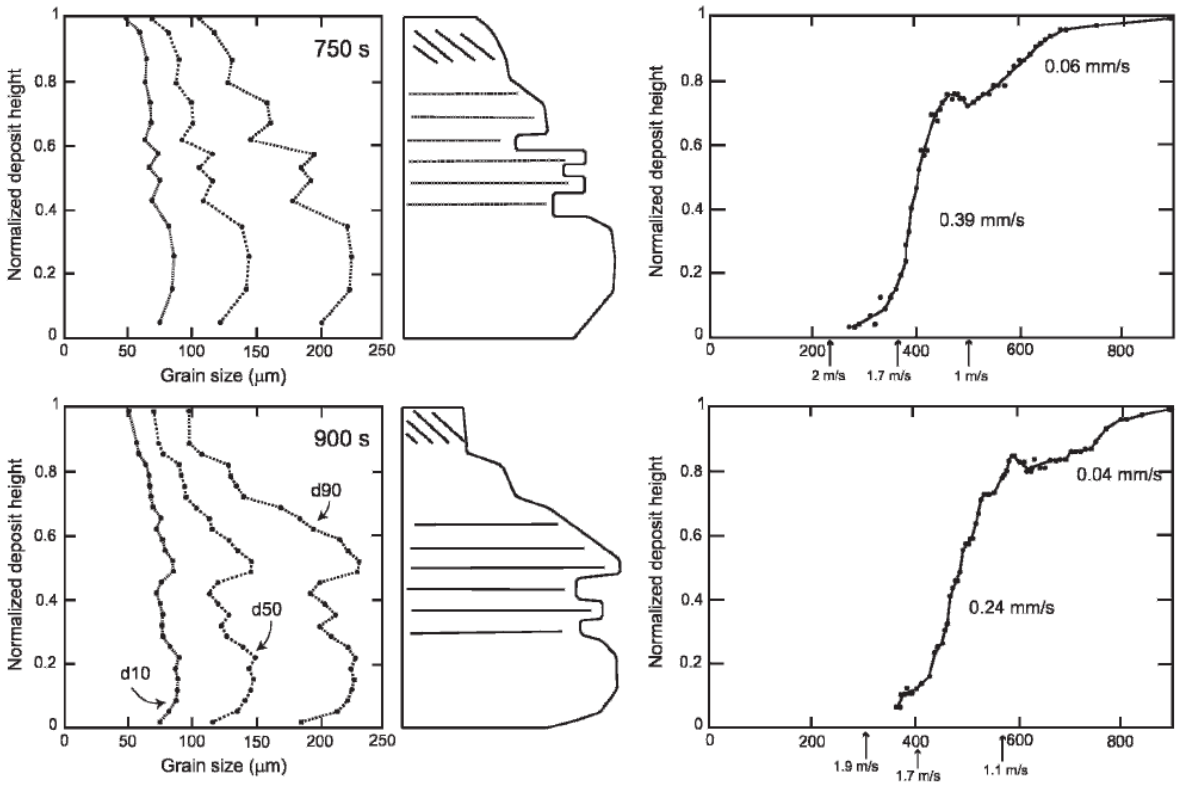

Fig.A7: *Vertical grainsize trends of two experiments performed by Sumner et al.. Also the sedimentary structures within the deposit and its growth over time is shown. Deposition was triggered by deceleration of the current during the run.(Sumner et al., 2008)*

8) Acknowledgements

This thesis was accomplished as part of my degree as Master of Science in Geology at the Faculty of Earth Sciences (University Utrecht). The project gave me the opportunity to perform a combination of sedimentary laboratory research and numerical modelling, which showed me the advantages and disadvantages of both. For the success of this project, I would like to thank:

- Dr. J. T. Eggenhuisen, for his supervision, opportunity to perform my experiments in the Eurotank, feedback on my work and many fruitful discussions
- Matthieu Cartigny, for his excellent support during the experimental phase of my thesis, support in learning the basics of Matlab, his ideas and many helpful comments
- Thony van der Gon Netscher, for supplying all materials and equipment and his excellent ideas in solving experimental problems
- Henk van der Meer, for his great support on solving numerous ICT-problems
- Jan de Leeuw and Natalie Duncan, for additional support during the performance of the experimental work
- All others which have not been mentioned but showed support during the accomplishment of my thesis.

9) Nomenclature

α/S	=	Slope/gradient of flume floor
C_i	=	Initial sediment concentration
C_f	=	Average flume sediment concentration
f_e	=	Flow expansion factor
Fr’	=	Densimetric Froude number
g’	=	Reduced gravity
H/h	=	Flow height (m)
h_T	=	Vertical position U_{max}
k	=	Von Kármán Constant
μ_a	=	Dynamic viscosity of ambient fluid
μ_s	=	Dynamic viscosity of flow
Re	=	Reynolds number
Ri	=	Bulk Richardson number
$\Delta\rho$	=	Density difference (ambient fluid & mixture)
ρ_a	=	Ambient fluid density (kg/m^3)
ρ_c	=	Average flow density (kg/m^3)
Q_i	=	Initial discharge (m^3/s)
Q_f	=	Flume discharge (m^3/s)
τ_b	=	Bed shear stress
$U;U_{mean}$	=	Average flow velocity (m/s)
U_{max}	=	Maximum velocity (m/s)
U*	=	Shear velocity (m/s)
ζ	=	Density profile shape factor
ξ	=	Ratio position of U_{max} to total flow height
w_f	=	Width flume (m)
w_s	=	Settling velocity of particles
Z	=	Vertical position in flow (m)
Z_0	=	Hydraulic (bed) roughness length

10) Appendices

10.1) Additional validation of experimental approach

10.1.1) Validation of UVP location

When the mixture is released in the flume tank, the current needs time to become stable, increase its velocity and develop in a fully mature turbidity current. Therefore it is necessary to retrieve the data some distance away from the inlet.
To test if the chosen location is sufficient, at two experiments UVP data was retrieved at three different laterally distinct locations (3.21m, 2.42m & 2.02m distance from discharge tank). The conditions of both experimental runs were the same (C=17%, Sf=75:25, A=9.0[deg]).

It was found that the differences between the mean velocities are minor at all three locations, which means that there is no major change happening over the interval (2.1% change between 2.02 and 3.21m.)
The U_{max} however does show a substantial (linear) increase at further distance from the inlet. This is on average about 0.1m/s per m distance (+/- 9% change).
But since the tank dimensions is limited and the mean velocities are more important for general flow properties, the position of 2.42m is considered sufficient.

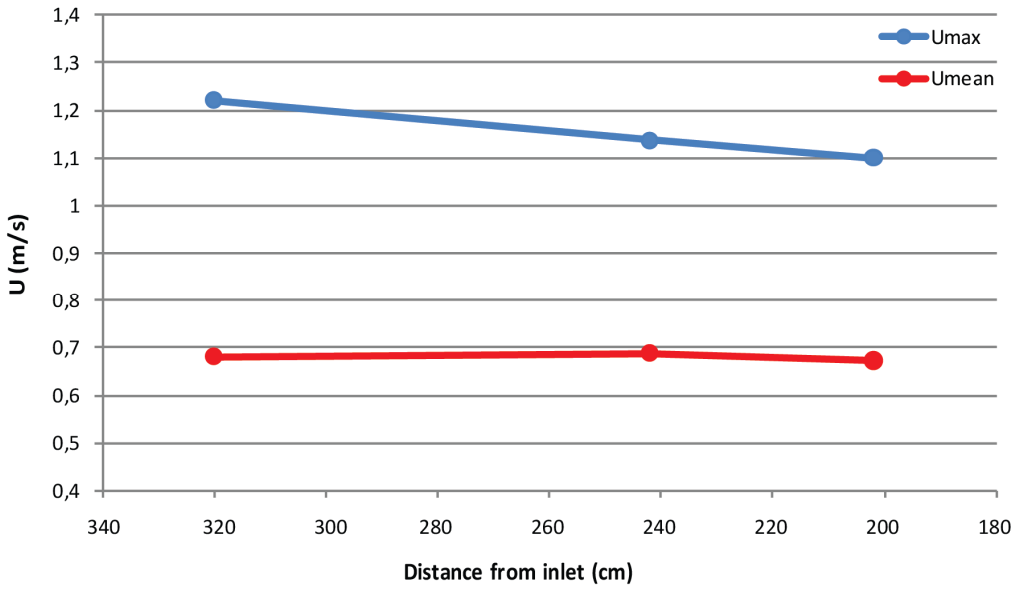

Fig 10.1: *Lateral variation in Umax & Umean measured at three individual locations (17v%, 9.0 [deg], 75:25)*

10.1.2) Initial versus actual volume concentration

The disadvantage of only having knowledge of the initial volume concentration, is that the exact concentrations at the UVP-location are lacking. Entrainment has a large effect on the dilution of the mixture and eventually on the measured velocities. When the current is depositional or depositing in front of the probe location, the flow dilutes even more extensively. This could not only have a large effect on concentrations, but also possibly influence the sediment fraction due to 'preferred settling' of the coarser sediments.

Since run#43 was the most extreme case of deposition from all experiments, it was calculated how much of the sediment in the current was deposited before arrival at the UVP probe. The total volume was estimated to be around 10.7L in total (corrected for porosity), which would mean that with a current of around 420L and 21v% sediment, around 12% of the sediment that was present in the mixing tank has settled. But since the probe is located around 3/4 of the tank, eventually only 10% of the total volume has settled in front of the probe. With

a volume concentration of 21%, this will mean an average reduction to 18.9% of the initial sediment concentration in the flow at point of measurement. However there is also a significant portion of late settling by the tail of the current, which occurred due to the drop of discharge at the far end of the experiment. With the help of the video data, this was estimated to consist of around 15.6% of the deposit. This would mean that the average sediment concentration during the run at measuring point was around 19.2% instead of 21%. This is a minor deviation from the original intended concentration.
All depositional experiments performed therefore had to be limited to low settling rates and total volume to prevent intensive concentration loss during the experiment.
Therefore they were limited to not more than half of the total volume deposit of the 10.7L in Run#43, which substantially reduces the concentration loss due to deposition. Relative to the entrainment (see Results) factor, the changes made to concentration by deposition are almost negligible.

10.1.3) Quality Comparison with previous experimental data

The distinct UVP setup of the previous 100% coarse grained runs has its effect on the quality of the data. The accuracy of the measurements clearly decline fast at greater distance of the probe and also the angle of the probe itself is of great influence. This results in conflicting velocity profiles.
Run#1 is compared with two runs of a previous set of experiments and share the same concentration (13.5v%), sediment fraction (100% coarse) and slope (~11[deg]). Only the discharge is different between the three runs (Fig. A2). As can be seen this results in a difference in average and maximum velocities. The relation between discharge and U_{max} looks to be quite linear from this figure.
The vertical position of U_{max} seems rather similar in all runs. But the overall shape of the profiles differs significantly.
The area between the U_{max} and the bed, which is of special interest for shear stress approximations, is quite different. Run#1 shows a much more realistic profile for a turbidity current with a fast declining velocity when nearing the bedding plain. This can be partially attributed to the decrease of reliability of the incoming data at greater distance from the probe.
A large number of experimental constructed profiles in this report do reach values of close to zero, attributed to the better quality of the inner region.
The reason for this increased quality has to be found in the distance from the bedding plane (10cm standard in this report) together with the angle of the probe relative to the bed.

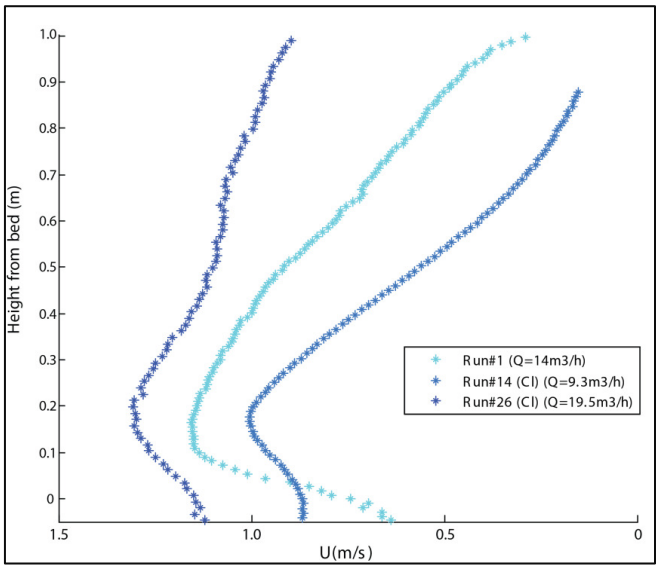

Fig. 10.2 : *Velocity profile comparison of three runs with distinct UVP angle (Run#1 = 60 [deg], Run#14&26 = 45 [deg]) and discharge. The run with 60 [deg] angle shows the most realistic inner region. Further on it shows the direct relationship between discharge and velocity. (13v%-11.3[deg]-100:00)*

The reason for the quality loss with distance can be found in the limited permeability of the probe signals into the mixture. The amount of signals that return are significantly less in dense mixtures thicker than 10cm, which makes the received data a lot more unreliable. Besides this, there is also an effect of the increased node surface with increasing distance (explained in 1.4)

The variable angle of the probe relative to the bed has effect on the vertical resolution of the measured nodes by the UVP. This is because every node or cell is averaged over a surface which increases with distance from the probe (Fig. A.4). When the angle between the bedding plain and the probe is smaller this will have a negative effect on the vertical resolution, which is especially unwanted in areas with strong velocity gradients as in the inner region. Therefore a higher angle (60 [deg]) will give better and more detailed results.

10.1.4) UVP Calibration and locating the bedding plain

One of the problems with UVP monitor used in previous analogue HDTC-experiments was to recognize the correct signals as the bedding plain of the flume tank. Even though the exact location of the probe relative to the flume floor is known, the probe does not measure distance, but time. It is questionable if the mixture has an effect on the travelling speed of the sound signals, and if the standard applied speed of sound in water (343.2 m/s) is sufficient.
It is of importance for near bed velocity studies to derive the exact location in the received data of the bedding plain.
During previous runs it seemed that the bed shifted down when sediment was in suspension. To gain a good understanding what affects these signals, a simple set-up (Fig. A.3) was created to investigate which and where the signals of a bedding plain could be pinned under different circumstances.
The probe (1hz) was fitted in the glass tank with an angle of 45° aiming towards the bottom of the tank. A mixer kept the mixture of water and sediment constantly in movement during all runs. During numerous runs the volume concentration of the sediment was increased to look if a shift in bedding plain signals could be observed.
Both velocity and amplitude data were collected from the UVP probe during all runs.
Since there is a large difference in acoustic impedance between the glass bedding and the water inside the tank, it is expected that a transition between these two mediums will result in a large amplitude peak. Further on, since the mixture is in constant movement, a fast decrease in velocities is expected at this transition as well.

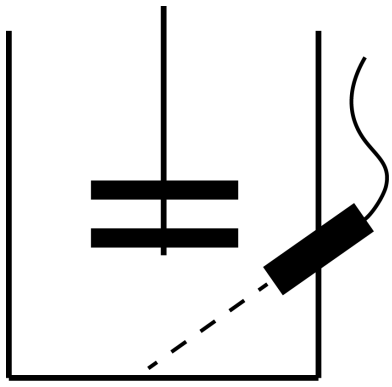

Fig. 10.3: *Sketch of UVP-test setup with small tank including mixer and probe in side-wall*

With the help of mean velocity and amplitude profiles, standard deviations and velocity maps the properties and behaviour of bedding plain signals was studied.

High amplitude signals at different distances from the probe were found which could possibly be linked to the glass floor of the tank. In the various experiments with
V-concentrations varying between 2-12%, the main amplitude-signal could shift and in some cases multiple signals were identified in one single profile.
The reason why the glass floor of the tank can be responsible for multiple and/or shifting strong amplitudes, can be found in the way the probe receives its signals.
A combination of two factors controls the range of the outgoing sound waves (Fig. 10.4):

1. The surface of the probe itself. This is shown by the dashed lines in figure A.4 The lower side of the probe needs less time/distance to reach the bedding plain than the upper side

2. The deviation angle of the signals coming from the probe (2.2°). This is shown by line D_{A2} and D_{B2} in figure A.4. This causes the signal density to decline over longer distances and the area reached to increase.

A large amount of the released signals reaching the glass bottom of the tank will be reflected. Since angle of incidence is angle of reflection, the data that has been recorded comes from the reflected ray at ±90 degrees from the incidence ray (Fig. 10.4). This reflected data disturbs the actual data at location between distance x, since all data has been averaged over the whole channel. After distance A, all data received must be from reflected signals. Since the reflected signals make a 90 degrees angle, this will give a mirror image (at distance k) of the earlier received data.
The shifting of the bedding plain signals is therefore a defect of the UVP-averaging over a channel taken in partially reflected particle signals, bedding signals and direct particle signals (Figure 10.4a). The combination of these distinct signals that correspond to the same distance or time and can fade out the exact location of the bed. When going deeper into the bed, the reflected signals will eventually dominate and a mirror image is obtained.

A major difference between the UVP test and the actual flume is that due to the coarse irregular characteristics of the sand-glued flume floor, the reflectance is minimal compared with a smooth glass floor. When trying to locate the flume floor in the HDTC-experiments a 'blurring-effect' can be expected and can explain the shift of dominant floor signals.

Since the character of this blurred bed is dependent on the height, angle and channel size of the probe, it is better to look at other details than the amplitude when trying to locate the exact position of the flume floor.

During the basic analysis of the velocity data of all experimental work a series of simple techniques were developed to pinpoint the location of the bedding plain as precisely as possible:
For non-aggrading runs:

- Use the actual distance as a rough indication for the flume floor. Since it is important to know the location on mm-level precision and the UVP-time is not distance, deviation from the measured value can be expected
- Look at zero-velocity points in constructed profiles or interpolate the inner region. A good indication is always given by the velocity map, which must show a constant indication over time of the flume floor
- Compare with experiments of the same series. If the measured location of the probe is the same before and after a series of runs, the location of the floor must be same in all runs. It was proven that this is independent of the contents of the mixture. The best velocity data of a series nearing the zero-velocity is therefore best used for retrieving the exact location.

Aggrading runs are much more challenging since the bedding plain is constantly shifting during the experiment and averaging of velocities over a time interval can give problems.

Aggrading runs:

- Try to locate the flume floor before the currents starts with deposition. This acts as the starting location. The settling rates are already known from the video data and therefore an approximation how fast the bedding signal will shift over time can already be made (with one measurement every 15ms).
- The velocity map can sometimes very clearly show a thickening of a distinct low-velocity area, indicating the slowly aggrading bed (Fig. 10.5).
- Compare a constructed profile of a certain point in time before deposition and at the point in time of the eventual general velocity profile and determine the vertical migration of U_{max} or other features during that time interval.

With the help of these techniques a reasonable indication can be given of the flume floor.

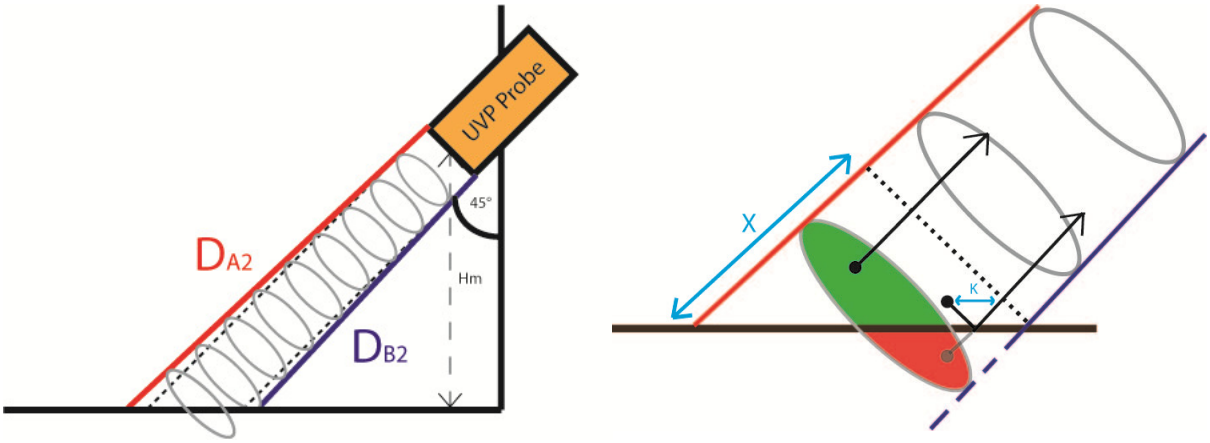

Fig. 10.4a&b: *Increase of the signal surface area with distance from the probe. Note the difference in distance (time) travelled between D_{B2} and D_{A2}*

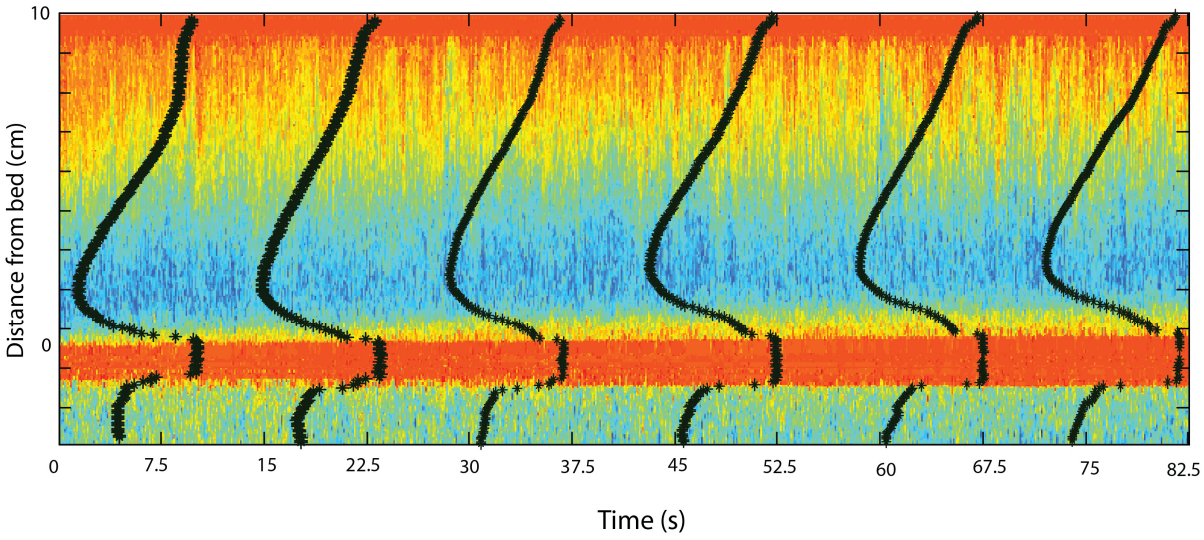

Fig. 10.5: *Run#24 as example for a depositional run which shows an increase of the bedding plain thickness over time (red = low velocity). The profiles are averaged over 500 nodes (7.5s). Below the thickening red bedding 'signal', a somewhat blurred mirror image of the profile is obtained.*

1.10.2 Appendix Tables

Run#	Initial Conc [v%]	Slope [deg]	SF(CS:FS)	Q1 (m3/h)	Probe distance from be	Probe distance from inlet (m)
2,1	0,135	11,3	90-10	9	0,0965	2,4
3	0,135	9	90-10	8,5b - 9,5e	0,094	2,4
4	0,135	7	90-10	7-10,5	0,094	2,4
5	0,17	9	90-10	8.0b-10e	0,094	2,4
6	0,17	7	90-10	9,5	0,102	2,4
7	0,135	11,3	75-25	9,5	0,098	2,4
8	0,135	9	75-25	9,5	0,098	2,4
9	0,135	7	75-25	9,2	0,098	2,4
10	0,17	9	75-25	9,3	0,098	2,4
11	0,17	7	75-25	9,5	0,098	2,4
13	0,21	9	90-10	9,1	0,1	2,46
14	0,21	7	90-10	9,1-9,2	0,1	2,46
15	0,21	5,5	90-10	9,1	0,1	2,46
17	0,09	11,3	90-10	9,5e	0,1	2,46
18	0,09	9	90-10	9,5	0,1	2,45
19	0,135	11,3	50-50	11b-9.5e	0,1	2,45
20	0,135	9	50-50	7.0b-8.9e	0,1	2,45
21	0,135	7	50-50	9.6e	0,106	2,45
22	0,17	9	50-50	8.8b-9.5e	0,106	2,45
23	0,17	7	50-50	9.5-9.6	0,106	2,45
24	0,17	5,5	50-50	9.4-9.7	0,106	2,45
25	0,09	11,3	75-25	8.8b-9.5e	0,104	2,45
26	0,09	9	75-25	9.5	0,104	2,45
27	0,21	9	50-50	8.8b-9.5e	0,104	2,45
28	0,21	7	50-50	8.8b-9.4e	0,104	2,45
29	0,21	5,5	50-50	8.5-9.0	0,104	2,45
30	0,21	4	50-50	9.5	0,104	2,45
32	0,09	11,3	50-50	9.1-9.5	0,104	2,45
33	0,09	9	50-50	9.5b-9.0e	0,104	2,45
34	0,09	7	50-50	9.5	0,104	2,45
36	0,135	11,3	00-100	9.1-9.5	0,106	2,45
37	0,135	9	00-100	9.5	0,106	2,45
38	0,135	7	00-100	9.5	0,106	2,45
39	0,135	5,5	00-100	9.5	0,106	2,53
40	0,21	9	75-25	9.5-9.8	0,105	2,53
41	0,21	7	75-25	8.9b-9.5e	0,105	2,53
42	0,21	5,5	75-25	9.5	0,105	2,53
43	0,21	4	75-25	11b-9.5e	0,105	2,53

Run#	Umean (m/s)	H High series (m)	H Medium series (m)	Fe [basic]	Fe [med]	Fe [high]	Real conc [basic] (v%)	Real conc [med] (v%)	Real conc [high] (v%)	Fr [basic]	Fr [med]	Fr [high]
2	0,538	-	-	1,37	-	-	9,86	-	-	1,48	-	-
3	0,541	-	-	1,38	-	-	9,80	-	-	1,49	-	-
4	0,505	-	-	1,29	-	-	10,50	-	-	1,35	-	-
5	0,590	-	-	1,50	-	-	11,31	-	-	1,53	-	-
6	0,610	-	-	1,55	-	-	10,95	-	-	1,61	-	-
7	0,672	-	-	1,71	-	-	7,89	-	-	2,04	-	-
8	0,666	-	-	1,70	-	-	7,96	-	-	2,02	-	-
9	0,568	-	-	1,45	-	-	9,33	-	-	1,60	-	-
10	0,688	-	-	1,75	-	-	9,71	-	-	1,91	-	-
11	0,614	-	-	1,56	-	-	10,87	-	-	1,62	-	-
13	0,713	-	-	1,81	-	-	11,57	-	-	1,83	-	-
14	0,631	-	-	1,61	-	-	13,06	-	-	1,55	-	-
15	0,588	-	-	1,50	-	-	14,03	-	-	1,40	-	-
17	0,589	-	-	1,50	-	-	6,01	-	-	2,02	-	-
18	0,584	-	-	1,49	-	-	6,05	-	-	2,00	-	-
19	0,688	0,12	0,10	1,75	1,73	2,19	7,71	7,79	6,17	2,11	2,11	2,09
20	0,608	0,11	0,09	1,55	1,37	1,77	8,73	9,85	7,61	1,76	1,78	1,75
21	0,563	-	-	1,43	-	-	9,42	-	-	1,58	-	-
22	0,623	-	-	1,59	-	-	8,50	-	-	1,83	-	-
23	0,576	-	-	1,47	-	-	9,20	-	-	1,64	-	-
24	0,538	-	-	1,37	-	-	9,85	-	-	1,48	-	-
25	0,553	-	-	1,41	-	-	9,59	-	-	1,54	-	-
26	0,437	-	-	1,11	-	-	12,14	-	-	1,10	-	-
27	0,666	-	-	1,70	-	-	7,96	-	-	2,01	-	-
28	0,590	-	-	1,50	-	-	8,98	-	-	1,69	-	-
29	0,461	-	-	1,17	-	-	11,50	-	-	1,19	-	-
30	0,521	-	-	1,33	-	-	10,17	-	-	1,42	-	-
32	0,513	0,12	0,10	1,31	1,29	1,63	6,88	6,96	5,51	1,66	1,66	1,64
33	0,438	-	-	1,12	-	-	8,06	-	-	1,32	-	-
34	0,473	-	-	1,20	-	-	7,47	-	-	1,47	-	-
36	0,602	0,13	0,09	1,53	1,43	2,00	8,81	9,45	6,77	1,74	1,75	1,71
37	0,572	0,13	0,10	1,46	1,54	1,94	9,27	8,77	6,96	1,62	1,61	1,59
38	0,542	0,11	0,09	1,38	1,30	1,60	9,77	10,37	8,45	1,50	1,51	1,49
39	0,491	0,11	0,10	1,25	1,25	1,46	10,80	10,80	9,26	1,30	1,30	1,29
40	0,666	0,13	0,10	1,70	1,70	2,26	12,38	12,35	9,29	1,67	1,67	1,63
41	0,598	0,10	0,08	1,52	1,32	1,65	13,79	15,85	12,73	1,43	1,45	1,42
42	0,530	0,12	0,09	1,35	1,28	1,65	15,55	16,41	12,76	1,21	1,22	1,19
43	0,507	0,11	0,08	1,29	1,10	1,49	16,27	19,17	14,07	1,14	1,16	1,12

Run#	Umean (m/s)	Angle [deg]	Initial Conc (v%)	Ri (basic)	Ri(med)	Ri (high)	Dyn Visc (Ruscoe 1953)	Re (basic)	Re(med)	Re(high)
2,1	0,538	11,3	13,5	0,47	-	-	1,83	3,42E+04	-	-
3	0,541	9	13,5	0,46	-	-	1,83	3,43E+04	-	-
4	0,505	7	13,5	0,56	-	-	1,83	3,24E+04	-	-
5	0,590	9	17	0,44	-	-	2,17	3,23E+04	-	-
6	0,610	7	17	0,40	-	-	2,17	3,32E+04	-	-
7	0,672	11,3	13,5	0,25	-	-	1,83	4,15E+04	-	-
8	0,666	9	13,5	0,25	-	-	1,83	4,12E+04	-	-
9	0,568	7	13,5	0,40	-	-	1,83	3,59E+04	-	-
10	0,688	9	17	0,28	-	-	2,17	3,68E+04	-	-
11	0,614	7	17	0,39	-	-	2,17	3,34E+04	-	-
13	0,713	9	21	0,31	-	-	2,60	3,27E+04	-	-
14	0,631	7	21	0,43	-	-	2,60	2,95E+04	-	-
15	0,588	5,5	21	0,53	-	-	2,60	2,79E+04	-	-
17	0,589	11,3	9	0,25	-	-	1,56	4,14E+04	-	-
18	0,584	9	9	0,26	-	-	1,56	4,12E+04	-	-
19	0,688	11,3	13,5	0,22	0,21	0,22	1,83	4,22E+04	4,02E+04	4,96E+04
20	0,608	9	13,5	0,32	0,30	0,31	1,83	3,78E+04	3,27E+04	4,10E+04
21	0,563	7	13,5	0,41	-	-	1,83	3,55E+04	-	-
22	0,623	9	17	0,31	-	-	1,83	3,89E+04	-	-
23	0,576	7	17	0,39	-	-	1,83	3,63E+04	-	-
24	0,538	5,5	17	0,47	-	-	1,83	3,42E+04	-	-
25	0,553	11,3	9	0,43	-	-	1,83	3,50E+04	-	-
26	0,437	9	9	0,85	-	-	1,83	2,87E+04	-	-
27	0,666	9	21	0,25	-	-	1,83	4,12E+04	-	-
28	0,590	7	21	0,36	-	-	1,83	3,71E+04	-	-
29	0,461	5,5	21	0,73	-	-	1,83	3,00E+04	-	-
30	0,521	4	21	0,52	-	-	1,83	3,33E+04	-	-
32	0,513	11,3	9	0,37	0,36	0,36	1,56	3,66E+04	3,48E+04	4,31E+04
33	0,438	9	9	0,59	-	-	1,56	3,18E+04	-	-
34	0,473	7	9	0,48	-	-	1,56	3,40E+04	-	-
36	0,602	11,3	13,5	0,33	0,31	0,32	1,83	3,75E+04	3,39E+04	4,55E+04
37	0,572	9	13,5	0,38	0,37	0,38	1,83	3,59E+04	3,61E+04	4,44E+04
38	0,542	7	13,5	0,44	0,42	0,43	1,83	3,43E+04	3,13E+04	3,73E+04
39	0,491	5,5	13,5	0,59	0,57	0,58	1,83	3,14E+04	3,02E+04	3,45E+04
40	0,666	9	21	0,37	0,36	0,37	2,60	3,09E+04	2,97E+04	3,78E+04
41	0,598	7	21	0,50	0,47	0,49	2,60	2,83E+04	2,42E+04	2,90E+04
42	0,530	5,5	21	0,71	0,67	0,71	2,60	2,56E+04	2,36E+04	2,89E+04
43	0,507	4	21	0,81	0,75	0,80	2,60	2,47E+04	2,09E+04	2,67E+04

Run#	Umean (m/s)	U* (av) (m/s)	Cz (Umean/U*)	T0 (pa)	Depo	Settling Rates (m/s)
2.1	0,538	0,11	4,74	15,7	no	-
3	0,541	0,32	1,67	128,8	eq	-
4	0,505	0,23	2,18	65,9	yes	4,00E-04
5	0,590	0,06	9,27	5,2	no	-
6	0,610	0,19	3,19	46,8	yes	1,50E-04
7	0,672	0,09	7,15	10,8	no	-
8	0,666	0,09	7,52	9,6	no	-
9	0,568	0,47	1,22	265,8	yes	2,60E-04
10	0,688	0,04	15,29	2,6	no	-
11	0,614	0,10	6,41	11,7	yes	2,00E-04
13	0,713	0,07	9,58	7,4	no	-
14	0,631	0,11	5,82	15,8	eq	-
15	0,588	0,16	3,70	34,0	yes	3,00E-04
17	0,589	0,23	2,58	59,8	eq	-
18	0,584	0,34	1,71	133,6	yes	1,50E-04
21	0,563	0,12	4,80	16,8	eq	-
22	0,623	0,09	7,18	9,6	no	-
23	0,576	0,07	8,78	5,5	no	-
24	0,538	0,13	4,18	21,3	yes	1,80E-04
25	0,553	0,05	10,66	3,1	no	-
26	0,437	0,10	4,37	11,5	yes	1,00E-04
27	0,666	0,12	5,51	19,6	no	-
28	0,590	0,12	4,74	20,9	no	-
29	0,461	0,10	4,51	14,1	eq	-
30	0,521	0,13	4,07	22,0	yes	2,00E-04
32	0,513	0,26	1,99	76,2	no	-
33	0,438	0,04	11,63	1,6	eq	-
34	0,473	0,11	4,12	15,1	yes	2,40E-04
36	0,602	0,09	6,93	9,2	no	-
37	0,572	0,04	15,24	1,7	no	-
38	0,542	0,05	11,28	2,8	no	-
39	0,491	0,09	5,50	9,7	yes	1,30E-04
40	0,666	0,27	2,48	97,1	no	-
41	0,598	0,48	1,24	314,3	no	-
42	0,530	0,09	6,19	9,9	eq	-
43	0,507	0,12	4,09	20,7	yes	2,75E-04

Run#	Pos Umax (m)	Angle [deg]	Initial Conc (v%)	U* (kneller)	U*(wall)	U*(k)/U*(w)
2.1	0,0087	11,3	13,5	0,061634256	0,113454493	0,543250906
3	0,0195	9	13,5	0,08215177	0,324589501	0,253094352
4	0,01206	7	13,5	0,056883838	0,232111676	0,245070991
7	0,01268	11,3	13,5	0,074408433	0,093957993	0,79193297
8	0,0154	9	13,5	0,073006239	0,088608883	0,823915577
11	0,0139	7	17	0,068529919	0,095773594	0,715540853
12	0,01925	9	17	0,091595167		
13	0,01336	9	21	0,084809716	0,07435093	1,140667857
14	0,01653	7	21	0,083060479	0,108487476	0,765622745
15	0,01765	5,5	21	0,076005833	0,15893828	0,47820974
19	0,01022	11,3	13,5	0,066801771		
20	0,01069	9	13,5	0,06082589		
21	0,01498	7	13,5	0,063397356	0,117243627	0,540731787
22	0,01205	9	17	0,072468741	0,086789294	0,834996318
23	0,01461	7	17	0,070258347	0,065644489	1,070285521
24	0,0159	5,5	17	0,064906463	0,128901099	0,503536926
25	0,01038	11,3	9	0,054968714	0,051852534	1,06009696
26	0,01231	9	9	0,053294576	0,099957778	0,53317088
27	0,01204	9	13,5	0,064552469	0,120767178	0,534519981
28	0,01396	7	13,5	0,06120092	0,124519039	0,49149849
29	0,01909	5,5	13,5	0,063377451	0,102332449	0,61932898
32	0,01011	11,3	9	0,054249093	0,257604613	0,210590533
33	0,01076	9	9	0,04982647	0,037689715	1,322017694
34	0,01076	7	9	0,043870819	0,114698497	0,38248818
36	0,01017	11,3	21	0,08311239	0,086816361	0,957335567
37	0,01051	9	21	0,075221803	0,037506589	2,005562379
38	0,01404	7	21	0,076549359	0,048087897	1,591863316
39	0,01788	5,5	21	0,076499453	0,089295588	0,856699129
40	0,0095	9	21	0,071516159	0,268510655	0,266343841
41	0,0119	7	21	0,070474416	0,483144457	0,145866137
42	0,0149	5,5	21	0,069834126	0,085634711	0,815488551
43	0,0194	4	21	0,06790611	0,123853077	0,548279556

Table 1.10 (1-5): *Full set of single value data. Only the experiments of interest are included. Red numbers indicate unrealistic and probably invalid values. In the discharge (Q1) column of the first table b= begin of run and e =middle/end of run. When no good video data was available, no medium or high estimates of the dimensionless parameters have been given.*

1.10.3) Full set of velocity profiles

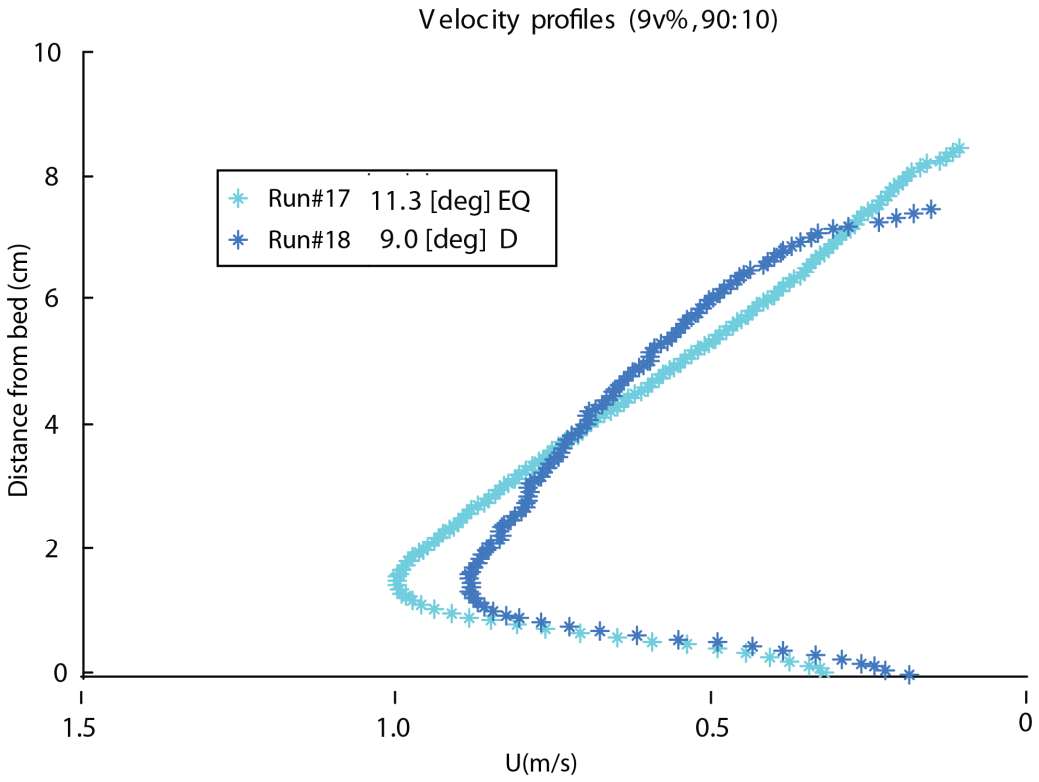

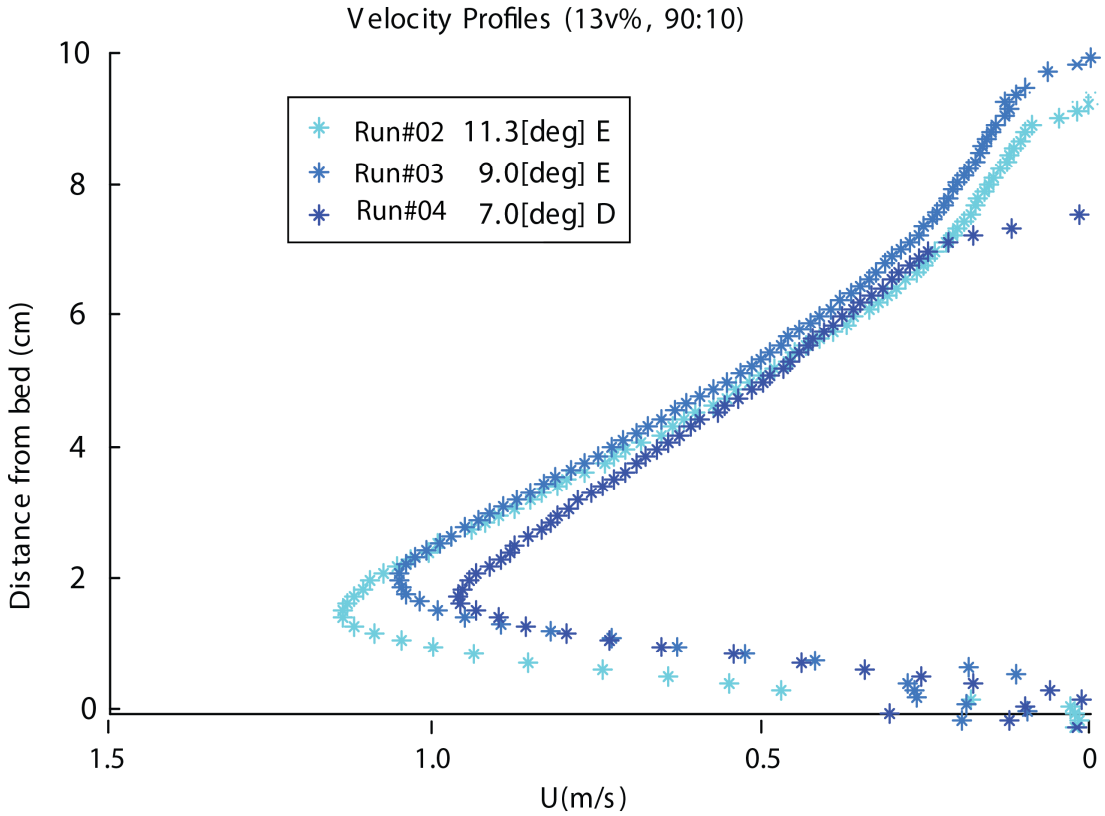

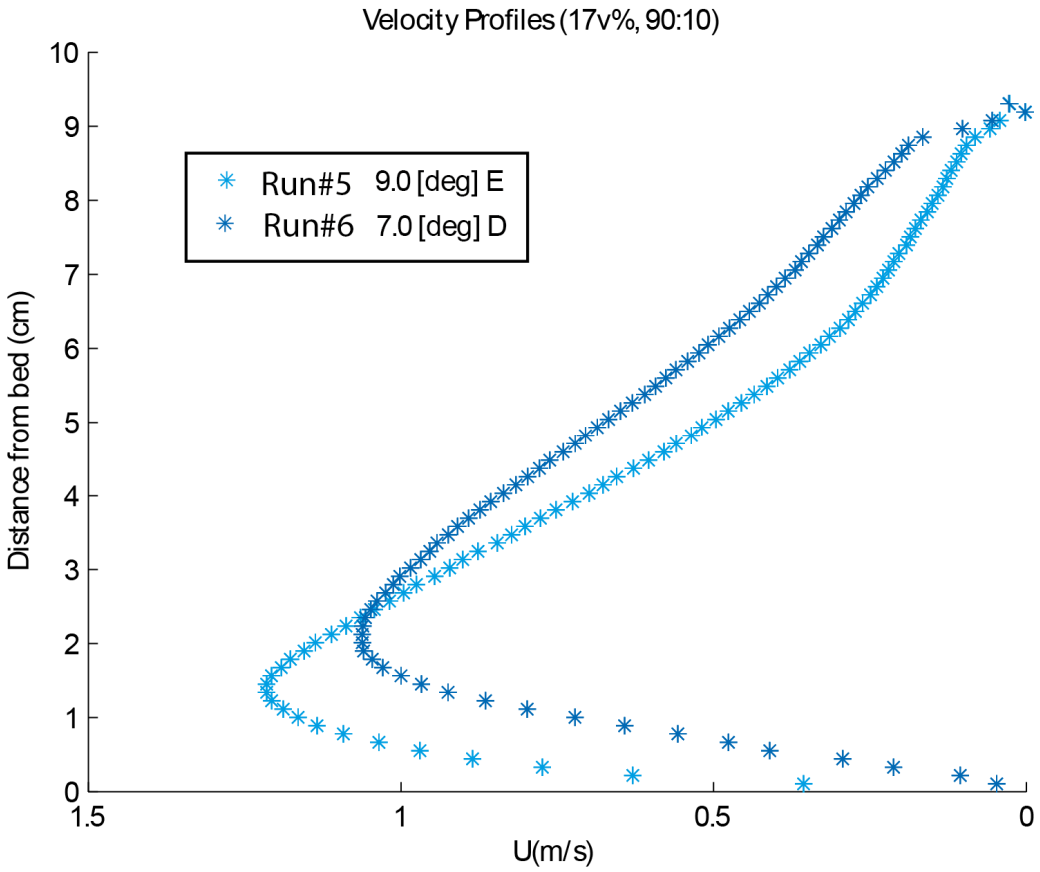
Velocity Profiles (17v%, 90:10)
Run#5 9.0 [deg] E
Run#6 7.0 [deg] D
Distance from bed (cm)
U(m/s)
10
9
8
7
6
5
4
3
2
1
0
1.5
1
0.5
0

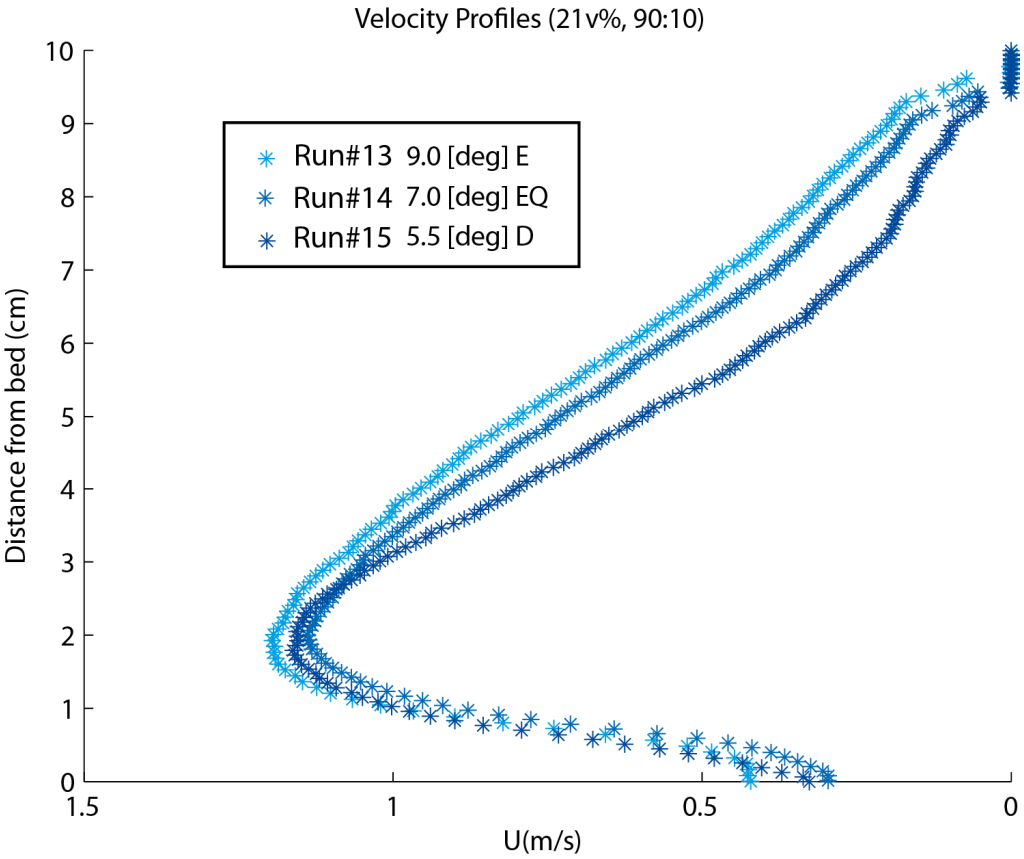
Velocity Profiles (21v%, 90:10)
Run#13 9.0 [deg] E
Run#14 7.0 [deg] EQ
Run#15 5.5 [deg] D
Distance from bed (cm)
U(m/s)
10
9
8
7
6
5
4
3
2
1
0
1.5
1
0.5
0

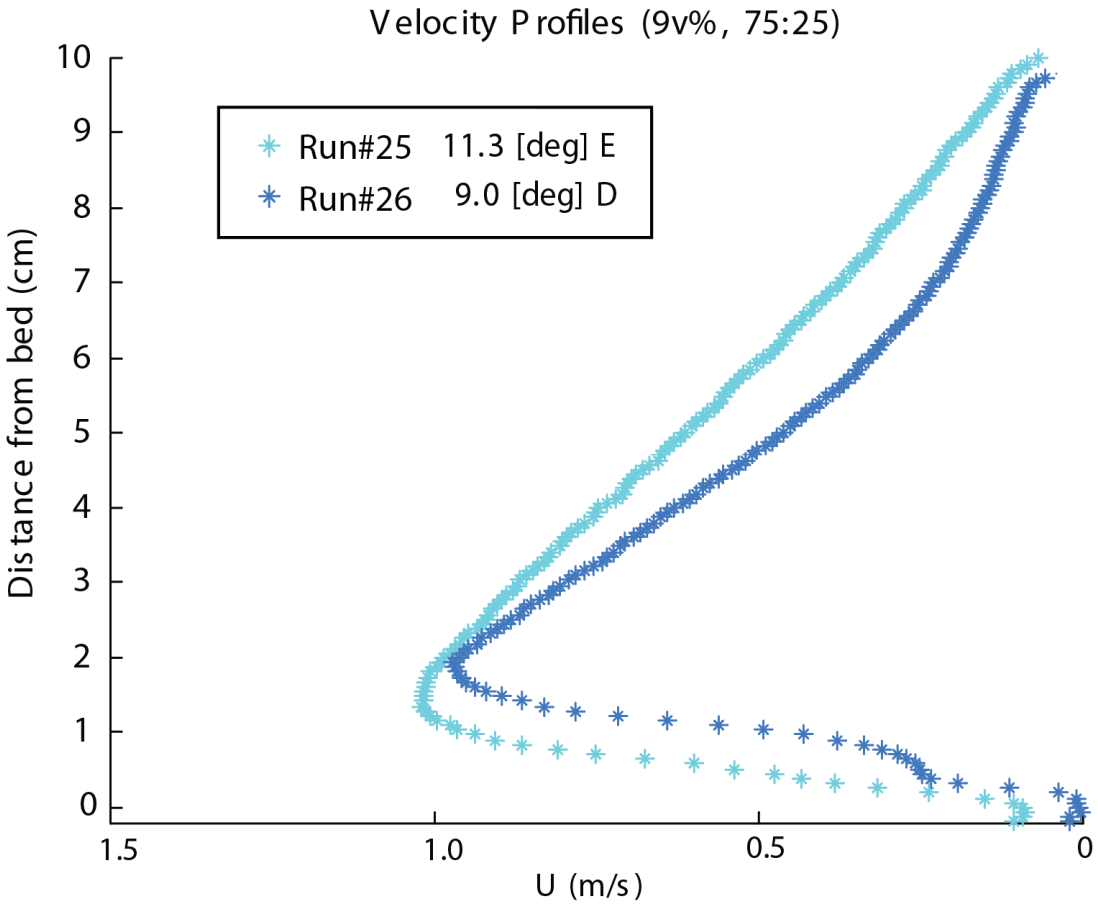
Velocity Profiles (9v%, 75:25)
Run#25 11.3 [deg] E
Run#26 9.0 [deg] D
Distance from bed (cm)
U (m/s)
10
9
8
7
6
5
4
3
2
1
0
1.5
1.0
0.5
0

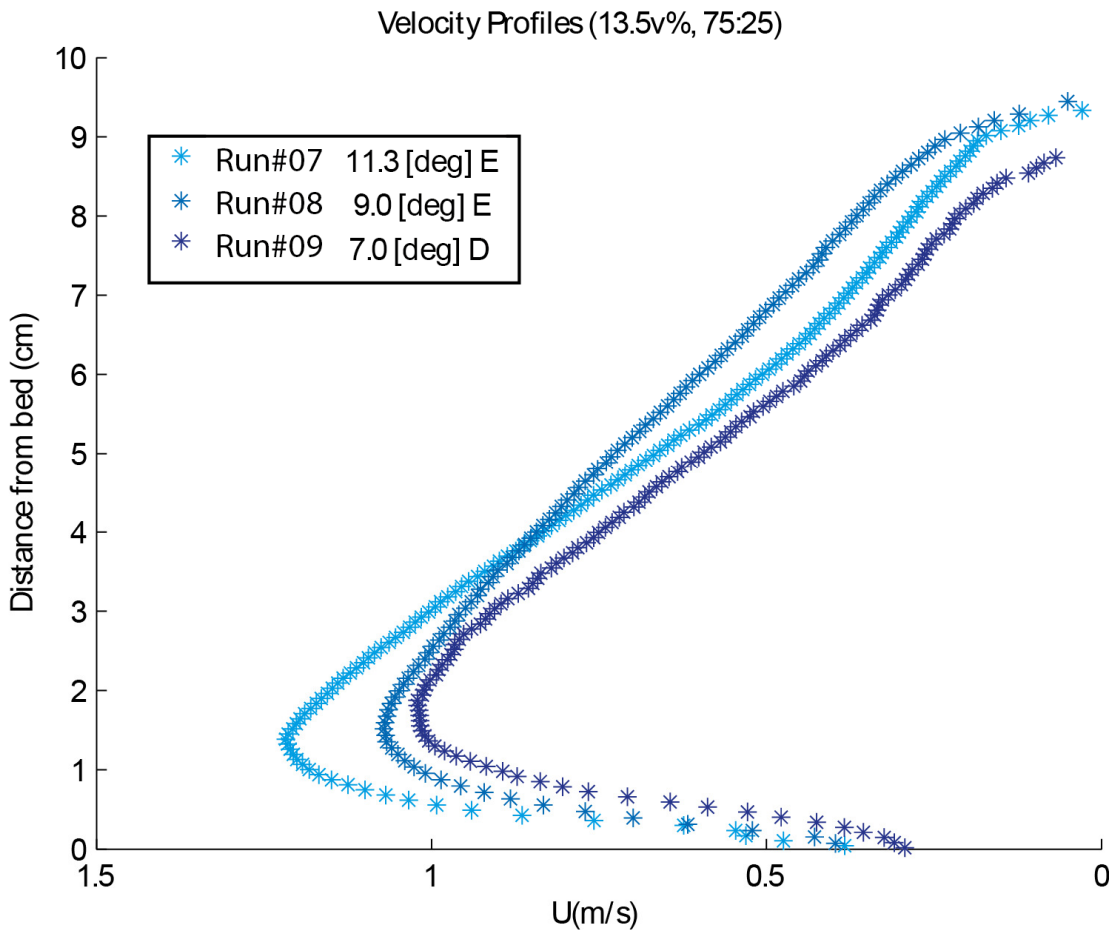
Velocity Profiles (13.5v%, 75:25)
Run#07 11.3 [deg] E
Run#08 9.0 [deg] E
Run#09 7.0 [deg] D
Distance from bed (cm)
U(m/s)
10
9
8
7
6
5
4
3
2
1
0
1.5
1
0.5
0

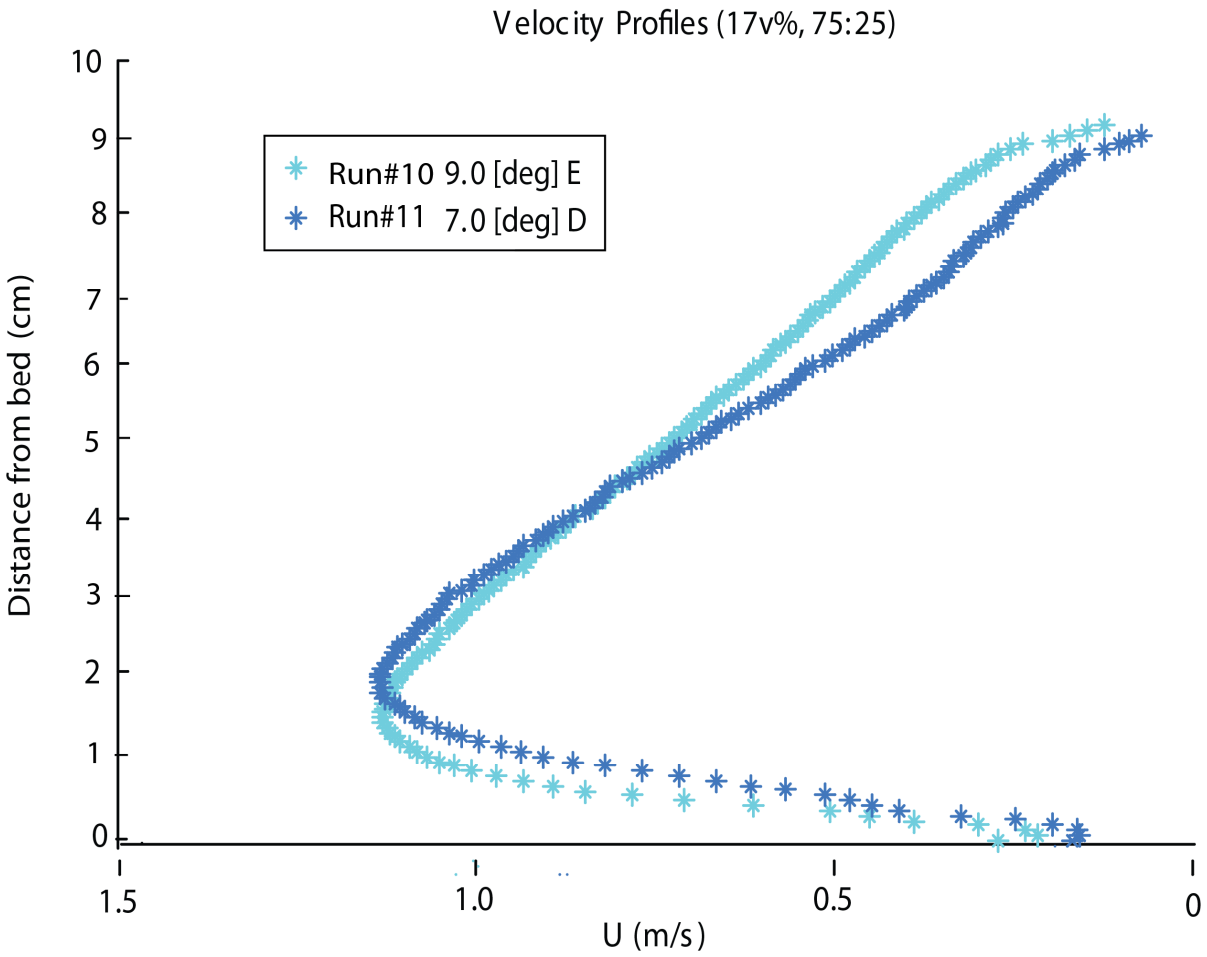
Velocity Profiles (17v%, 75:25)
Run#10 9.0 [deg] E
Run#11 7.0 [deg] D
Distance from bed (cm)
U (m/s)
10
9
8
7
6
5
4
3
2
1
0
1.5
1.0
0.5
0

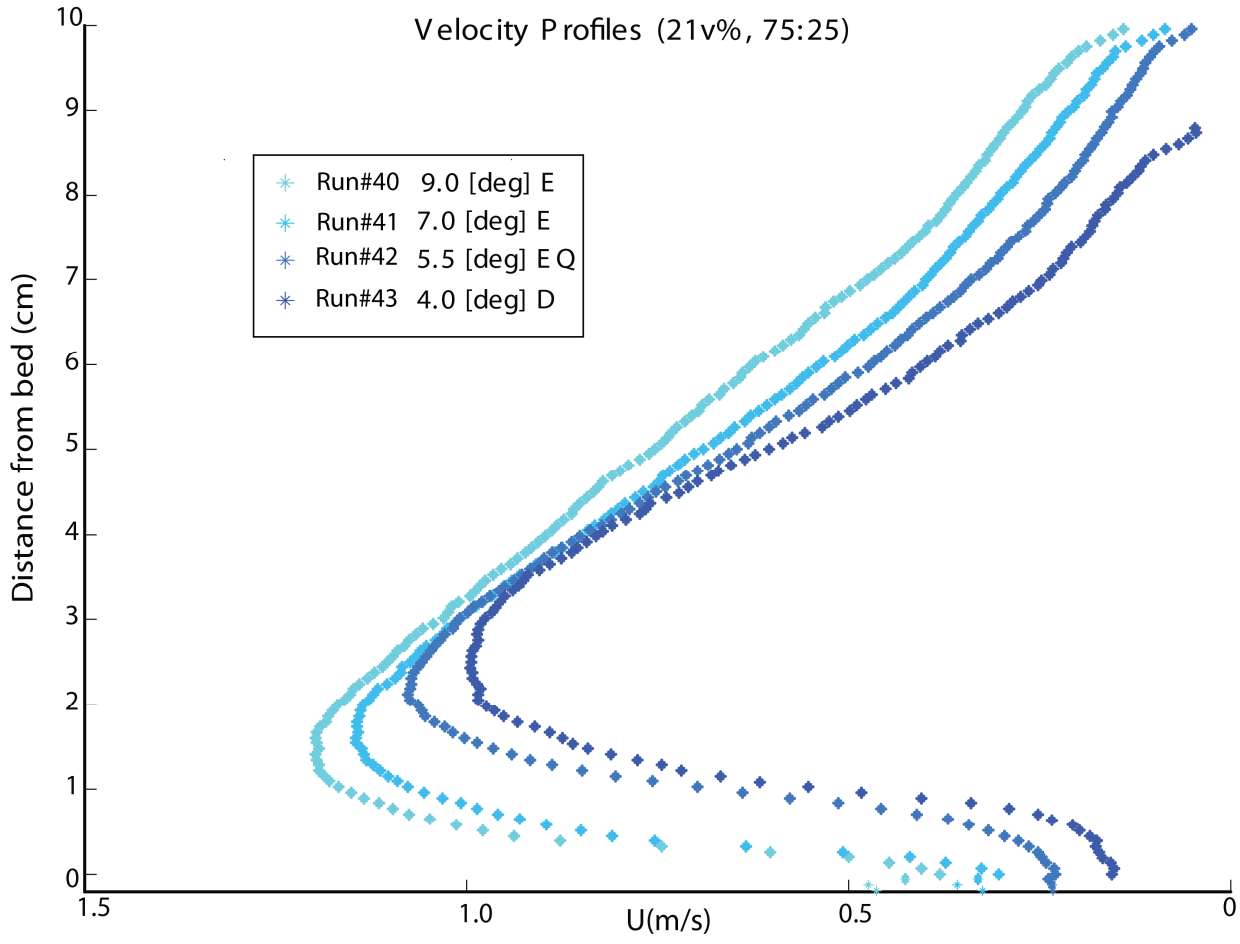
Velocity Profiles (21v%, 75:25)
Run#40 9.0 [deg] E
Run#41 7.0 [deg] E
Run#42 5.5 [deg] E Q
Run#43 4.0 [deg] D
Distance from bed (cm)
U(m/s)
10
9
8
7
6
5
4
3
2
1
0
1.5
1.0
0.5
0

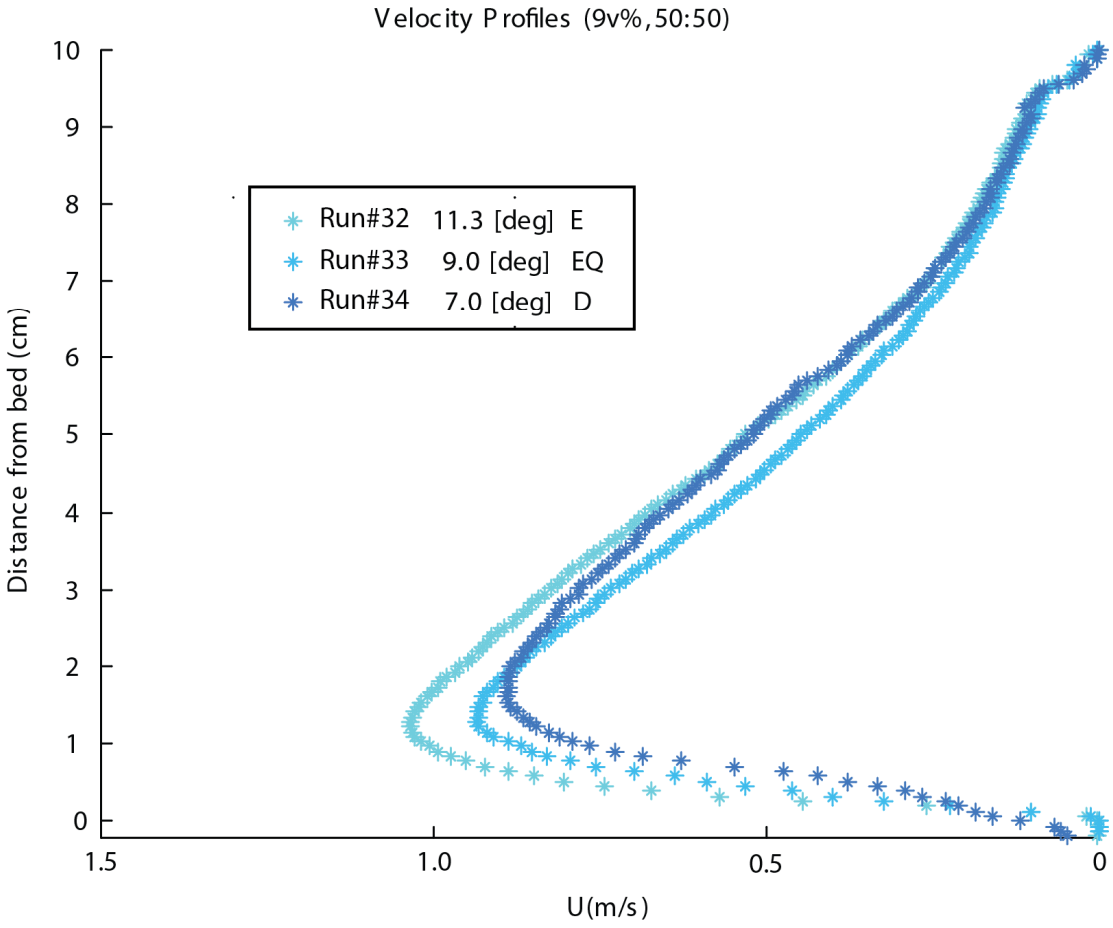
Velocity Profiles (9v%, 50:50)
Run#32 11.3 [deg] E
Run#33 9.0 [deg] EQ
Run#34 7.0 [deg] D
Distance from bed (cm)
U(m/s)
10
9
8
7
6
5
4
3
2
1
0
1.5
1.0
0.5
0

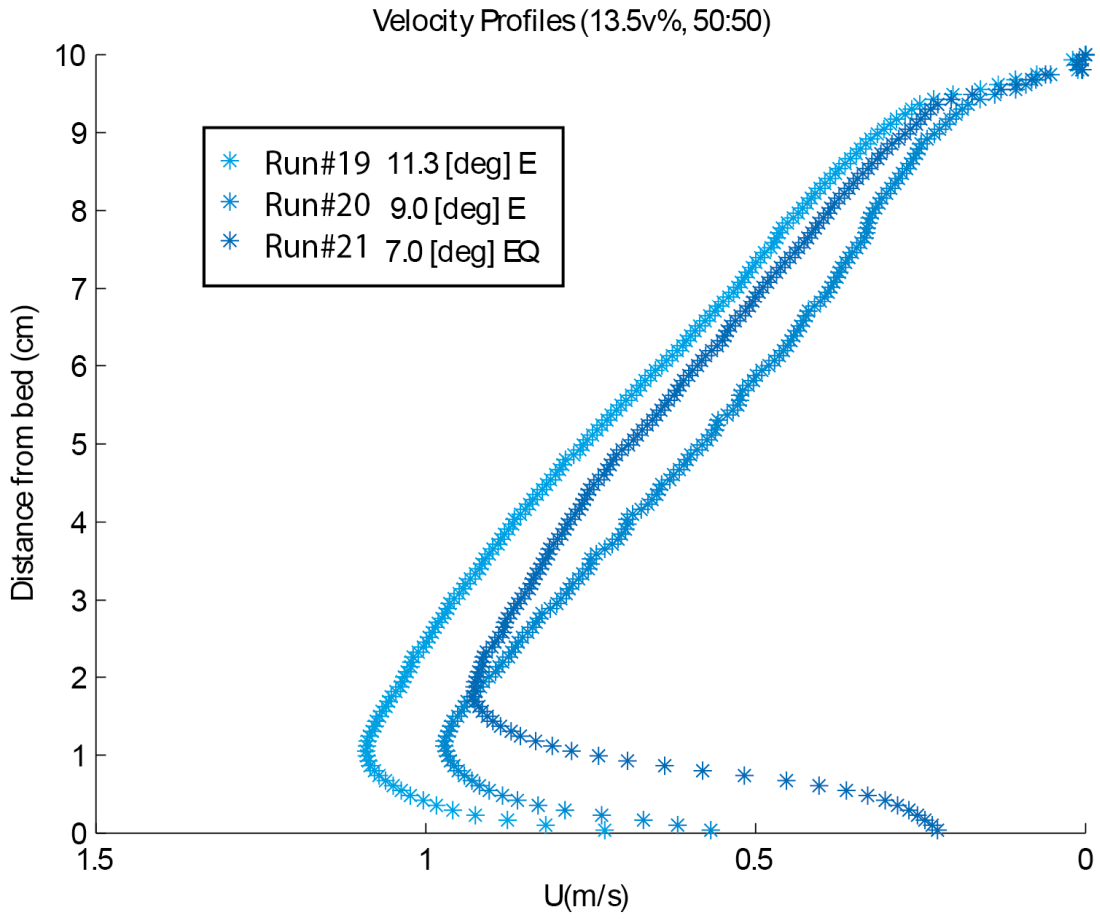
Velocity Profiles (13.5v%, 50:50)
Run#19 11.3 [deg] E
Run#20 9.0 [deg] E
Run#21 7.0 [deg] EQ
Distance from bed (cm)
U(m/s)
10
9
8
7
6
5
4
3
2
1
0
1.5
1
0.5
0

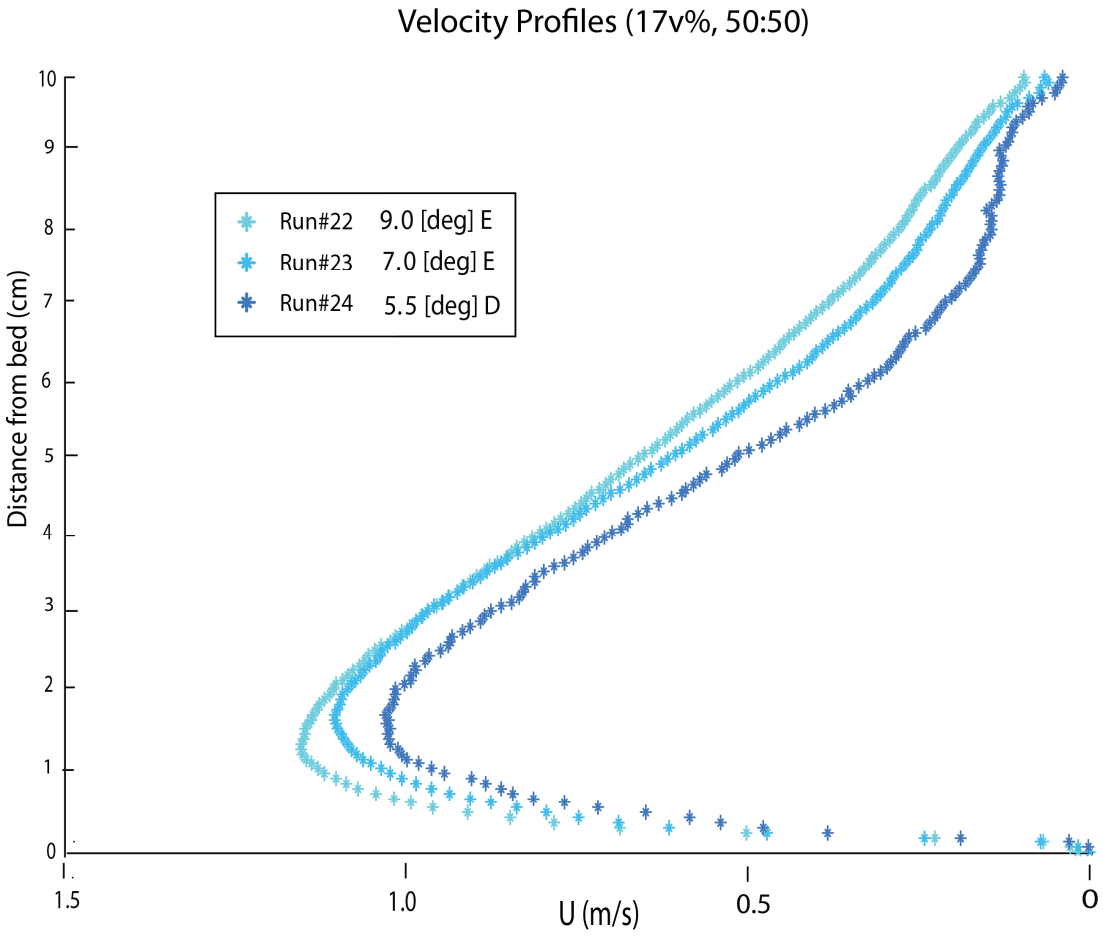
Velocity Profiles (17v%, 50:50)
Distance from bed (cm)
U (m/s)
Run#22 9.0 [deg] E
Run#23 7.0 [deg] E
Run#24 5.5 [deg] D

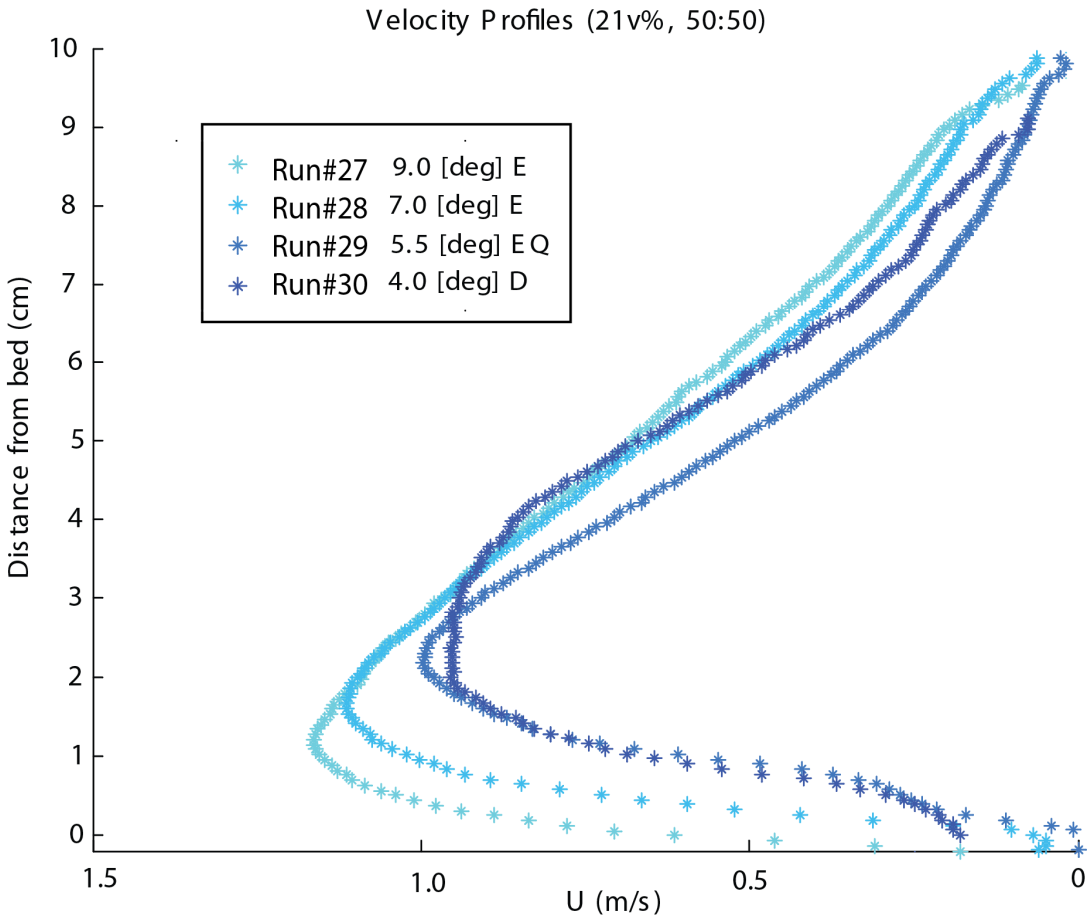
Velocity Profiles (21v%, 50:50)
Distance from bed (cm)
U (m/s)
Run#27 9.0 [deg] E
Run#28 7.0 [deg] E
Run#29 5.5 [deg] EQ
Run#30 4.0 [deg] D

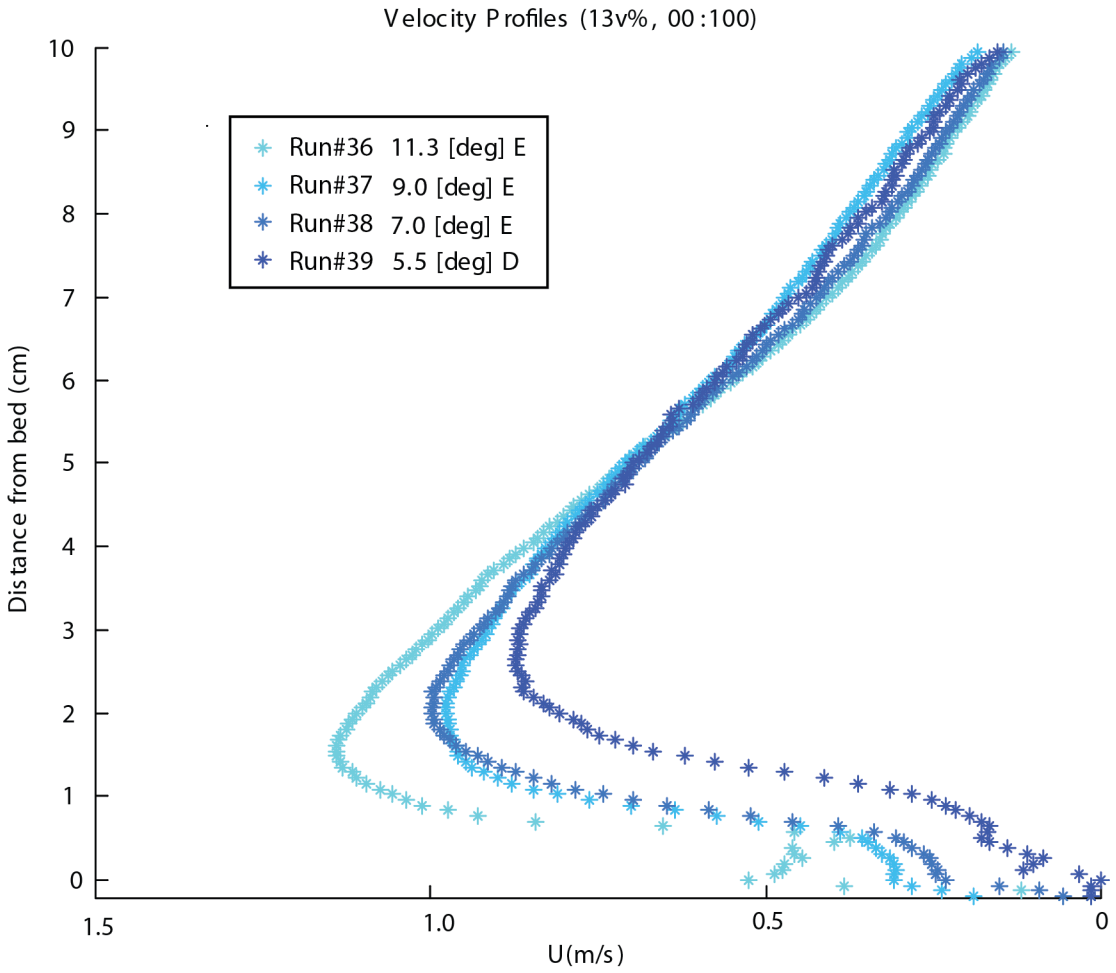

Fig. 10.6: *The full range of velocity profiles plotted by slope series. The aggrading character has been given in the legend (E = non-aggrading, EQ= equilibrium, D = depositional). The decrease in slope generally gives lower velocities and higher position of $U_{max.}$. The equilibrium and non-aggrading runs often show an inflection point near the bedding plain.*

11) References

Altinakar, M.S., Graf, W.H. and Hopfinger, E.J. (1996) Flow structure in turbidity currents. *Journal of Hydraulic Research,* **34**, 713.

Amy, L.A., Peakall, J. and Talling, P.J. (2005) Density- and viscosity-stratified gravity currents: Insight from laboratory experiments and implications for submarine flow deposits. *Sedimentary Geology,* **179**, 5-29.

Amy, L.A., Talling, P.J., Edmonds, V.O., Sumner, E.J. and Lesueur, A. (2006) An experimental investigation of sand-mud suspension settling behaviour: implications for bimodal mud contents of submarine flow deposits. *Sedimentology,* **53**, 1411-1434.

Amy, L.A., McCaffrey, W.D. and Talling, P.J. (2009) Special Issue Introduction: Sediment gravity flows: Recent insights into their dynamic and stratified/composite nature, *Marine and Petroleum Geology*, **26-10**, 1897-1899

Baldock, T.E., Tomkins, M.R., Nielsen, P. and Hughes, M.G. (2004) Settling velocity of sediments at high concentrations. *Coastal Engineering,* **51**, 91-100.

Basson, D.K., Berres, S. and Bürger, R. (2009) On models of polydisperse sedimentation with particle-size-specific hindered-settling factors. *Applied Mathematical Modelling,* **33**, 1815-1835.

Blanchette, F., Piche, V., Meiburg, E. and Strauss, M. (2006) Evaluation of a simplified approach for simulating gravity currents over slopes of varying angles. *Computers & Fluids,* **35**, 492-500.

Bonnecaze, R.T., Huppert, H.E. and Lister, J.R. (1996) Patterns of Sedimentation from Polydispersed Turbidity Currents. *Proceedings: Mathematical, Physical and Engineering Sciences,* **452**, pp. 2247-2261.

Buckee, C., Kneller, B. and Peakall, J. (2009) Turbulence Structure in Steady, Solute-Driven Gravity Currents (eds W. McCaffrey, B. Kneller and J. Peakall), *Blackwell Publishing Ltd*., Oxford U.K., doi:10.1002/9781444304275.ch13

Carling, P.A., (1992) The nature of the fluid boundary layer and the selection of parameters for benthic ecology, *Freshwater Biology,* **28, 2,** p. 273-284

Choux, C.M. and Druitt, T.H. (2002) Analogue study of particle segregation in pyroclastic density currents, with implications for the emplacement mechanisms of large ignimbrites. *Sedimentology,* **49**, 907-928.

Choux, C.M.A., Baas, J.H., McCaffrey, W.D. and Haughton, P.D.W. (2005) Comparison of spatio–temporal evolution of experimental particulate gravity flows at two different initial concentrations, based on velocity, grain size and density data. *Sedimentary Geology,* **179**, 49-69.

Clerx, N., (2010) Structure and Properties of High Density Turbidity Currents*, BSc-thesis*, University Utrecht

Eggenhuisen, J.T. and McCaffrey, W.D. (in press) The vertical turbulence structure of experimental turbidity currents encountering basal obstructions: implications for vertical suspended sediment distribution in non-equilibrium currents. *Sedimentology*

Ellison, T.H. and Turner, J.S. (1959) Turbulent entrainment in stratified flows, *Journal of Fluid Mechanics*, **6**, 423-448

Felix, M. (2004) The significance of single value variables in turbidity currents / Signification des variables de valeur simple caratariстique dans des courants de turbidity. *Journal of Hydraulic Research,* **42**, 323-330.

Felix, M., Sturton, S. and Peakall, J. (2005) Combined measurements of velocity and concentration in experimental turbidity currents. *Sedimentary Geology,* **179**, 31-47.

Ferguson, R.I. and Church, M. (2004) A Simple Universal Equation for Grain Settling Velocity. *Journal of Sedimentary Research,* **74**, 933-937.

Garcia, M.H. (1994) Depositional Turbidity Currents Laden with Poorly Sorted Sediment. *Journal of Hydraulic Engineering,* **120**, 1240-1263.

Gladstone, Phillips and Sparks (1998) Experiments on bidisperse, constant-volume gravity currents: propagation and sediment deposition. *Sedimentology,* **45**, 833-843.

Gladstone, C. and Woods, A.W. (2000) On the application of box models to particle-driven gravity currents. *Journal of Fluid Mechanics,* **416**, 187-195.

Hand, B.M. (1997) Inverse grading resulting from coarse-sediment transport lag. *Journal of Sedimentary Research,* **67**, 124-129.

Harris, T.C., Hogg, A.J. and Huppert, H.E. (2002) Polydisperse particle-driven gravity currents, *Journal of Fluid Mechanics*, **472**, 333-371

Haughton, P., Davis, C., McCaffrey, W. and Barker, S. (2009) Hybrid sediment gravity flow deposits – Classification, origin and significance. *Marine and Petroleum Geology,* **26**, 1900-1918.

Hodson, J.M. and Alexander, J. (2010) The Effects of Grain-Density Variation on Turbidity Currents and Some Implications for the Deposition of Carbonate Turbidites. *Journal of Sedimentary Research,* **80**, 515-528.

Huang, H., Imran, J. and Pirmez, C. (2007) Numerical modeling of poorly sorted depositional turbidity currents. *J.Geophys.Res.,* **112**, C01014.

Huppert, H.E. (2006) Gravity currents: a personal perspective. *Journal of Fluid Mechanics,* **554**, 299-322.

Islam, M.A. and Imran, J. (2010) Vertical structure of continuous release saline and turbidity currents. *J.Geophys.Res.,* **115**, C08025.

Julien, P.Y. ASCE, M., Klaassen, J., Ten Brinke, W.B.M. and Wilbers, A.W.E. (2002) Case Study: Bed Resistance of the Rhine River during 1998 Flood, Journal of Hydraulic Engineering, DEC, 1042-1050

Kneller, B. and Buckee, C. (2000) The structure and fluid mechanics of turbidity currents: a review of some recent studies and their geological implications. *Sedimentology,* **47**, 62-94.

Kneller, B. (2003) The influence of flow parameters on turbidite slope channel architecture. *Marine and Petroleum Geology,* **20**, 901-910.

Kneller, B.C., Bennett, S.J. and McCaffrey, W.D. (1999) Velocity structure, turbulence and fluid stresses in experimental gravity currents. *J.Geophys.Res.,* **104**, 5381-5391.

Kostic, S., Parker, G. and Marr, J.G. (2002) Role of Turbidity Currents in Setting the Foreset Slope of Clinoforms Prograding into Standing Fresh Water. *Journal of Sedimentary Research,* **72**, 353-362.

Lowe, D.R. (1982) Sediment gravity flows: II. Depositional models with special reference to the deposits of high-density turbidity currents. *Journal of Sedimentary Petrology,* **52**, 279-297.

Leeder, M. (1999) Sedimentology and Sedimentary Basins; From Turbulence to Tectonics: Oxford, U.K., Blackwell Science, 608 p.

Lüthi, S. (1981) Some new aspects of two-dimensional turbidity currents, *Sedimentology*, **28**, 1, 97-105

McCaffrey, W.D., Choux, C.M., Baas, J.H. and Haughton, P.D.W. (2003) Spatio-temporal evolution of velocity structure, concentration and grain-size stratification within experimental particulate gravity currents**,** *Marine and Petroleum Geology*, **20,** 6-8, 851-860

Meiburg, E. and Kneller, B. (2010) Turbidity Currents and Their Deposits. *Annual Review of Fluid Mechanics,* **42**, 135-156.

Middleton, G.V. (1993) Sediment deposition from turbidity currents. *Annual Review of Earth & Planetary Sciences,* **21**, 89-114

Middleton, G.V., Southard, J.B. (1984) Mechanics of Sediment Movement, *Society of Economic Paleotologists and Mineralogists,* Providence, Rhode Island

Middleton, G.V., (1967) Experiments on density and turbidity currents. III. Deposition of sediment, *Canadian Journal of Earth Sciences*, **4**, 475-505

Middleton, G.V., (1966a) Experiments on Density and Turbidity Currents: I. Motion of the Head, *Canadian Journal of Earth Sciences*, **3:(4),** 523-546

Mueller, S., Llewellin, E.W. and Mader, H.M. (2010) The rheology of suspensions of solid particles. *Proceedings of the Royal Society A: Mathematical, Physical and Engineering Science,* **466**, 1201-1228.

Mulder, T. and Alexander, J. (2001) The physical character of subaqueous sedimentary density flows and their deposits. *Sedimentology,* **48**, 269-299.

Nourmohammadi, Z., Afshin, H. and Firoozabadi, B. (2011) Experimental observation of the flow structure of turbidity currents. *Journal of Hydraulic Research,* **49**, 168-177.

Parker, G., Fukushima, Y. and Pantin, M. (1986) Self-accelerating turbidity currents*, Journal of Fluid Mechanics*, **171**, 145-181

Peakall J, Asworth P and Best J (1996)
Physical Modelling in Fluvial Geomorphology: Principles, Applications and Unresolved Issues.

Postma, G. (1986) Classification for sediment gravity-flow deposits based on flow conditions during sedimentation. *Geology,* **14**, 291-294.

Postma, G., Nemec, W. and Kleinspehn, K.L. (1988) Large floating clasts in turbidites: a mechanism for their emplacement. *Sedimentary Geology,* **58**, 47-61.

Ribberink, J.S. (1998) Bed-load transport for steady flows and unsteady oscillatory flows. *Coastal Engineering,* **34**, 59-82.

Roscoe, I.R. (1953) Suspensions, In Hermans, J.J., ed. Flow properties of disperse systems. Amsterdam, North-Holland, p.1-38

Salaheldin, T.M., Imran, J., Chaudhry, M.H. and Reed, C (2000) Role of fine-grained sediment in turbidity current flow dynamics and resulting deposits, *Marine Geology*, **171/1-4**, 21-38

Sequeiros, O.E., Spinewine, B., Beaubouef, R.T., Sun, T., Garcia, M.H. and Parker, G. (2010) Bedload transport and bed resistance associated with density and turbidity currents. *Sedimentology,* **57**, 1463-1490.

Shin, J.O., Dalziel, S.B. and Linden, P.F. (2004) Gravity currents produced by lock exchange. *Journal of Fluid Mechanics,* **521**, 1-34.

Simpson, J.E. (1987) Gravity Currents in the Environment and the Laboratory, New York: Wiley, 244pp

Sohn, Y.K. (1997) On traction-carpet sedimentation. *Journal of Sedimentary Research,* **67**, 502-509.

Stacey, M.W. and Bowen, A.J. (1988) The Vertical Structure of Density and Turbidity Currents: Theory and Observations. *J.Geophys.Res.,* **93**, 3528-3542.

Sumner, E.J., Amy, L.A. and Talling, P.J. (2008) Deposit Structure and Processes of Sand Deposition from Decelerating Sediment Suspensions. *Journal of Sedimentary Research,* **78**, 529-547.

Thompson, C.E.L., Amos, C.L., Angelaki, M., Jones, T.E.R. and Binks, C.E. (2006) An evaluation of bed shear stress under turbid flows. *Journal of Geophysical Research C: Oceans,* **111**.

Turner, J.S. (1973) Buoyancy Effects in Fluids, Cambridge U.K., Cambridge University Press, 367 p.

Van Kessel, T. and Kranenburg, C. (1996) Gravity Current of Fluid Mud on Sloping Bed, *Journal of Hydraulic Engineering*, **122-12**, 710-718

Wilcock, P.R. (1993) Critical Shear Stress of Natural Sediments. *Journal of Hydraulic Engineering,* **119**, 491-505.

Xu, J.P., Noble, M.A. and Rosenfeld, L.K. (2004) In-situ measurements of velocity structure within turbidity currents. *Geophysical Research Letters,* **31**, L09311.

Chapter 2

Simulating Bidisperse High Density Turbidity Currents in MassFLOW-3D™

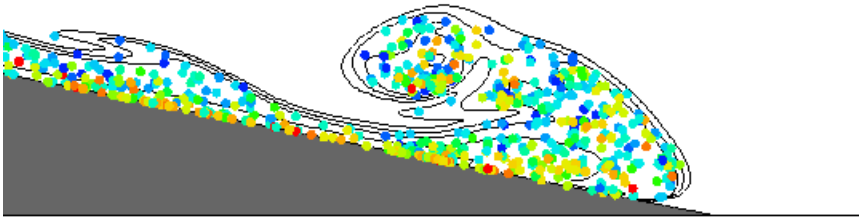

Menno Hofstra
University Utrecht

Complex Flow Design

Universiteit Utrecht

Abstract

This report includes the results of numerical simulations with MassFLOW-3D™ software of the earlier performed Eurotank flume experiments with bidisperse High Density Turbidity Currents (HDTC). The main objectives are to cross-check both approaches, doing sensitivity tests to create identical flow conditions as was observed int the flume, retrieving additional information about the rheology of the flow and as a main objective: gain specific knowledge on the effect of bidisperse grainsize-distributions on the flow properties in HDTC's.

It was found that a relative large turbulent mixing length of 2.5mm (80% of smallest cell) and small bedload coefficient (0.3) gives the most realistic or identical results. Due to lack of complex grain-to-grain interactions such as 'hindered settling' and 'traction carpets' in this version of Massflow-3D™, the modelled turbidity currents show deposition at higher gradients and total concentrations than what was observed in the actual flume. Also the simplicity of the usage of only the D50's in the numerical model is of importance.

Great similarities in the results are found in the effect of sediment fraction on the dimensionless velocity profiles. The addition of fines increases the width of the area around the Umax (nose) due to its thicker concentration distribution. Dynamic viscosities and turbulence kinetic energy also increase with addition of fine sediments in the mixture, however its influence on the vertical profiles is rather distinct relative to changes in slope or total volume concentration.

1- Introduction

The commercial computational fluid dynamics (CFD) software MassFLOW-3D™ is used for the numerical modeling of high density turbidity currents. An identical experimental setup as the physical flume experiments has been created for the numerical flow-software and when conditions are similar both are expected to show highly identical results in flow behaviour.

MassFLOW-3D™ is based on finite volume, discretizising and solving standard flow process equations for each individual cell, such as the Navier-Stokes equation.
This is done due to the employment of specially developed numerical techniques to solve the fluid-motion equations in transient, 3-Dimensional, multi-scale and multi-physis problems.
The big advantage of numerical modelling is that more and better resolution data about the rheology and flow behaviour of the turbidity current can be retrieved than with the physical flume experiments. This is of special interest in the field of bidisperse grainsize distributions

Further on it yields as a cross-check mechanism for the consistency and the realistic value of as well the 3D-flow modelling as the physical flume experiments. Certain modelling parameters (TLEN, BLC, etc.) are not fully understood how they specifically influence conditions in gravity flows. Better understanding of their working is hoped to be acquired by sensitivity tests.

Therefore to conclude the aims of this numerical study are as follows:

1) Cross-checking the results of the Eurotank physical experiments with the MassFLOW-3D™ numerical solutions

2) Doing sensitivity tests for various physical parameters that are not well defined for this typical turbidity model

3) Retrieving additional information about the flow conditions and rheology of the modelled \turbidity currents

4) Getting specified knowledge on the effect of sediment fraction on bidisperse grainsize distributions on flow behaviour in HDTC's and its difference relative to the effect of changes in slope and total volume concentration

2- Method

2.1) Geometry & Mesh

For this numerical model a geometrical set-up was constructed with the same relative dimensions as the actual flume used in the Eurotank experiments with the help of simple rectangular components. Different attempts have been made to make the geometrical setup as realistic as possible, while preventing numerical flow-model problems such as an excessive number of pressure iterations. These iterations are caused by pressure adjustments in incrompressible flows made of large distances, since the calculating pressure formula are based on local processes in the neighbouring grid. Complex geometry can cause more complex pressure differences and therefore result in pressure iteration problemss

Since no fluctuations are expected (Nicole, 2010) of the initial velocity in the inner part of the inlet, only the outer horizontal part of the inlet has been included in the model. Also the outflow tank and the top-seal of the flume tank have been left out of the model.

Extensive testing shows that using a highly identical geometry with a flat triangular inlet produces pressure problems at the top corner of this particular subcomponent.
To prevent the large amount of pressure iteration problems and the instability of flow, a one-cell inlet was attempted, but when looking at the local dynamic viscosities close to the inlet (figure 1), it can be seen that a maximum is formed due to the effect the abrupt transition to the open flume has on the current.

With the knowledge that the shape of the inlet has effect on the current, the final model was constructed as can be seen in figure 2. The thickness of the rotated sub-component, making the triangular inlet, can be assumed to have no effect on the current. In the triangular-inlet model it was necessary to maintain a constant initial velocity from the Xmin boundary. The flume floor as a subcomponent can be tilted to the right angle for every individual run.

The eventual mesh chosen for this MassFLOW-3D model (table 1) included a total of 367.5e3 cells with the smallest cells in the z-direction (2.9e-3m) and 1.1e-2 m and 1-2e-2 m for the x and y direction. There was no internal variation in cell size. This gives a X-Z and Y-Z ratio of around 4, which is considered to be reasonable for solving flow-processes in Flow-3™ software (Manual). The small cell-size in the z-direction gives the opportunity for better detail in the constructed profiles.

Direction	X	Y	Z
Total Cells	350	3	350
Cell-size (m)	1.11e-02	1.17e-02	2.86e-03
Total Number	367500		

Table 1: *Cell-dimensions used for the bidisperse Massflow-3D™ model*

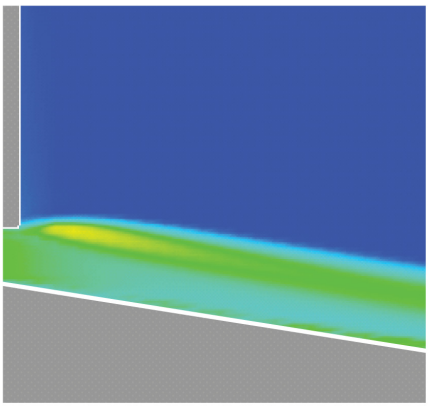

Fig.1: *one-cell inlet with viscosity maximum near the flow entrance*

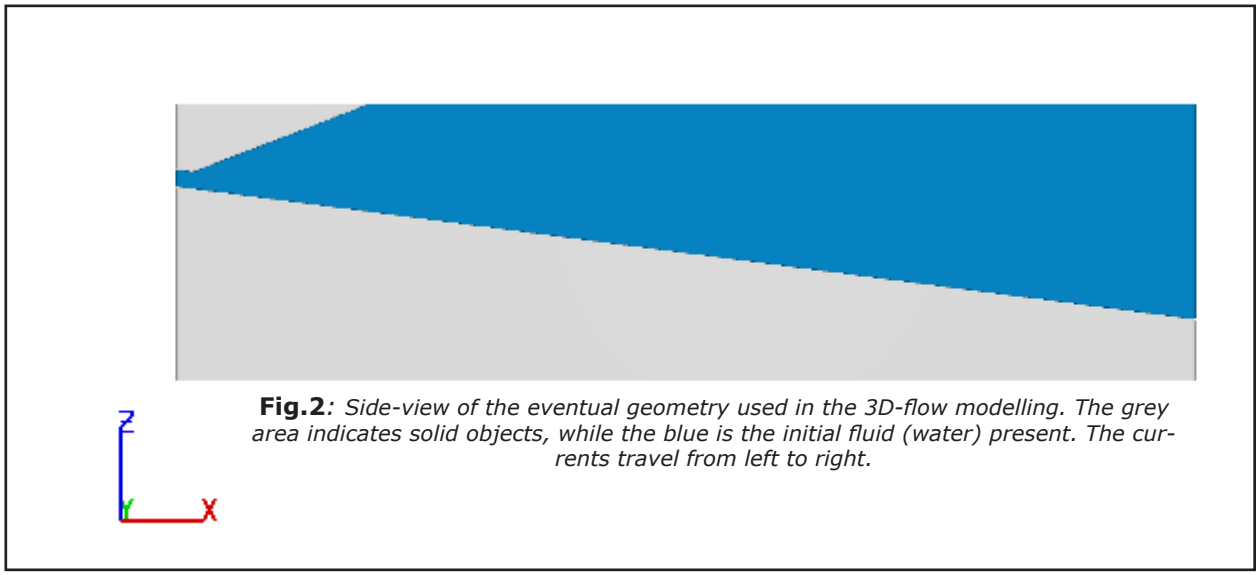

Fig.2: *Side-view of the eventual geometry used in the 3D-flow modelling. The grey area indicates solid objects, while the blue is the initial fluid (water) present. The currents travel from left to right.*

2.2) Boundary conditions

The MassFLOW-3D™ model contains a total of six boundaries, including two walls (one side-wall and the flume floor), one symmetry boundary (reduces computation time), one specified pressure (air pressure from top), one specified velocity (inlet) and one outflow boundary (outlet) (figure 3).
Since the surface of the Eurotank flume contained a thin mm-layer of sand-carpet (144mu), a similar surface roughness was provided in the model as a property for the tank floor.
The specified velocity was set on a constant value over the whole run which was equivalent to the constant discharge of 9.5 m3h-1, while the dimensions of the modelled inlet are known.
Because the flume is tilted, the initial velocity was divided into two vectors (X & Z), to give it a direction parallel to the bed.

When the velocity is set only in the x-direction, the flow jets a short distance from the flume floor after which it continues along the bed. This has a slight effect on the continuing current and the data retrieved at the point of measurement.
The outflow boundary gives the allowance for continuation of the flow through the boundary with minimum reflection. Since the current in the physical experiment dropped down in the open space of the outflow-tank, no or neglect able resistance is expected.

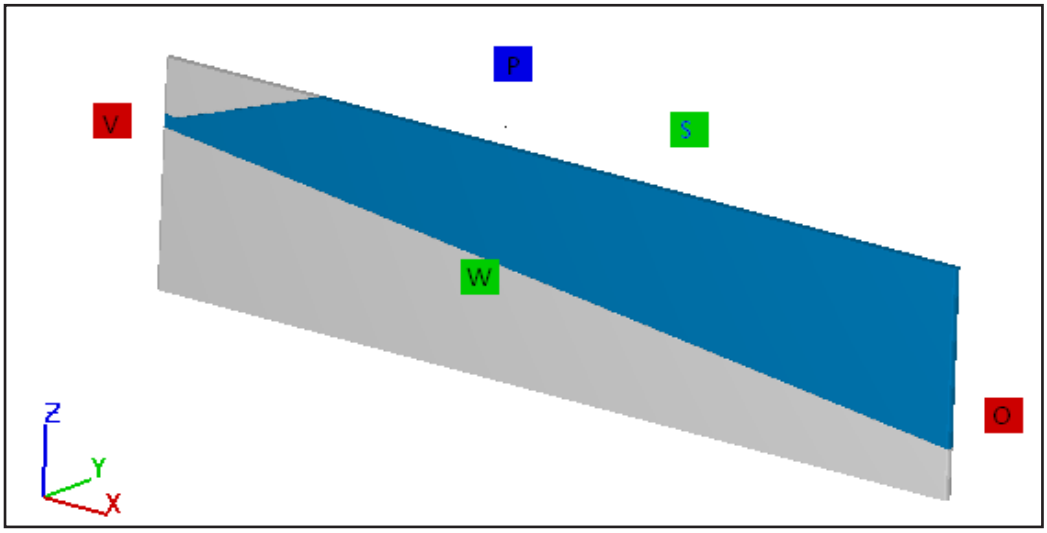

Fig. 3*: skewed view of the geometry with boundary indications in each individual axis.*

2.3) Physics

The gravity-flow based models that are active in all simulations are: gravity, density evaluation, viscosity-turbulence and sediment scour. Also the particle model is incorporated, which can have the same function as the tracer particles used in the physical experiments. The model-flume was filled with water (temperature of 20 C) over its full height (0.5m).
In the inflow boundary with initial velocity of the primary fluid (water) different sediment concentrations are included with various grainsizes.

For simplicity, each grainsize fraction (fine and coarse) of the flume experiments is represented by one uniform grainsize (D50) and the same density known for silica-quartz (2650 kgm-3). This results in a bidisperse distribution with only two grainsizes, representing mixtures of sand and silt. This has major advantages when considering the modelling-time and preventing calculation problems. Probably for the high-slope, high-concentrated runs this gives quite a good representation of the flow. However when nearing depositional conditions, problems may occur with its accuracy.
In the following the most important hydrologic models used for these simulations are shortly explained.

2.3.1) Sediment Scour Model

The model for bedload transport included in MassFLOW-3D™ has the basics of the Meyer, Peter & Muller equation (1948) which predicts the volumetric flow of sediment per width unit at the surface of the packed sediment bed with the dimensionless bed-load transport rate Φi.

$$\Phi_i = \beta_i(\theta_i - \theta"_{cr,i})^{1.5} \qquad (1)$$

This includes the local Shields number (θi), the dimensionless critical Shields parameter ($\theta_{cr,i}$) and a so called bed load coefficient βi or BLC.
(1) is originating from a combination of (2) & (3) with q_b being the volumetric bedload transport rate, ρ the density of water, τ_0 the bed shear-stress for a flat bed, s the ratio of densities of the sediment and water and d being the grain diameter.

$$\Phi = \frac{q_b}{\left[g(s-1)d^3\right]^1} \qquad (2)$$

$$\theta = \frac{\tau_0}{g\rho(s-1)d} \qquad (3)$$

According to Meyer-Peter and Müller (1948) the typical value for βi in steady flows is in the order of 8.0 with a critical Shields parameter of 0.047. However this was developed for use in rivers, maintaining relative coarse gravel grainsizes.
The behaviour of bedload transport rate with very fine sands as was used with the physical experiments (D50 = 144 & 50 mu) is mostly a grey area and has only been speculated.
Fernandez Luque & Van Beek (1976) did perform experiments with smaller grains (D50 > 0.9mm) and found the same relationship with βi = 5.7. Ribberink (1998) concluded this yields for bed-load conditions very close to the threshold of motion.
Nnadi and Wilson (1992) used D50 = 0.7mm and found βi = 12, but according to Ribberink this was more for a sheet flow regime.
In MassFLOW-3D™ this value is standard set to 8, but can be easily altered to modify the bed-load transport rates.
Into the scour model also the effect of armoring is included. This is a representation of the fact that the larger particles protect the fines from being entrained, which is added as a modification for the determination of the critical Shields parameter.

2.3.2) The RNG turbulence model

The RNG-model is based on renormalization-group methods (Yakhot and Orszag, 1986; Yakhot and Smith, 1992), which applies general statistical methods for retrieving average equations for turbulence associated parameters, which includes turbulent kinetic energy and the dissipation rate.
An advantage of this model is that it does not rely heavily on empirical constants, while its equations look similar to the k-e turbulence model (Harlow & Nakayama, 1967). This makes it more widely usable at variable conditions. Further on it is known for accurate low-intensity turbulence flows and modelling characteristic strong shear regions.

TLEN

As part of the turbulence renormalized group model, the most uncertain and sensitive parameter for the turbulent flow is the maximum turbulent mixing length. It yields as a limit of the amount of turbulent energy resulting from the turbulence model, by restraining the size of eddies/vortexes in the flow.
kinetic energy (k) can be described in three different components giving the turbulent velocity fluctuations in all three directions (u', v' & w').

$$k_T = \frac{1}{2}\left(\overline{u'^2} + \overline{v'^2} + \overline{w'^2}\right) \qquad (4)$$

The turbulent energy dissipation (e) includes the kinetic energy (assuming it is isotropic), a constant parameter C_{nu} assumed to be 0.085 in the RNG model (Isfahani & Brethour, 2009) and the TLEN.

$$\varepsilon = C_{NU}\sqrt{\frac{3}{2}}\frac{k_T^{\frac{3}{2}}}{TLEN} \quad (5)$$

From this the turbulence viscosity (Vt) can be calculated, which yields as the best way to simulate turbulence with the Reynolds Averaged Navier Stokes equations.

$$\nu_T = C_{NU}\frac{k_T^{\,2}}{\varepsilon_T} \quad (6)$$

It can be seen the influence of the TLEN on the energy dissipation is that a greater TLEN will decrease the dissipation an eventually, due to its effect on (6), increase the turbulent viscosity. Changes in momentum can be seen as turbulence which causes small variations in the local fluid viscosity by internal and external shear. In Massflow-3D™ this acts as an alternative option to give a measure for the turbulence of the system. It has to be kept in mind that this is based on assumptions of isotropic behavior, which may not always be valid.

Dynamic viscosity

Massflow-3D is able to calculate approximations of the dynamic viscosity. This is done by a combination of the turbulent viscosity and the molecular viscosity (7)

$$\mu = \rho \cdot (\nu_m + \nu_T) \quad (7)$$

The general known empirical viscosity expression of fluid-sediment mixtures in gravity flows is a function of fluid viscosity and sediment volume concentration (Roscoe, 1953, Davidson et al. 1977):

$$\mu_s = \mu_a(1-1.35C)^{-2.5} \quad (8)$$

According to (8), when sediment volume concentrations reach a percentage of 74%, the sediment is so tightly packed no shear movement is allowed.
With μa (15.6[deg]) = 1.129x10-3 Ns/m^2) this gives 1.561x10-3 Ns/m^2 for 9% volume concentration and 1.867x10-3 Ns/m^2 for 13.5% volume concentration.
However the prescribed maximum packing fraction of 3D-flow is 64% which is a good assumption for mono-disperse sediments. But there is no recall for changes occurring in this fraction when there is better packing due to bi or polydisperse sediment mixtures.
Pal & Rhodes (1985-86) introduced an empirical approach for viscosity data in emulsions, where a factor for maximum packing was incorporated. This makes it possible to calculate the dynamic viscosity independent of the effect of alterations in the maximum packing fraction.

$$\mu_s = \left[1+\frac{C/C_p}{1.187-(C/C_p)}\right]^{2.49} \quad (9)$$

It is not intended for sediment-laden suspensions, but can yield as a good indicator in gravity flows. Next to (8) & (9) also the empirical equations of Eilers (1941-1943) (10), Bridge (2008) (11) and Krieger & Dougherty (1959) (12) are introduced to get a feeling for the range for the empirical calculated dynamic viscosities of these low-concentration mixtures.

$$\mu_s = \left(1+\frac{1.25C}{1-K\cdot C}\right)^2 \quad (10)$$

$$\mu_s = \mu_a(1+2.5C+6.25C^2+15.26C^3) \quad (11)$$

$$\mu_s = \left(1-\frac{C}{C_p}\right)^{-B\cdot C_p} \quad (12)$$

(9) & (12) both include a maximum packing factor, however show rather differing results. The factor B (= 2.5) in (12) stands for the 'Einstein coefficient' and is mostly called 'intrinsic viscosity'. With the typical Cp of 0.74 the Krieger & Dougherty solution gives the same relationship as the equation of Eilers. The most widely used (8) by Roscoe (1953) gives the highest values for the viscosity above all others (figure 4)

Assumption is made that the molecular viscosity making up part of the dynamic viscosity is neglectable compared with the turbulent viscosity. Therefore:

$$\nu = \nu_m + \nu_t \approx \nu_t = \frac{\mu}{\rho} \qquad (13)$$

The range that is given by all different empirical relations for dynamic viscosity can be used as a reference of what would maximally be expected in these turbulent flows.

2.4) Sensitivity Tests

Some model parameters are assumed to be known correctly: drag coefficient, entrainment coefficient, angle of repose, grainsize and density. A number of sensitivity tests are needed to get a basic knowledge of the effect the other model parameters have on flow behavior. This has to be specified on X-direction velocity profiles.
The following parameters will be tested: TLEN, cell-size, Bedload Coefficient (BLC) & fill-height.

TLEN

By sensitivity tests the effect of TLEN on the behaviour of flow in the simulation of the bidispere turbidity currents has been studied. It was found that the TLEN has a big influence
on the stability in the flow and also on the flow thickness. Limiting the TLEN into small values
(≤ ~ 2.5mm) increases instabilities in such a manner that the body of the current is not stable and 'jumps' over the bedding plane (figure 5). A relative large TLEN (≥ ~ 2.5mm) however, shows fully uniform x-velocities and no extreme fluctuations in conditions over time (figure 6).
Further on this instability is of great influence on the diffusion and therefore the total flow height. A rather large TLEN (4 mm) results in a thick flow with higher velocities at greater distance from the bed (figure 7). The reverse yields for a low stable TLEN (2.5mm) number.
Not only is the width of the profile or flow altered, but also the size and the intensity of the Umax, getting more similar results with the UVP data by using the TLEN of 2.5mm.

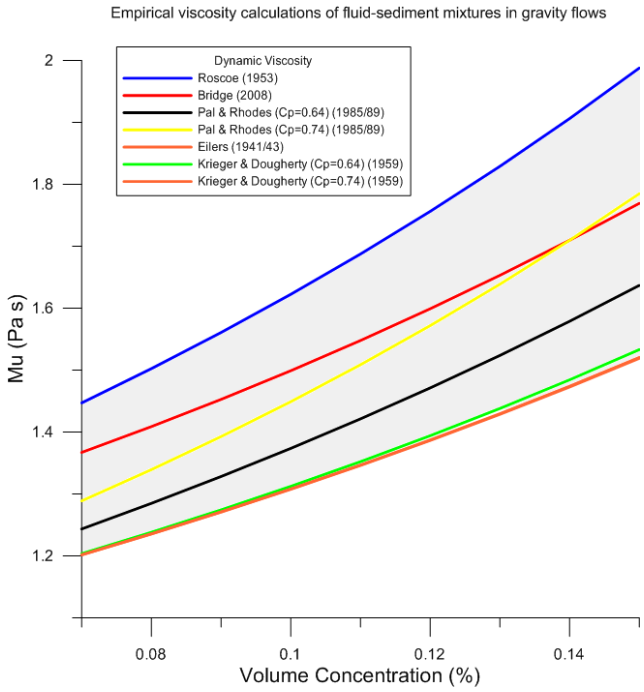

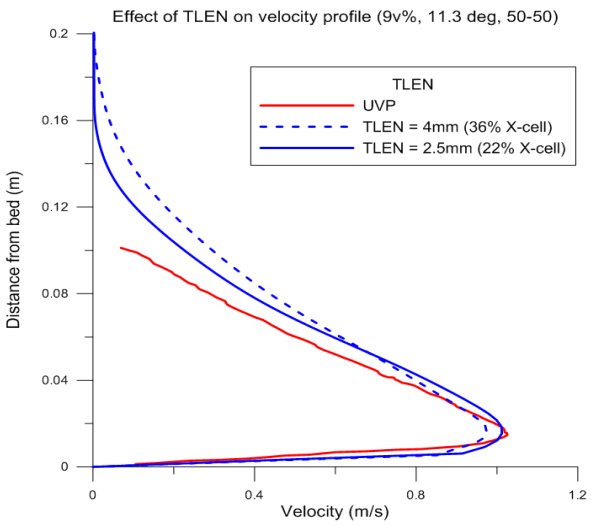

Fig. 5: *Effect of the maximum turbulence length in the RNG-model on x-direction velocity profiles*

Fig. 4: *Various common used empirical relations for viscosities in sediment gravity flows with varying volume concentration (1=100%). The grey area indicates the range of values.*

Since all UVP-velocity profiles are relatively thin with high velocity gradients, the lower TLEN is obviously preferred. Together with the knowledge that a lower TLEN than 2.5mm gives too unstable flow, this must be the optimum for this model.
However TLEN is dependending on the chosen cell size as was shown by Dircks (2010).
He showed that in his numerical model a TLEN of 3.5% or 1% of the smallest cell-size gives the most realistic depositional behaviour.

The smallest cell in this model is 3.1 mm in the Z-direction, which is similar to the chosen value of the TLEN itself. This is two orders of difference relative to the values used by Dircks. But TLEN's very much smaller than 2.5mm, are in no way giving good and wanted current conditions. This shows that the correct chosen TLEN length is very case dependent.

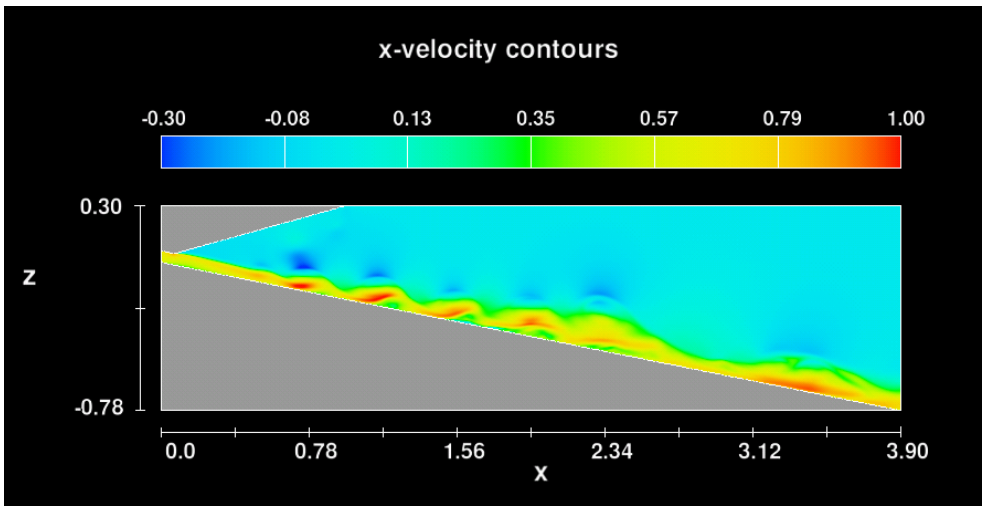

Fig. 6*: An example of too unstable flow due to reduction of the TLEN (1 mm) in the simulation of run 19. As can be seen, the current is jumping over the bedding plain in the x-direction, giving rather unrealistic flow behaviour. Velocities in m/s*

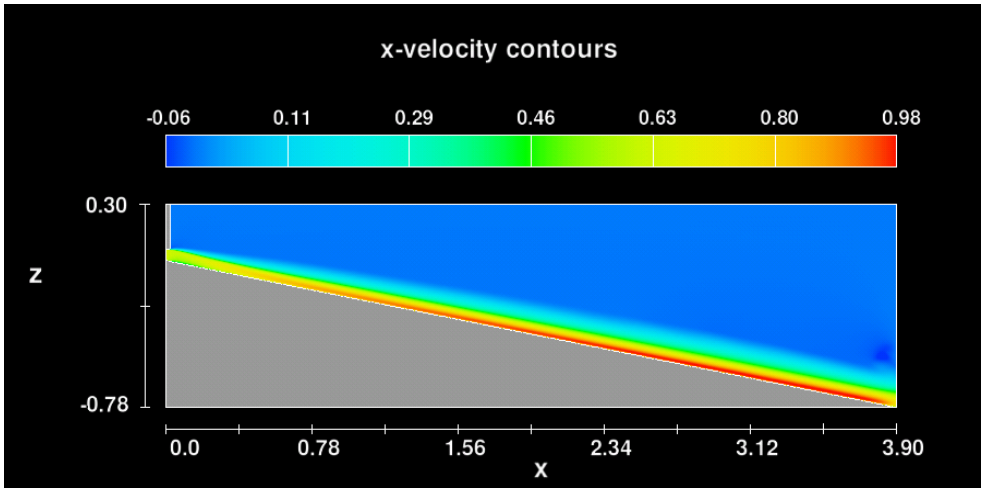

Fig. 7*: An example of stable flow due to increase of the TLEN (5 mm) in the simulation of run 19 (one-cell inlet). As can be seen there is no variation at all over time when looking at lateral velocity differences. Velocities in m/s*

BLC (βi)

Not much is known about the effect of the βi coefficient (BLC) on the depositional behaviour of the modelled bidisperse currents. From the scour model it is known that it has a direct effect on the dimensionless bed-load transport rate (5), which increases with larger coefficients. It was found that in the cases of very minimum or no bedload-transport, changes in BLC do not make a difference to the eventual x-direction velocities in the current. When parameters are altered in the direction of equilibrium conditions (f.e. lower slope), bed load transport increases and the BLC starts to have an effect on velocity structures (figure 8), due to its effect on (1).

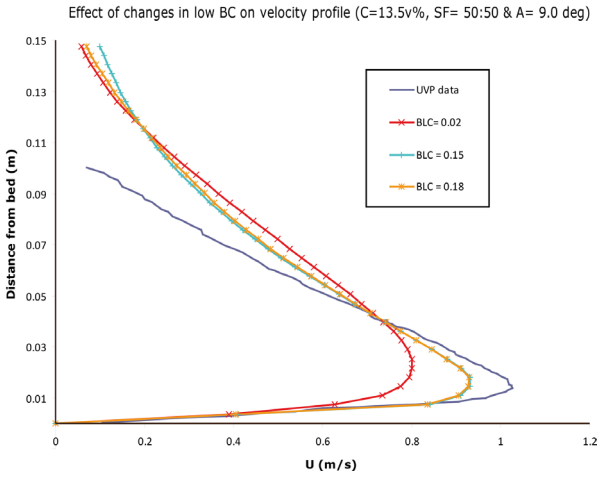

Fig. 8*: Effect of the Bedload Coefficient in the Sediment Scour model on the x-direction velocity profile*

A very low BLC of 0.1-0.3 has a positive effect on the realism of the velocity profile when directly comparing with the UVP results of the experimental data. This is primarily found in an increase in the velocity maximum and more skewed gradients. A BLC of 0 was found to has a negative effect by reducing velocities in general to too low values.
Further analysis of the effect of the BLC can be done by looking at differences in deposit structures. It was found that it can greatly influence the position and the amount of deposition occurring in the modelled flume.

A good idea about the sedimentation patterns is present for all the aggrading runs that have been done with the physical experiments and this can act as the main framework for sedimentary structures in the Massflow-3D™ model. Figure 9 show a simulation of a 9v% run at 11.3 degrees slope and 100% coarse sediment after 15s, which shows direct deposition after the head has passed. The only difference between both simulations is the value for the bed load coefficient (0.3 & 8). The original BLC is resulting in a constant deposit from about 1.6m until the outlet with about the same thickness over this whole area of the flume. The BLC of 0.3 however results in much more local variation in thickness, giving a spherical bump around the 1.6m and eventually thinning in the direction of the outlet.

The result given by the BLC of 0.3 is much more realistic for what is known about the sedimentation patterns generally found in the Eurotank flume. When depositional conditions occurred, there was in most cases a bump of sediment deposited some distance before the probe location, thinning further away from the inlet. This corresponds best with the results of the lower value of BLC.

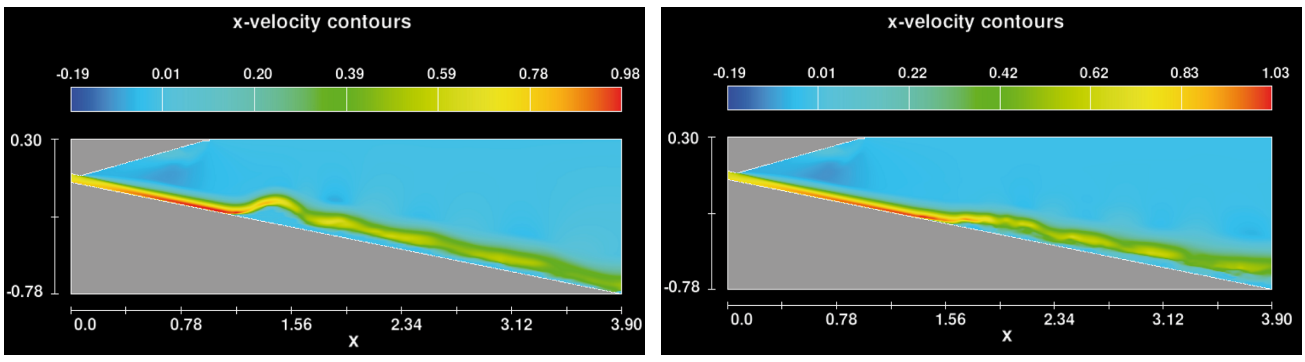

Fig. 9a&b: *side-view showing velocity contours of a depositional 9v%/11.3deg/100-00 run with varying Bedload Coefficient --> 9a (left) = 0.3 & 9b (right) = 8.*

Fill height

Of interest is also the initial fill height of the fluid (water at 20C), since it contributing to the hydrostatic pressure in the z-direction. A too low filling height could allow backflow at the top of the current, while this is obstructed by the pressure if the fill height is much more significant.

This is tested by some basic sensitivity tests on a simulation of a 9v%, 11.3 deg, 50:50 run. The best way to trial the concept is by increasing fill height together with the mesh in z-direction while keeping the size of the z-cells constant. This causes an increase in the amount of cells in the z-direction.

As can be seen in figure 10, when increasing fill height from 0.5 to 1 m, the effects on x-velocity is not very significant. There is only a small increase in Umax detectable (1.5% max) and some minor deviations at the outer region of the profile.

Since the differences between a doubled fill height and the original 0.5m is so minor, it can be assumed that the fill height of 0.5m is reasonable for this model and it does not create problems such as current back-flow.

In all physical experiments the fill height has always been around 0.5-0.8 m. But when the fill height is increased in the 3D-flow model it needs an increase in cells, which affects computation time. Therefore the fill heightof 0.5m will be persistently used in all furtherMassflow-3DTM modelling.

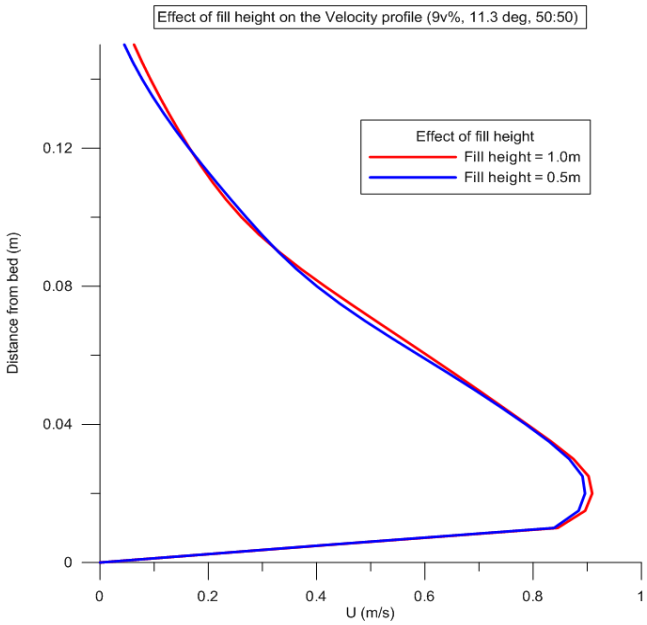

Fig. 10*:Effect of fill height (hydrostatic pressure) on x-direction velocity profile.*

The effect of mesh-variations on velocities

The choice of cell-size in all three directions is of great importance for the eventual reliability and value of the model results. Averaging the calculated data over one cell can have a large effect on the chaotic behaviour of the turbulent flow.

Especially the z-direction is important since it will determine the amount of datapoints on all z-profiles. A high amount of z-cells is therefore desirable; however cautions have to be taken. One of the basic rules for modelling dynamic flows is to keep the cell-ratio low. This means that when the number of z-cells is expanded, the x-cells and y-cells have to be taken into account as well.

Further more it is unknown which effect cell size will have on the boundary conditions at the bedding plane which is calculated as an assumption in MassFLOW-3D™. This averaging effect can have substantial influence on the lower contours in all profiles. Computation time is mainly depended on the mesh and increasing the amount of cells logically increases the duration for solving the model. Figure 11 is an example of what the effect is of the amount of x and z-cells on the velocity profile in the simulation of Eurotank run 31-35-36.

An increase of cells seems to have mainly effect on the Umax of the velocity profiles, giving higher and more realistic values with a greater amount of total cells. However this seems to be contributed only by an increase in z-cells, when looking at the difference between 600x300 and 400x400. It can be explained by an averaging effect, which is most substantial in the vertical direction than the horizontal direction, since variation over time is minimal.
It can be concluded that a relative low amount of x-cells will be sufficient, but a high amount of z-cells is desirable, while keeping the cell ratio's low enough for realistic results.

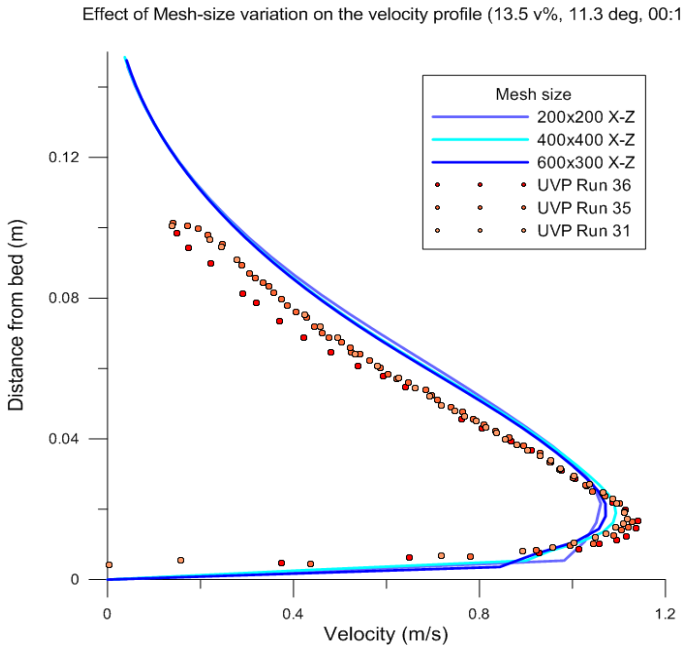

Fig. 11*: Variation in x-direction velocity profiles due to changes in cell-size (mesh). 200x200 (1.9e-2m x 5e-3m) 400x400 (9.7e-3m x 2.5e-3m) & 600x300 (6.4e-3m x 3.3e-3m)*

2.5) Modelled runs

The version used of MassFLOW-3D™ does not include a model for hindered settling. Therefore there is great risk that the model will not be functioning properly with the more highly concentrated HDTC. Since it is assumed (Baldock et al., 2003), that hindered settling will be less important in the low concentration runs, only the 9% and 13% volume concentration runs are simulated.
From these low-concentrated runs only the non-depositional runs are of interest. This is due to:

- Problems with the cell resolution occur when the velocity profile shifts vertically when the current is depositing
- MassFLOW-3D™ does not include the behaviour of 'traction carpets' in the scour model yet, while there are strong indications they are present in the equilibrium/depositional runs of the physical experiments
- There is still much unclear about the working of the Bedload Coeficient, (BLC) which is of great influence at deposi tional currents.

Ratio C/F	100/00	90/10	75/25	50/50	25/75	10/90	00/100
Conc/slope							
9%/11.3	x	x	x (TLEN=2.5 & 4)	x (TLEN =2.5 & 4)	x	x (TLEN =2.5 & 4)	x
9%/9.0	-	-	x	x	x	x	x
11%/9.0	-	-	-	-	-	x	-
13-14%/11.3	x (BLC 0.3 & 8)	x (BLC 0.3 & 8)	x	x	x	x (SR =144mu & 0)	x
13-14%/9.0	-	x	x	x (Q=9.5 & 8.5)	x	x	x
13-14%/7.0							x

Table 2*: Overview of all modelled Massflow-3D™ experiments + sensitivity tests. x= performed , - = lacking*

A full summary of experiments is given in Table 2. Since the depositional runs are not of interest, not the total matrix is performed

Additional simulations with SF of 25-75 and 10-90 are added for a more complete data set, which have not been modelled in the physical experiments. Most of interest are the angles of 11.3 /9.0 degrees and the concentration of 13.5/9.0 v%.

3- Results

All profiles and additional illustrations of the result chapter are combined in the Appendix (9)

3.1) Comparing velocity data

The UVP velocity data was the main component that was retrieved from the moving flow in the physical experiments; this has to yield as the major comparison with the numerical model, to create identical flow conditions.
The assumption was already made in the flume experiments that the velocities measured by the UVP are all parallel to the bedding plane (x-direction). Only the x-direction velocity factor of the Massflow-3D™ model should therefore be enough for comparison. A small correction is needed for the angle of the flow, since all UVP-profiles have been corrected for being perpendicular to the bedding plane.

In a semi-stable or lightly unstable turbidity current, velocities fluctuate heavily and one time slice is far from being a good representation of the whole flow. The UVP-data therefore has been averaged over 500 to 1500 individual measurements. To do the same with the MassFlOW-3D™ model, over a time-interval of several seconds multiple time slices are averaged until a good average velocity profile has been constructed.
The basic features which are of importance are: velocity maximum, velocity maximum height, velocity nose thickness and the outer region velocity gradient.

Also the inner region gradient is of importance, but since this is calculated by a standard boundary model in 3D-flow and is rather limited by cell size, it can not really yield as a good indicator.
With the process of 'trial and error' the best conditions (TLEN, bed coefficient, mesh) by which the numerical model shows best similarities with the UVP-data are obtained.

3.2) Dimensionless profiles (Fig.12 a-b)

Since the comparison of the actual UVP velocity profiles with the numerical model is far from perfect an alternative is to make both dimensionless. This also reduces the great uncertainty that is present in the physical experiments.
Dimensionless profiles are constructed by dividing all velocities by its maximum, making the Umax the origin of the x-axis and half umax in positive x-direction value 1.

This gives a better view of what actually occurs to the velocity 'nose'. In both approaches it shows that the nose significantly increases in size with addition of fines in the mixture. The profiles start to deviate further away from the nose, but the main structure is similar, with the 100% fines showing the thickest nose with the steepest velocity gradient, giving lower velocities in the top outer region.

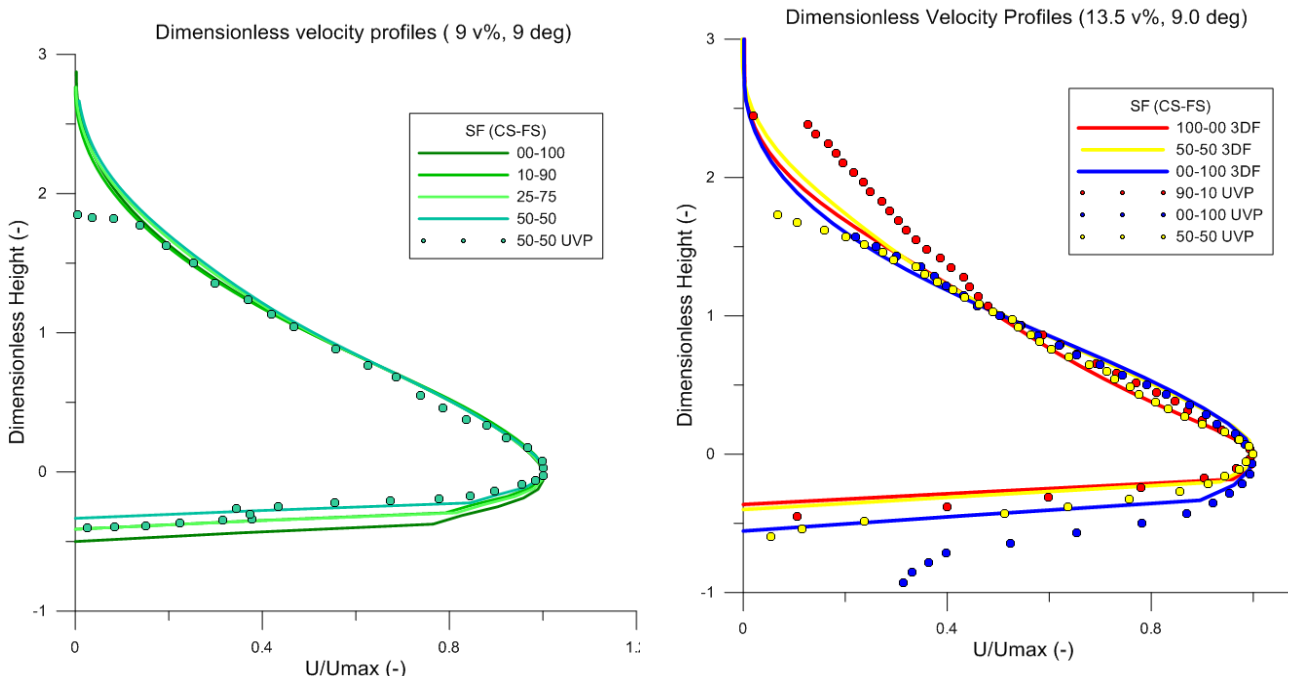

Fig. 12*: (a-b) dimensionless profiles of 9.0 [deg] runs including UVP velocity data of the flume experiments.*

3.3) The effect of sediment fraction on velocity profiles (Fig. 13 a-b)

When comparing modelled runs with only differences in the proportions of both sediment fractions, interesting results are found in the variance of the velocity profiles.
As can be seen, it has the biggest effect on the outer region velocities and in a minor way also the position and magnitude of U_{max}. In general it can be concluded that the addition of fines to the sediment mixture, widens the tip of the nose, but narrows the top outer region. Meaning that the flow gets thinner and a more uniform velocity-structure when the fraction of fines is high.

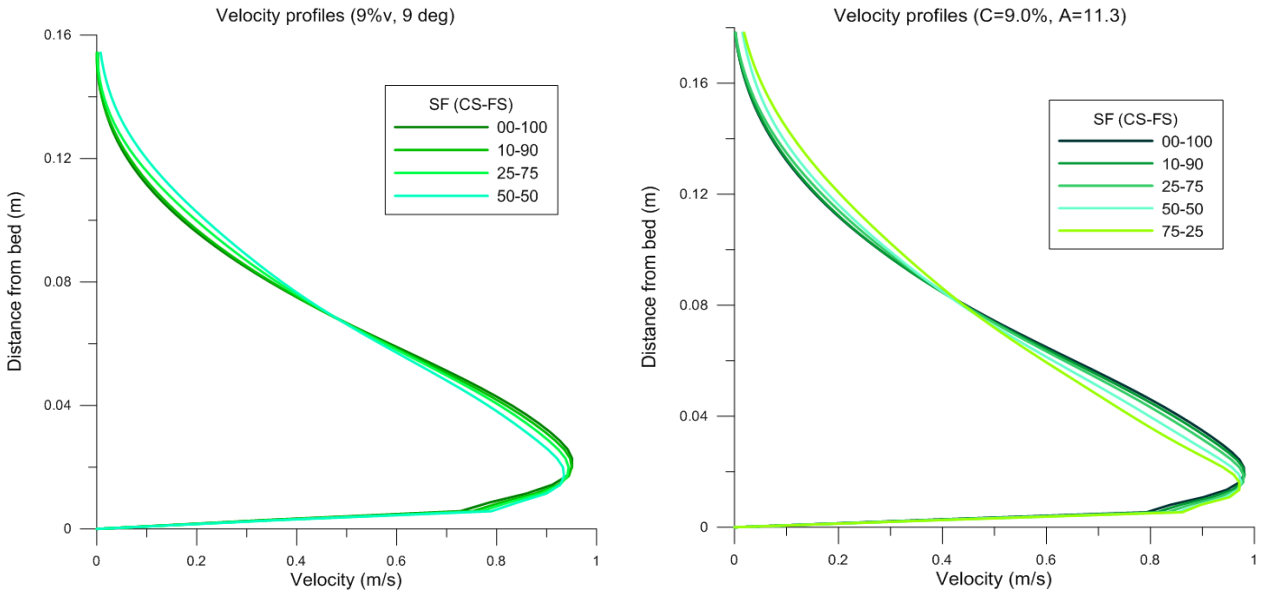

Fig. 13*: (a-b) X-direction velocity profiles of the 9v% runs (9.0 & 11.3 [deg])*

3.4) Observations regarding aggrading behaviour

The addition of the fine-fraction in the sediment has as expected a great influence on the sedimentational behaviour of the turbidity current. For example, when looking at the C=13.5%, A=11.3 deg runs, both in the physical and the 3D-flow experiments the current is depositional when there are only coarse sediments in the mixture, while the addition of a small amount of fines (10%) is enough to prevent deposition.
A full overview of the depositional behaviour of both the numerical and the physical model can be seen in Table 3.

Massflow-3D™	100/00	90/10	75/25	50/50	25/75	10/90	00/100
9%/9.0	D	D	D	E/EQ	E	E	E
9%/11.3	D	D	D	E/EQ	E	E	E
13-14%/11.3	D	D	EQ?	E	E	E	E
13-14%/9.0	D	D	D	E	E	E	E
Physical model	100/00	90/10	75/25	50/50	25/75	10/90	00/100
9%/9.0	D	D	D	EQ	-	-	-
9%/11.3	D	EQ	E	E	-	-	-
13-14%/11.3	D/EQ	E	E	E	-	-	E
13-14%/9.0	D	EQ	E	E	-	-	E

Table 3*: Stability table for both the numerical model and the Eurotank (physical model) flume. (D=Aggrading, EQ=Equilibrium, E=Non-aggrading)*

A clear difference exists in the results of both approaches. In general the physical model can stay longer non-depositional with lower concentration and gradients than the numerical model. Only the 9v%/ 9.0 deg runs are similar in both.

3.5) Internal concentration/density structures (Fig.14-15)

The numerical model gives the opportunity to analyze the concentrations of the sediment mixture in the flow for the whole, but also for each individual fraction.This makes it possible to explain the structure of the concentration profile by the individual additions of each of the two fractions in the flow. The total volume concentration profiles in Fig. 14 show rather strange transformations in shape with the addition of fines. When the CS-fraction is increased high concentrations persist close to the bed, while concentration higher up are reduced. Fig. 15, shows that the thickness of flow is always around the 7cm, with only the finer fraction reaching these heights. The coarse fraction, when present, only persists in the lower 2cm of the flow. Higher concentrated coarse fractions lightly increase this height, but no coarse sediment can be found above the 4cm. Further on, it seems especially at the 13.5v% runs that when the coarse fraction increases, the fine fraction is relatively reduced near the bedding plane.

Influence of flume gradient is rather insignificant, indicating only a small increase in near-bed concentration at the lower slope (9.0 deg). Increasing total volume concentration does not affect flow height and mainly increases concentrations in the lower region.

Due to the concentrated character of the coarse fraction there is especially in the high Cs runs a fast increase in total concentration (Fig. 14) near the bedding plane.

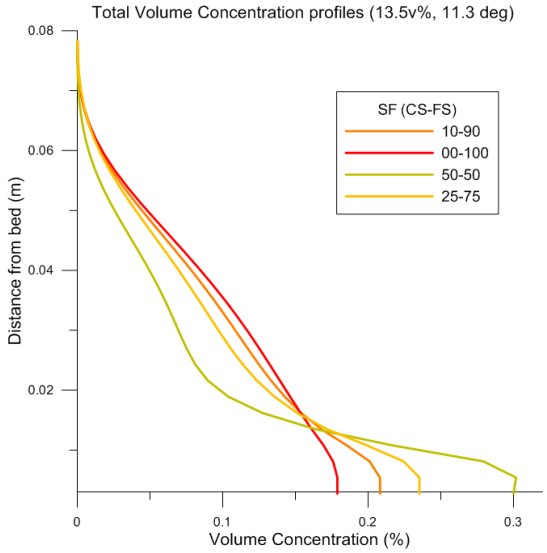

Fig. 14*: Alterations in Concentration profiles due to changing sediment fractions in bidisperse flows*

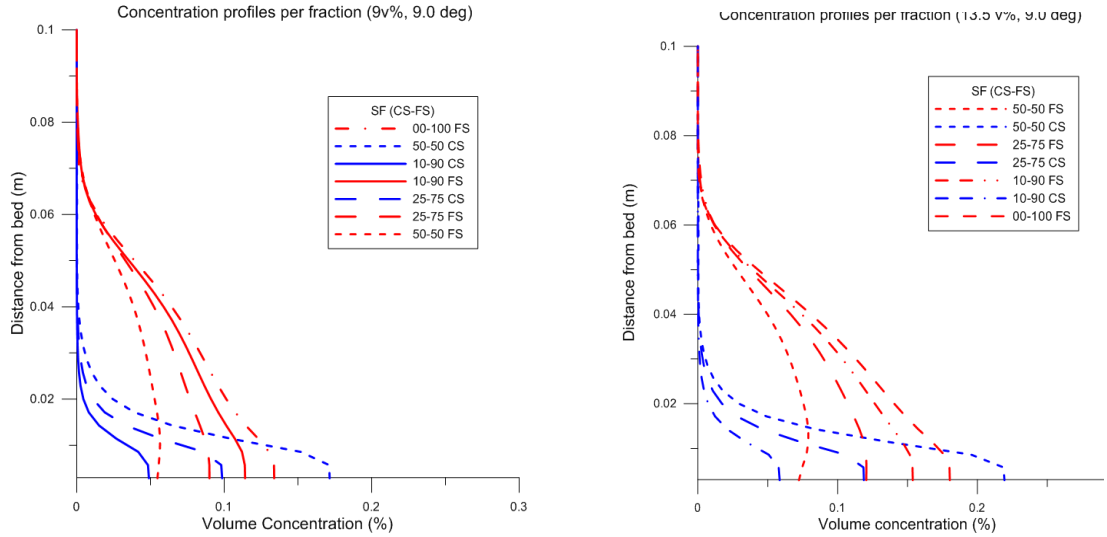

Fig. 15*: (a-b): Sediment Concentration profiles of each individual fraction divided by total volume concentration and slope*

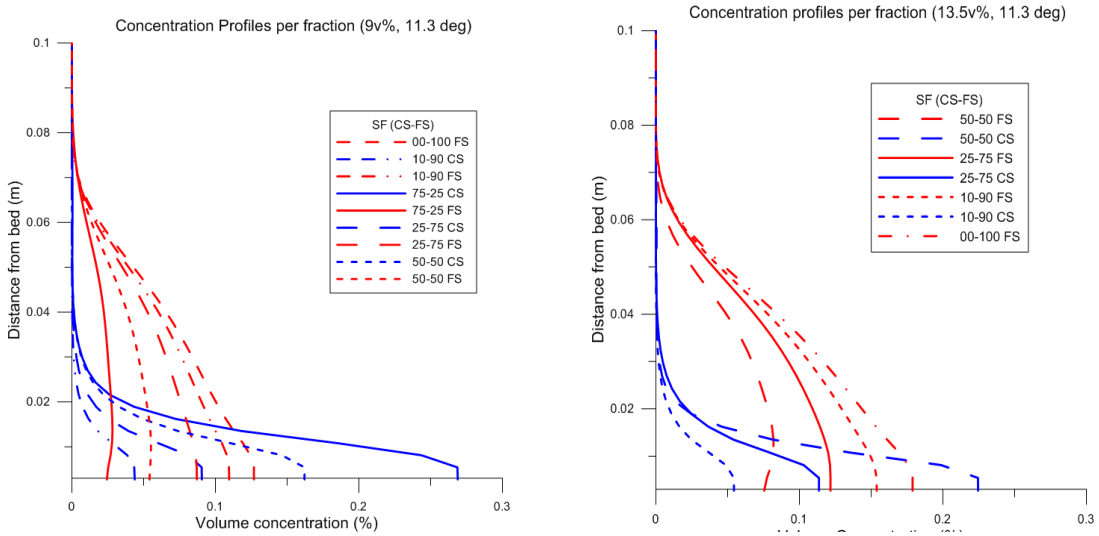

Fig.15: *(c-d): Sediment Concentration profiles of each individual fraction divided by total volume concentration and slope*

3.6) Turbulence kinetic energy & dynamic viscosity (Fig.16-18)

All turbulence kinetic energy profiles show two characteristic maxima in their profiles: A big wide peak around 6 cm from the bed and a narrow peak close to the bedding plane (Fig.16). It has been tested if the lower bed-peak could be a side-effect of the models boundary conditions, but with a surface roughness of '0' , this second peak remains (Fig.17).
The effect of the reduction in surface roughness is that the energy in the outer region peak becomes larger, while there is less turbulence energy near the bedding plane. This can easily be explained by the higher velocities due to less friction, increasing turbulence, while near the bed it has an opposite effect due to major reduction of shear forces. Turbulence energy of the upper maximum is increasing with addition of more fines, as well as its vertical position Sediment fraction seems to not alter significantly the first minor maximum near the bedding plane, while there can be observed a major influence due to the gradient of the flume. Further on, the combination of greater angles and higher concentrations is levelling both maxima.

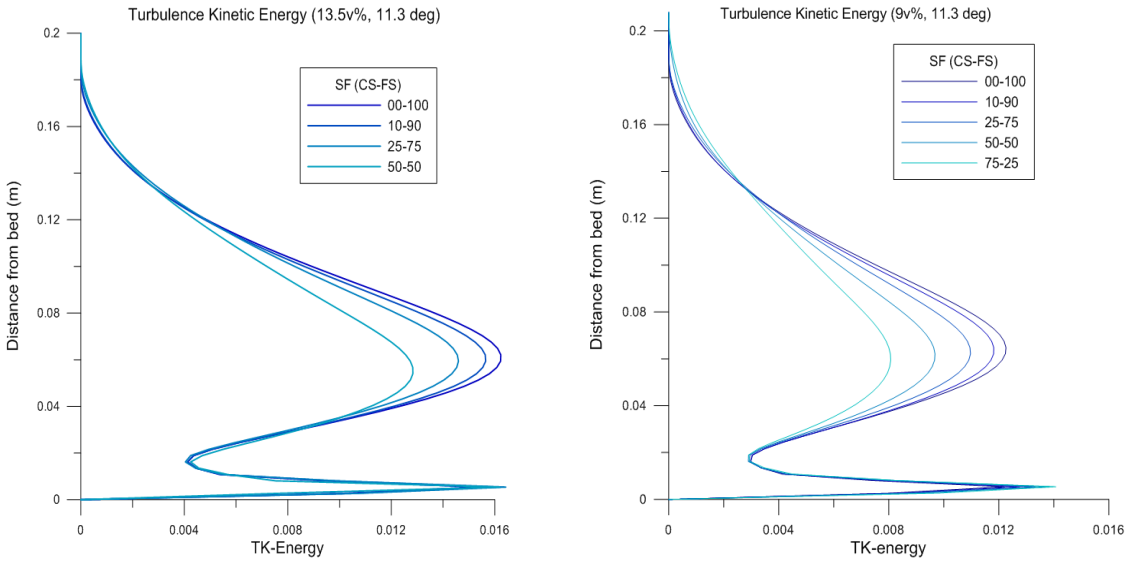

Fig.16: *(a-b): Turbulence Kinetic Energy profiles of each individual fraction divided by total volume concentration and slope*

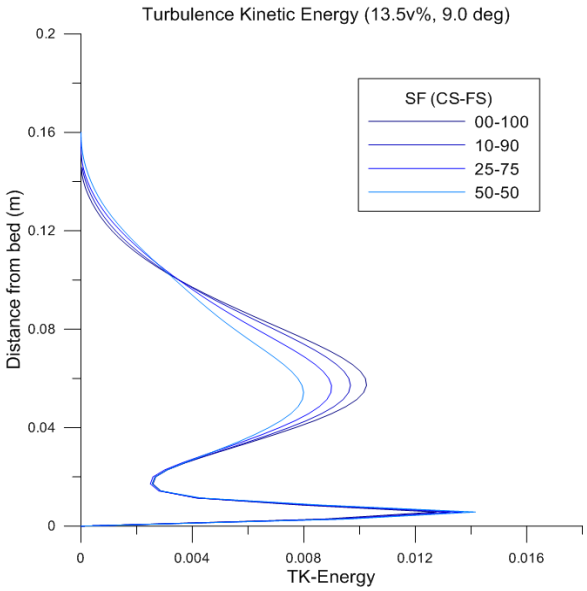

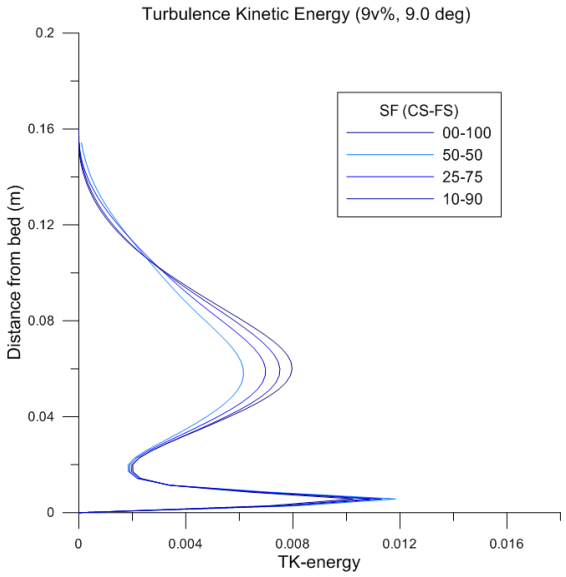

Fig. 16(c-d): *(top) Turbulence Kinetic Energy profiles of each individual fraction divided by total volume concentration and slope*

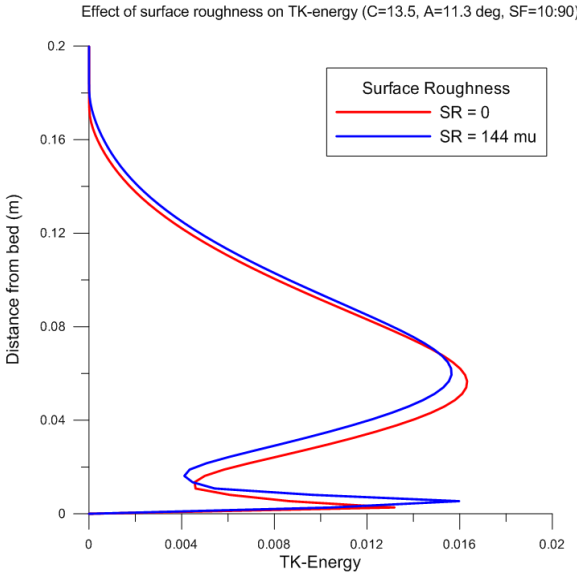

Fig. 17: *(left) The influence of surface roughness on turbulence kinetic energy, increasing very close to the bedding plane with increased surface roughness, while decreasing higher up in the flow.*

The dynamic viscosity profiles show a concave shape with a small peak near the bedding plain (Fig.18). With an increased fine fraction in the mixture the nose of the profile increases, while at the top the viscosity is lower. This looks rather similar to the general trend found in all the velocity profiles.

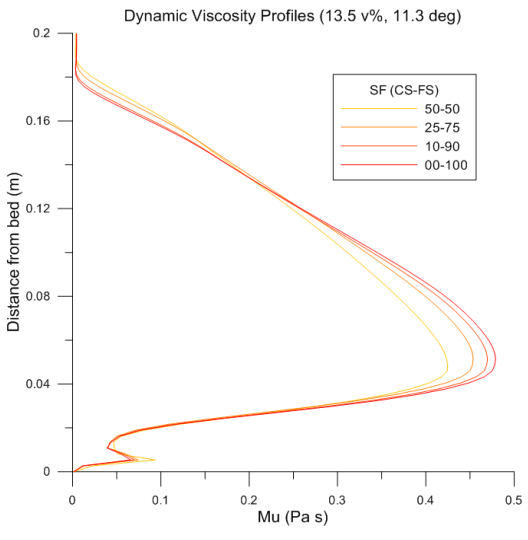

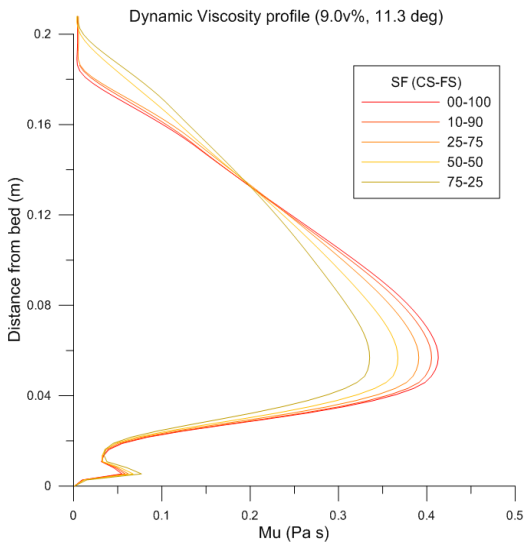

Fig. 18(a-b): *Dynamic viscosity profiles of each individual fraction divided by total volume concentration and slope*

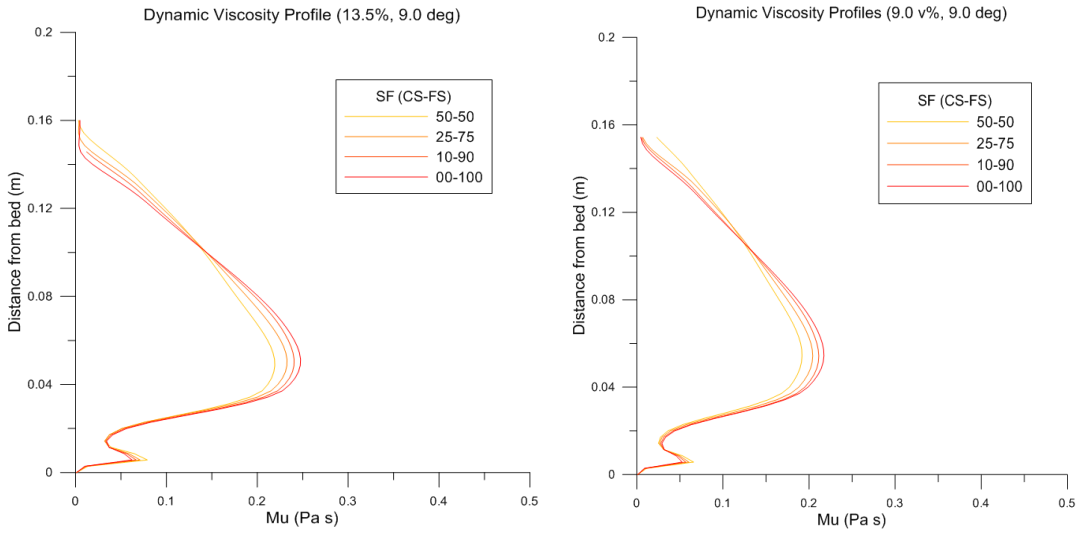

Fig.18 (c-d): *Dynamic viscosity profiles of each individual fraction divided by total volume concentration and slope*

3.7) Variations in initial volume concentration (Fig.19)

With the addition of one numerical simulation with 11v% (9 deg, 10:90), the effect of changes in sediment concentration in the MassFLOW-3D^{Tm} model can be properly examined and illustrated.
As can be seen in figure x, on the velocity profiles it has only major effect on the velocity maximum, increasing with higher volume concentrations.

No unexpected behaviour is seen in the concentration profiles, except for the fact that it seems to slightly influence the concentrated height of the coarse fraction (Fig.19b)
Both TK-energy peaks are enhanced due to increased concentration, but also the minimum in between increases in energy when there is more sediment in the mixture. Above 10cm away from the bed, there seems to be no influence of sediment concentration.

The same increasing of both peaks can be seen in the dynamic viscosity profiles; however there is a crossing around 14cm above the bed, giving the low-concentration simulations higher viscosities at top of the profile.

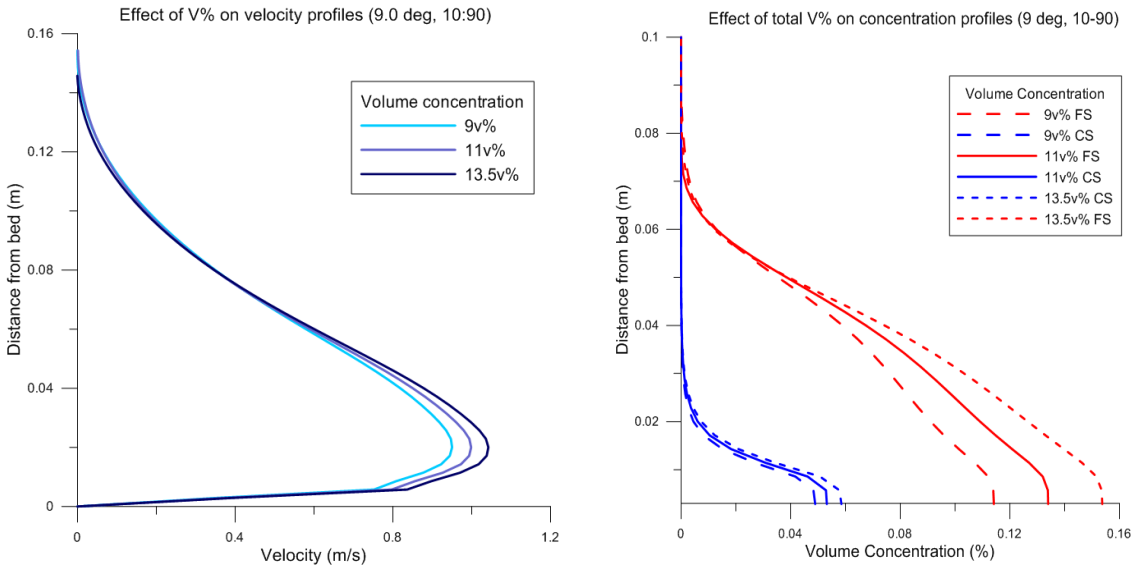

Fig. 19 (a-b)*: Effect of total volume concentration on velocity and concentration profiles*

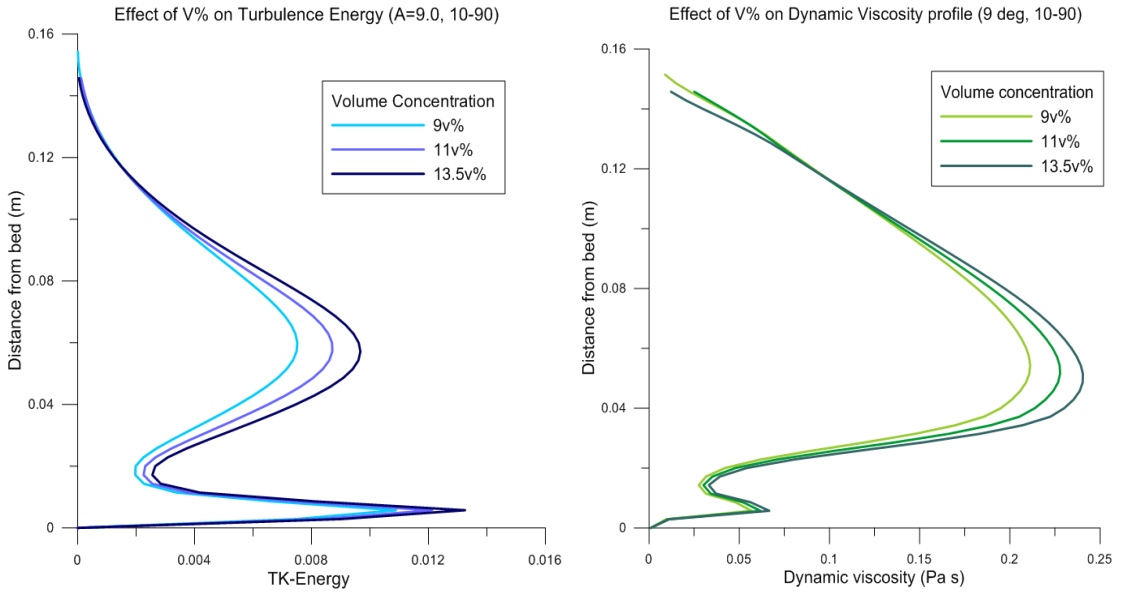

Fig. 19 (c-d): *Effect of total volume concentration on turbulence kinetic energy and dynamic viscosity profiles.*

3.8) Variations in slope/gradient (Fig.20)

With the addition of one 7.0 degree run (C=13.5, SF=00:100) detailed analysis on the effect of the gradient of the flume on the current can be performed. As expected, velocity increases significantly as well as the dynamic viscosity and the biggest TK-energy peak with increasing slope (Fig.20). A few degrees change in slope has a bigger effect on velocities than a change of a few percentage in volume concentration. Further on, when the velocity profiles are plotted dimensionless (Fig.20b) no change in shape can be detected with varying gradient. When the dimensionless profiles of the physical experimental data is plotted in the same diagram (Fig.20b), it shows at first sight rather distinct behaviour.

But only Run 37 deviates significantly from the rest, while Run 36 & 38 look very similar. Therefore, these deviations can not be attributed to changes in slope, but is more probable a defect in the physical conditions of Run 36 relative to the others.

Other conditions yield near the bedding plain, showing no clear relationship between gradient and dynamic viscosity and turbulence energy.

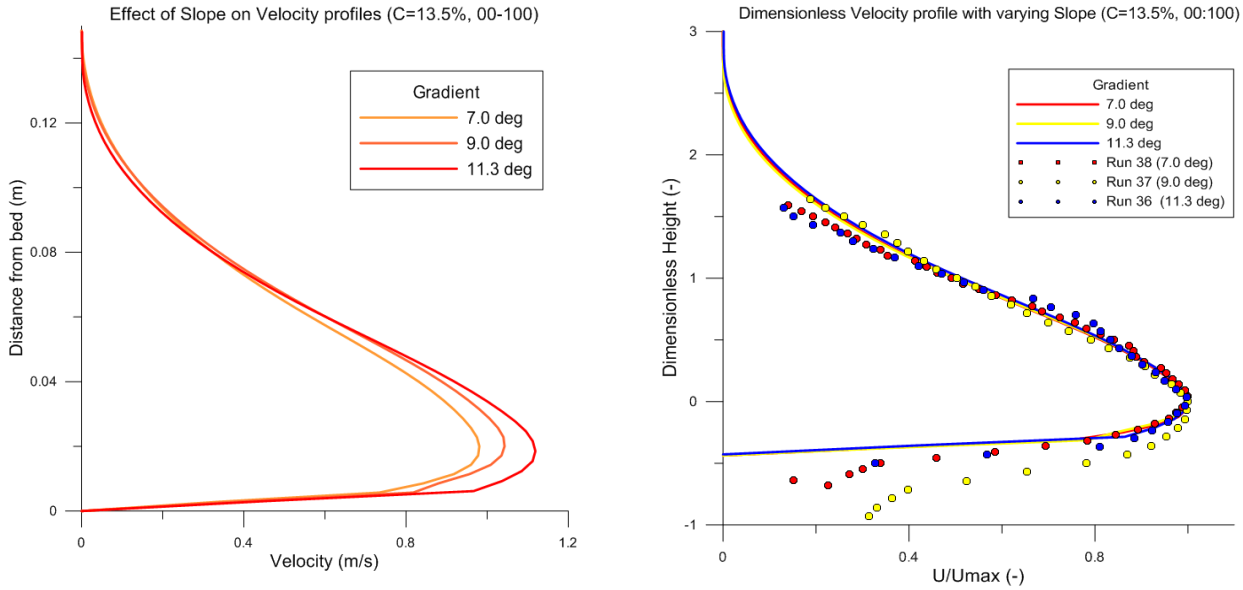

Fig. 20: (a-b): *Effect of slope on velocity and dimenstionless velocity profiles*

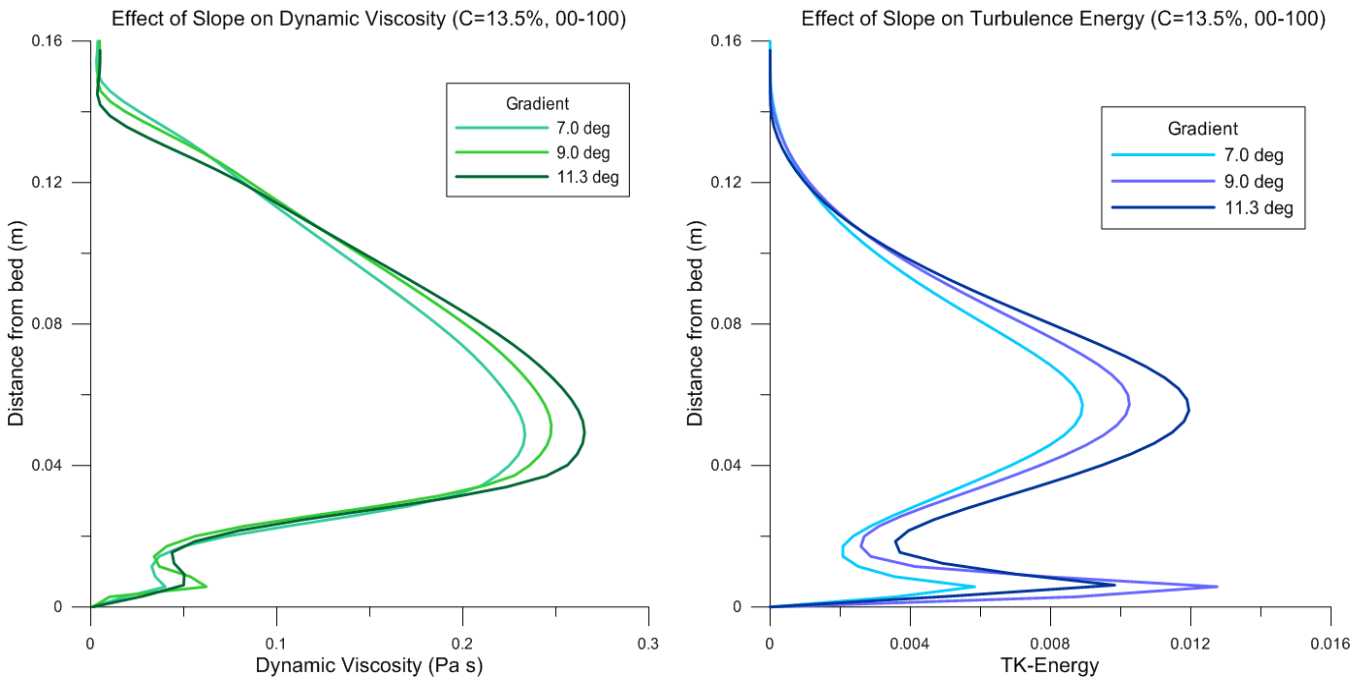

Fig. 20 (c-d): *Effect of slope on turbulence kinetic energy and dynamic viscosity profiles.*

4- Discussion

From the results it can be seen that there are similarities but also many differences between the numerical and physical approach regarding the effect of bidisperse grainsize distribution. Especially the distinct differences in the stability field is remarkable.

Reasons can be found in a couple of simplified concepts in this version of Massflow3D™:

4.1) Grainsize distributions

Differences in sedimentational behaviour between the numerical model and the physical experiments can partially be explained by the grainsize distibution. Since it is known that the fine fraction does maintain the non-depositional behaviour of the current more sufficient, the 50 v% that is smaller than the D50 with grains until 1e-6 m is very probable even more efficient. For simplicity only the D50's of both fractions have been incorporated in Massflow-3D™ which therefore results in distinct equilibrium conditions. The opposite effect also yields for the coarser 50v%.

To take into account the total distribution of both fractions, it has been tested what the effect is when the inflow sediment is divided in several different fractions. The differences in size represent a rough estimate of the known distribution from the laser-diffraction analysis (Fig. A2).

When only a small number of different grain species are added (2-4) no significant effect can be observed. However if a more realistic distribution as in figure A2(a-b) is applied, with five species for each fraction, different results are obtained. A direct effect of the distribution can be seen in figure A8(c-d). In the case of a bi-grainsize model at these conditions (11.3deg, 13.5v%, 50:50) no noticeable deposition takes place. But when there is addition the coarser fraction in the distribution, deposition starts suddenly early and close to the inlet.

This has a big effect on the current itself, forming an obstruction and reducing speed as well due to reduction in sediment concentration. As a result also the finer fraction is deposited at the same location, but in smaller quantities.
Since the deposit is growing, the obstruction hindering the current is getting bigger, decreasing flow velocities even more and eventually totally alters flow conditions.

4.2) Hindered settling

Since the 9.4 version of Massflow-3D™ (Flow-3D) has been used for all the numerical modelling, no model for the effect of hindered settling has been incorporated. For HDTC this gives significant problem, because it is of great influence on settling velocities and the stability field.
The semi-empirical Richardson and Zaki (1954) equation is the most widely used measure for the reduction in settling velocity due to higher concentrations in sediment mixtures.

More recent data was obtained by Baldock et al. (2003) which shows there is a significant difference between spherical particles (Richardson & Zaki) and the deviating shape of sand particles in reduced velocities. At volume concentration of 15% the effect of hindered settling will reduce settling rates to half of what it would be in fully clear water.
Fig. 20 shows the combined results of a great number of performed experiments plotted against relative settling velocity and concentration. At low relative concentrations (0-0.2) the settling velocities are reduced till 40% and seem to be rather insensitive to their properties.

At greater concentrations it not only depends on the particle properties but also on the rheology of the flow. Hindered settling even at low concentrations can have a major impact on the depositional behaviour of the model and explain partially the differences with the physical approach.

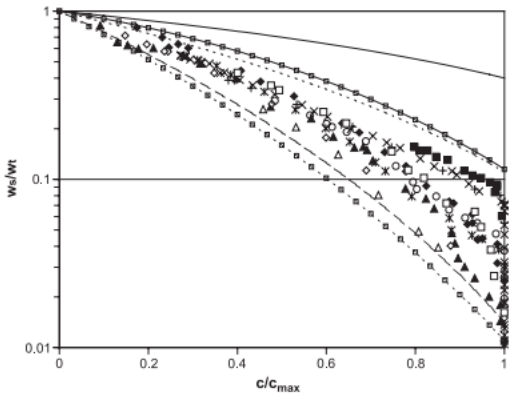

Fig. 20: *Relative settling velocity versus relative concentration including a large number of experimental data of various materials (open symbols = silica) (Baldock, 2003)*

4.3) Similarities in velocity profiles

The non-aggrading experimental runs in both approaches do show a great quantity of similarities when looking at the velocity properties of the current. The same increase of thickness in the 'velocity nose' is recognizable when the fine fraction is increased, made clear by the dimensionless velocity profiles. There is also a slight increasement of the U_{max} itself. This latter effect was more obvious in the Eurotank experiments, showing a curved structure with increased FS-fraction. This curve contained a great increase with a small addition of fines and becoming quite stable after reaching its maximum. The average velocities showed a similar pattern but not as clear.

These U_{mean} fluctuations are however not found in the MassFLOW-3D™ simulations for the average velocities over the whole flow height. All UVP data was obtained from 10cm above the bedding plane which is in someway rather restricted in representing the whole flow. A great number of UVP-profiles miss the outer low-velocity region and contain false or low-resolution data close to the probe. The general velocity fluctuations of the U_{mean} in the physical flume experiments could therefore also be explained by only increased velocities in the lower region of the flow, while the top outer region with reduced velocities (due to added fines) is left out.

In the MassFLOW-3D™ model, where the whole current is taken into account, there is no average change in velocities present and the alterations in sediment fraction results in local shape variations.
The data obtained from MassFLOW-3D™ limits due to its depositional behaviour to mostly relative high fine fraction simulations. This makes it harder to compare, since the UVP results are limited in most cases till 50v% fine fraction.
When looking at **Fig.13b** (9 v%, 11.3 [deg]) it shows that the shape-changes occurring between 75:25 & 00:100 are uniform. But when these profiles are averaged over the first 10cm (**Fig. 21**), the linear relationship seems to be lost. This is more conform with the general trend of the U_{mean}-U_{max} sediment fraction behaviour of the experimental results.
In general the mean velocities from the simulations are about 0.1m/s to high relative to the physical approach, mainly caused by the great width of the nose in most of the simulations. The deviations in the lower region between the numerical results and the physical experiments is very probable due to the lack of incorporation of a model for 'traction carpets' in Massflow-3D™

4.4) Explanations regarding velocity structures

The pattern of the fluctuations in velocities and especially changes in the shape of the profiles are similar in both approaches. Dimensionless they all show an increase in the max velocity region or 'velocity nose' thickness. The reason for this can very probably be found in the difference of 'concentration behaviour' between both fractions. The coarse grains are all localized in the lower region, however when more fine sediments are added, they cause a better spreading of sediment vertically in the moving current. This better spreading of suspended sediments has its influence on the velocity structure giving a vertically wider area of high velocities.

When looking at the tracer particle model (**Fig. 22**), the coarse grains sink relatively fast to the lower region of the flow and is almost fully separated at 1m distance from the inlet. This will increase the concentration locally and therefore maintaining velocity, creating a narrow velocity maximum very close to the bed. Since the finer grains do not diffuse as fast to lower regions, a wider high-velocity flow region is created directly above the bed.

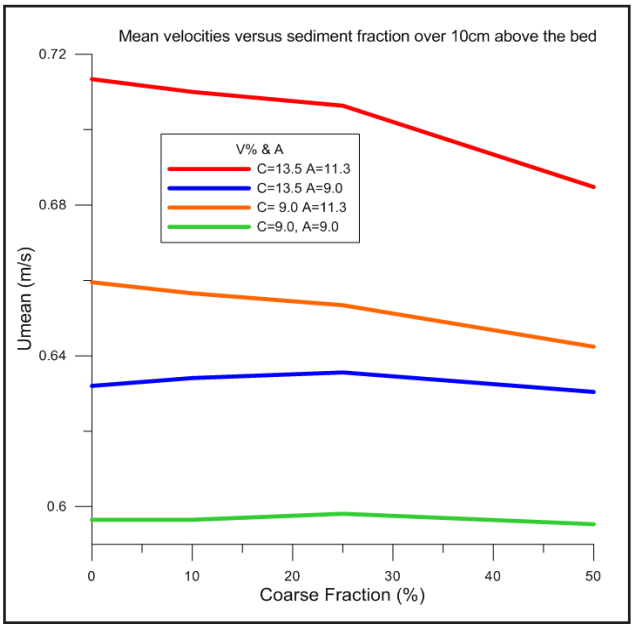

Fig. 21: *U_{mean} (massflow) calculated over the first 10cm above the bedding plane showing mainly variations at the high angle runs*

The reasoning for the crossing around 8cm from the bed giving higher velocities to the coarser grained mixtures in the top outer region remains unclear. No direct evidence can be found in the concentration profiles, since the mixture gets heavily diluted around the 7cm distance. The only noticeable change is that, when the coarse fraction is increased, the concentration of coarse particles enhances at greater distance from the bed. But this is no direct explanation for enhanced velocities at distances of more than 8cm.

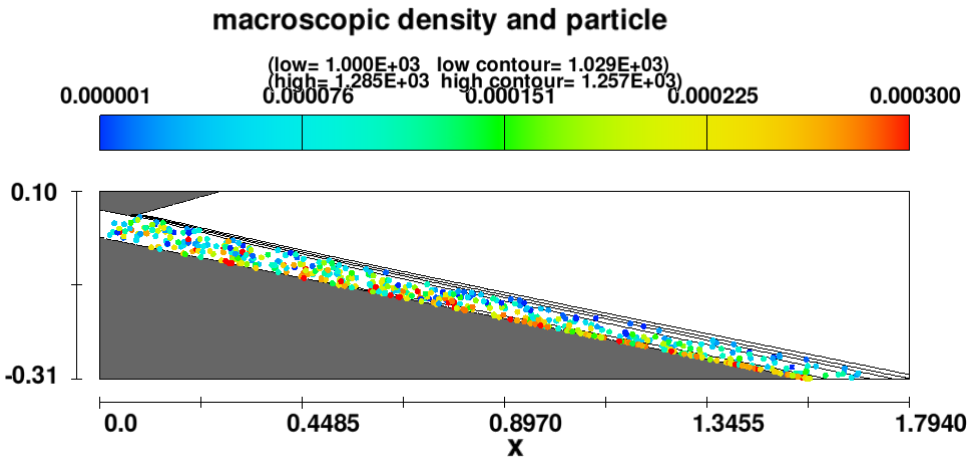

Fig. 22*: Zoomed-in section of various sized particles in a non-backcoupled particle model, showing diffusion in the flow of the coarser particles*

4.5) Additional Flow properties and comparison with previous work

Since flow velocity, viscosity & turbulence energy are all highly dependent and relatible to each other, it explains the identical trends found in all profiles.
The basic effect of enhanced slopes, total concentration and addition of fines is all increasing velocities, viscosities and turbulence energy. However how this is translated in the vertical profiles is quite distinct for every case.
Concentration and slope only affect the area around the velocity maximum, with the varying gradient showing a wider area of change. Further on it can be seen that all three variables have a different effect on turbulence kinetic energy, with only slope also having an effect on the near-bed peak.

The dynamic viscosity shows very similar behaviour in all three cases.The strange variance in the inner region seen with the slope-runs might be caused by the shape of the subcomponent having its effect on the model's mesh. When the gradient is changed the averaging of conditions in the boundary cells are altered, resulting in strange fluctuations and no clear trend with varying slope.

Better understanding of the internal meaning of TKE-peaks in vertical profiles was gained by Felix et al. (2005). Felix et al. performed lock-exchange turbidity experiments with various concentrations and sediments and did measurements on velocities and concentration.

According to the results of Felix et al. (2005) the interaction of the turbulence maxima is of importance for the vertical distribution of sediments in the flow. The TKE-minima located just below the biggest velocity maximum is of main influence on the capability of segregation in the flow, since turbulence is the mechanism to transport the particles in the vertical direction. When the TKE is very minimal the vertical movement of the sediment upwards is limited. From the numerical simulations from this report it shows that this minimum can be altered by total volume concentration and the gradient of the flume. Greater concentrations and gradients therefore would increase vertical mixing in the flow.

However this effect on vertical distribution can not be concluded from the concentration profiles including both individual fractions. There is only slight indication **(Fig. 19b&20a)** that the coarse sediments reach greater heights with the increased TKE-minimum. It can be concluded that the slight changes in the TKE minima are not enough to have a great effect on the vertical mixing of both fractions. In the interpretation of Felix (2005), the high-density plug-like flow reaches minima of 0 TKE, decoupling two regions and ceasing the vertical mixing **(Fig.23).** At these high-concentrated flows the stratification is much more effective to prevent vertical mixing.

In these numerical simulations, sediment fraction alters the occurrence of all concentration profiles and it indicates that the current becomes more stratified due to the bidisperse distribution of the mixture. Accoridng to Felix (2005) stratification should be a direct effect due to reduced TKE. When TKE is low, it becomes more difficult for the dense concentrated undercurrent to move upwards and the higher low-concentrated flow to go downward. Therefore the generated turbulence in the middle of the flow becomes less significant. However there is no decrease of TKE in the near bed located minima in the numerical model, since it is located at the stratification boundary (transition from high concentrated coarse to high concentrated fines).

There is only a direct effect on the higher situated TKE maximum, which dampening could be caused by stratification in the higher flow, but is more logically explained by the decreased concentrations and velocities.

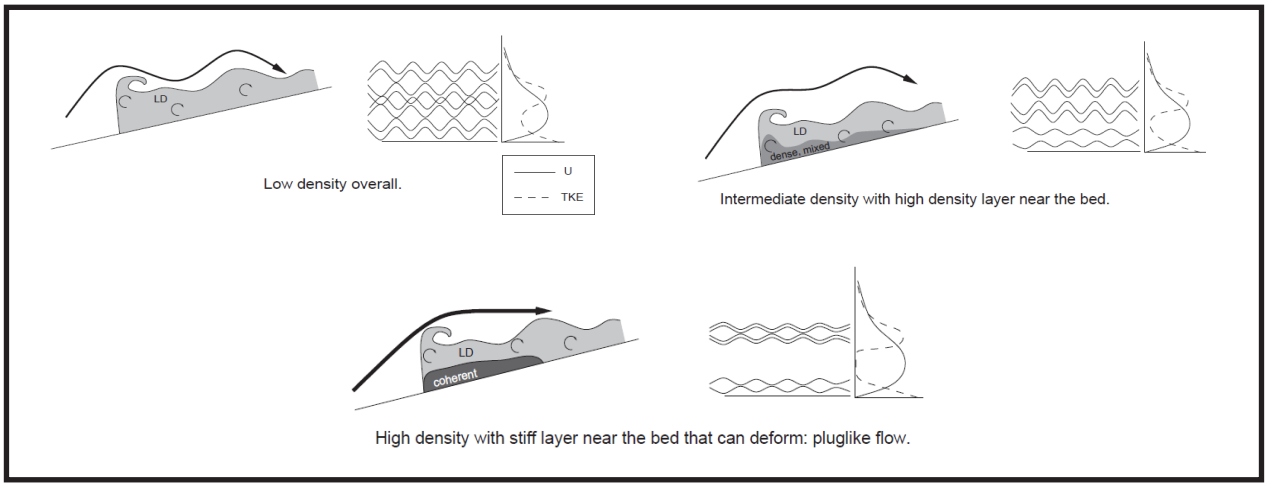

Fig. 23: *Schematic diagram showing three different flows, with a 2D-sketch of the current on the left and the velocity + TKE-profiles on the right. The sketch of the current shows distinct concentration regimes (LD= low-density region). The lowest flow is most stratified with decoppeling of the HD and LD regions, resulting in a TKE minimum of zero. The vertical position of U_{max} corresponds with the position of the TKE-minimum. The black arrow represents the general path of the ambient fluid. (Felix et al., 2005)*

In the field of vertical dynamic viscosity profiles almost no work has been published. Since turbulent gravity flows have to maintain low viscosities to show turbulent behaviour, values are expected to be lower than the calculated dynamic viscosities of all the empirical formulas for standardized gravity flows **(figure 4**). The maxima reached by all simulation profiles is around 0.5 Pa s, which is not in any way near the empirical values of the '9-13.5v%' concentration field. (3) shows that greater TLEN values result in higher turbulent viscosities. The relative high value of 2.5mm chosen for these simulations, is therefore not pushing flow condition out of the turbulent field. Stacey & Bowen (1988) made theoretical predictions of eddy viscosity and diffusivity, which look most similar to the results of this report (**Fig. 24**). It was concluded that the lower peak (which is relatively large in **Fig.24** compared to the results of this model) is located below the U_{max} and is not much greater than standard molecular viscosity, indicating that molecular processes are influencing the current.

Because computer power has only recently reached levels to be sufficient for the direct simulation of the complex Navier-Stokesequations with turbulent flow, previous work in the field of internal turbidity flow properties is limited. Further on, most models have been developed for well sorted and dilute suspensions.

Direct numerical simulation with Reynolds-average Navier-Stokes equations and special interest for poorly sorted mixtures has however been conducted by Huang et al. (2007). Huang simulated both 2-dimensional as 3-dimensional depositional currents in a canyon-fan transitional system and constructed velocity, concentration & TKE-profiles **(Fig. 25-27).** The experimental results of Garcia (1990) with badly sorted suspensions were numerically recreated and very close matching results in concentrations and velocities were found. As with the results of this report they found that the finer 'classes' were more evenly vertically distributed and the coarser particles more stratified concentrated close to the bedding plain.

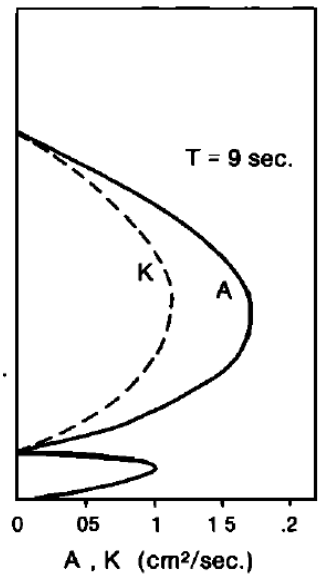

Fig. 24: *Theoretical predictions of eddy viscosity (A) and eddy diffusivity (K) obtained from numerical modelling by Stacey & Bowen (1988)*

The variation of the used grainsize classes (5-32mu) is limited, relative to the more bidisperse character (50 & 144 mu) of the MassFLOW-3D™ model.
This explains the much more subtle differences in **Fig. 23** compared to concentration profiles of this report. Next, the lateral variation of vertical concentration structures was studied for a depositional current by comparing at two fixed points (4m & 9m from inlet). It showed from the total volume concentration structures that the degree of vertical variation is reduced over distance due to deposition close to bedding and increase mixing at further distance. From the distinct fractions it shows that the coarser particles are mostly responsible for deposition, while the fines have most influence on the vertical mixing.

From the combined dimensionless fraction profiles **(Fig. 26)** it was found that the point at which all coincide is at the same vertical distance as the U_{max}. Further on, the coarser particles were highly concentrated below the U_{max}, while the finer particles were mostly concentrated above this point. The cross point is also the inflection point between the concave up and concave down concentration profile structures. When from this report as for example all TKE and velocity profiles of the 9.0v%-11.3[deg] runs are plotted together **(Fig.29)**, the same coincidens of the U_{max} and TKE-minimum can be found. Only the increase of height of U_{max} with sediment fraction does not correspond with the same increase in the TKE minimum, slowly placing the U_{max} above the TKE minimum with increased fine fraction. When all constructed profiles of the 9.0v%-11.3 [deg]-50:50 run are plotted together **(Fig.28)**, not only is the TKE minimum located close to the position of U_{max}, also the height of crossing of both fractions corresponds as with Huang et al. (2007). Furthermore the minor maximum of the TKE profile is located at roughly the same height as the minor dynamic viscosity maximum.

Huang et al. (2007) states the suggestion that the velocity structure with two distinct flow regions (inner and outer) is causing contrasting concentration structures of the different sediment classes.
However the reverse is probably of much more importance. The basic density differences caused by the vertical concentration variance and distribution is of major influence on the velocity structure. Density structures can be altered due to its effect on velocity, but this yields more as a feedback mechanism.

Further of interest are the constructed TKE-profiles **(Fig. 27)** of Huang et al. (2007). They have been normalized and are compared at two distinct distances from the inlet. As was also stated by Felix (2005), all TKE minima coincide with the position of Umax. The overall shape of these profiles are very similar to the results of this report (at 4m distance).
The near bed maximum has the highest local energy and is responsible for sediment entrainment and near bed mixing due to shear with the bedding, while the much wider maximum at the top is responsible for water entrainment and mixing in the outer region.

The reduction of the outer region maximum between the 8m and 4m is explained by the depositional character of the current, which reduces entrainment.
By Huang (2007) the relationship between U_{max} and the TKE minimum is not only attributed to the low velocity gradient, but also due to local high concentration and gradient Richardson number. This indicates strong local stratification, which prevents mixing.

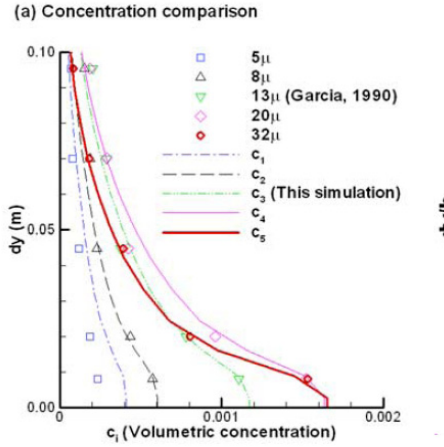

Fig. 25: *Comparison of vertical concentration profiles in the numerical experiments of Huang et al. (2007). Larger particles are concentrated near the bedding plain.*

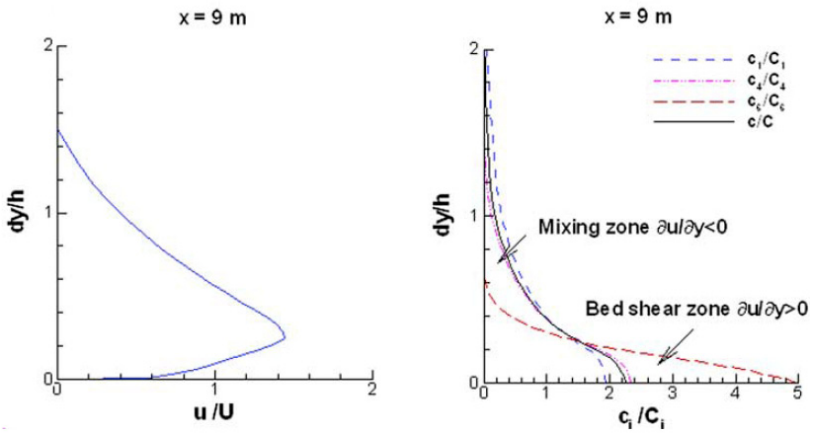

Fig. 26: *Normalized velocity and concentration profiles (run DEPO3) at 9m distance from inlet. All dashed lines reprensent individual fractions and solid line total concentation. All size classes coincide near the velocity maximum (Huang et al. ,2007)*

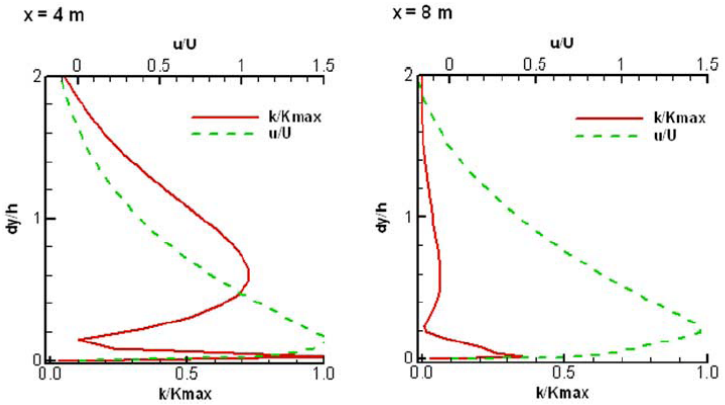

Fig. 27: (left) *TKE-profiles at 4 and 8m distance from the inlet, together with the normalized velocity profiles. The TKE-minima coincide with the U_{max} (Huang et al.,2007)*

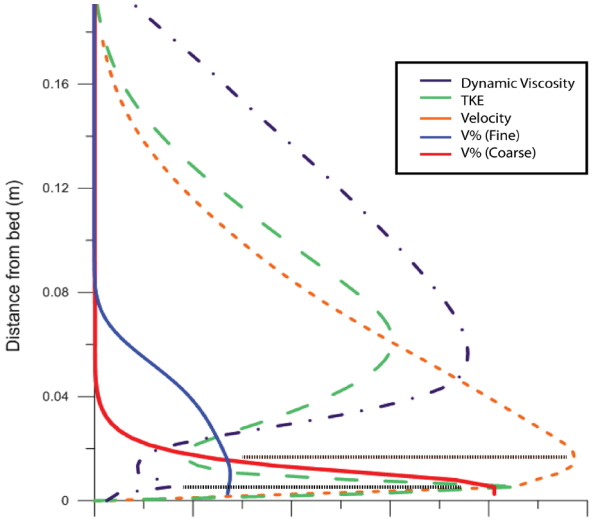

Fig.28: *Combination of all constructed profiles (Dyn visc, TKE, U & v%) of a 9.0v%-11.3[deg]-50:50 run. Horizontal scale is not indicated, since only the structures with vertical distance are of interest. The horizontal dashed lines indicate the coincidense of certain features.*

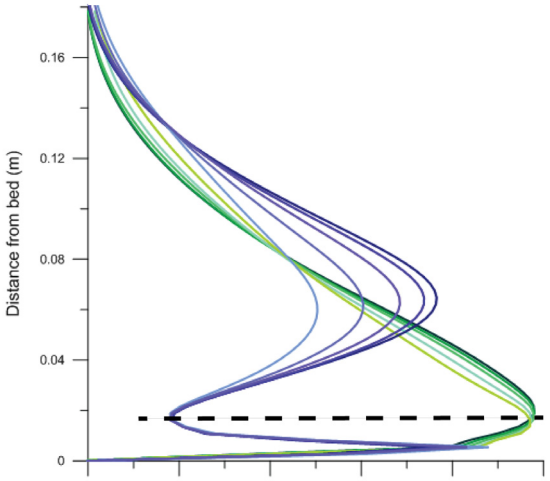

Fig.29: *Combination of all TKE and velocity profiles of the 9.0v%-11.3 [deg] runs. (Fig. 13b &16b). Horizontal scale is not indicated, since onyl the structures with vertical distance are of interest. The dashed line indicates the coincidense of the TKE-minimum with U_{max}. However the position of U_{max} exceeds the TKE-minimum , when the fine fraction is increased. (Blue = TKE ; Green = U)*

5- Conclusions

The conclusional remarks can be subdivided in three major fields:

Sensitivity test

- X & Y-cells of around 1 cm and Z-cells of 3mm give the best combination of high detail and short computation time. The effect of changes in the X direction is minimum, while the high detailed Z direction is of great importance
- Small changes in fill height (0.5m) is not of much influence in this Mashflow-3D model
- For the chosen cell-size the TLEN has an optimum of 2.5mm, which is of the same order as the size of one z-cell. Smaller TLEN's give unstable and unwanted flow behaviour.
- A low BLC (0.3) gives more realistic depositional behaviour than the standard used value of 8. However much remains vague about the exact consequences the BLC has on the deposition in modelled turbidity currents.

Stability field and deposition

- The addition of fine sediments to the sediment mixture enhances the ability to sustain non-aggrading currents at lower slopes and lower total volume concentrations. This is true for as well the MassFLOW-3D™ model as the Eurotank flume experiments
- Results are different in each approach, with the physical model being able to sustain non-aggrading conditions more efficient. This can be explained by lack of processes as hindered settling and traction carpets in this version of Massflow-3D™. A second reason can be found in the usage of both D50's instead of the real distribution, which as has been showed a significant effect on the depositional behaviour.

Profiles

- Sediment fraction influences velocity profiles by the different concentration distribution of each fraction. Mix-tures with greater coarse fractions have narrower 'velocity noses', while showing greater velocities at the top outer region.
- When plotted dimensionless, a thickening of the region around U_{max} can be found when the proportion of fine materials is increased, as well in the MassFLOW-3D™ model as the Eurotank experiments
- Bidisperse grainsize distributions have a great influence on the shape of the total volume concentration profiles. The difference in dilution of both fractions results in a typical layered flow system and stepped concentration profile.
- Greater gradients and volume concentrations also have a positive effect on velocities, turbulence kinetic energies and viscosities; however there are many distinctions in how this is of influence vertically in the flow.
- The various TKE-profiles reveal that volume concentration and gradient significantly influ ence stratification, but the variation in sediment fraction does not.
- The vertical position of U_{max} corresponds with the TKE-minimum as well as the crossing point in the concen tration profile of both fractions. This agrees with the numerical work of Huang et al. (2007). However in the nummerical work of this report the coincidence of the TKE-minimum and U_{max} fades when the fine fraction is increased with the U_{max} situated higher than the TKE-minimum.

6- Acknowledgments

I am especially grateful to Ernst Hansen for giving me the opportunity to accomplish this project at Complex Flow Design AS (Trondheim). I would also like to thank him for his hospitality, great support, fruitful discussions and enthusiasm during my stay.

I am also grateful to Romain Rouzairol for his excellent support while learning the basics of the MassFLOW-3D™ software aswell as Evgeniy Tantserev & Ricardo Basani for additional help and comments during all meetings.

7- Nomenclature

B	= Einstein Coefficient
BLC/β_i	= Bedload Coefficient
C	= Sediment volume concentration
C_p	= Maximum packing concentration
C_{NU}	= Energy dissipation parameter (=0.085)
d	= D50 grainsize diameter
ε	= Turbulent energy dissipation
Φ	= Dimensionless bedload transport rate
g	= Gravity factor (=9.81m/s^2)
k_T	= Turbulent kinetic energy
μ_a	= Dynamic viscosity of ambient fluid (Pa s)
μ_s	= Dynamic viscosity of mixture (Pa s)
q_b	= Volumetric bedload transport rate (m^3/s)
ρ	= Density of mixture (kg/m^3)
s/σ	= Density difference (ambient fluid & mixture)
τ_0	= Bed shear-stress (Pa)
$TLEN$	= Maximum turbulent mixing length
θ_i	= Local Shields number
$\theta''_{cr,I}$	= Critical Shields parameter
V_s	= Settling velocity (m/s)
v_m	= Molecular Viscosity
v_T	= Turbulent Viscosity

8- References

Altinaker MS, Graf WH, Hopfinger EJ, 1996. Flow structure in turbidity currents, Journal of Hydraulic Research, V 34: 5, p. 713-718

Baldock TE, Tomkins MR, Nielsen P & Hughes MG, 2003. Settling velocity of sediments at high concentrations, Coastal Engineering, V 51, p. 91-100

Bridge JS, Demicco RV, 2008. Earth Surface Processes, Landforms and Sediment Deposits, Cambridge

Felix M, Sturton S, Peakall J, 2005. Combined measurements of velocity and concentration in experimental turbidity currents, Sedimentary Geology, V. 179, p. 31-47

Huang H, Imran J, Pirmez C, 2007. Numerical modelling of poorly sorted depositional turbidity currents, Journal of Geophysical Research, V 112, C01014

Schramm LS, 1991. Emulsions; Fundamentals and Applications in the Petroleum Industry, Advances in Chemistry Series 231

Stacey MW, Bowen AJ, 1988. The Vertical Structure of Density and Turbidity Currents: Theory and Observations, Journal of Geophysical Research, V. 93, p. 3528-3542.

Mastbergen DR, Von den Berg JH, 2003. Breaching in fine sands and the generation of sustained turbidity currents in submarine canyons. Sedimentology, V. 50, p. 625-637.

Mueller BS, Llewellin EW & Mader HM, 2010. The rheology of suspensions of solid particles. Proceedings of the Royal Society A, 466: 1201-1228

Ribberink JS, 1998. Bed-load transport for steady flows and unsteady oscillatory flows. Coastal Engineering, 34, p. 59-82

Flow-3D User Manual Version 9.4

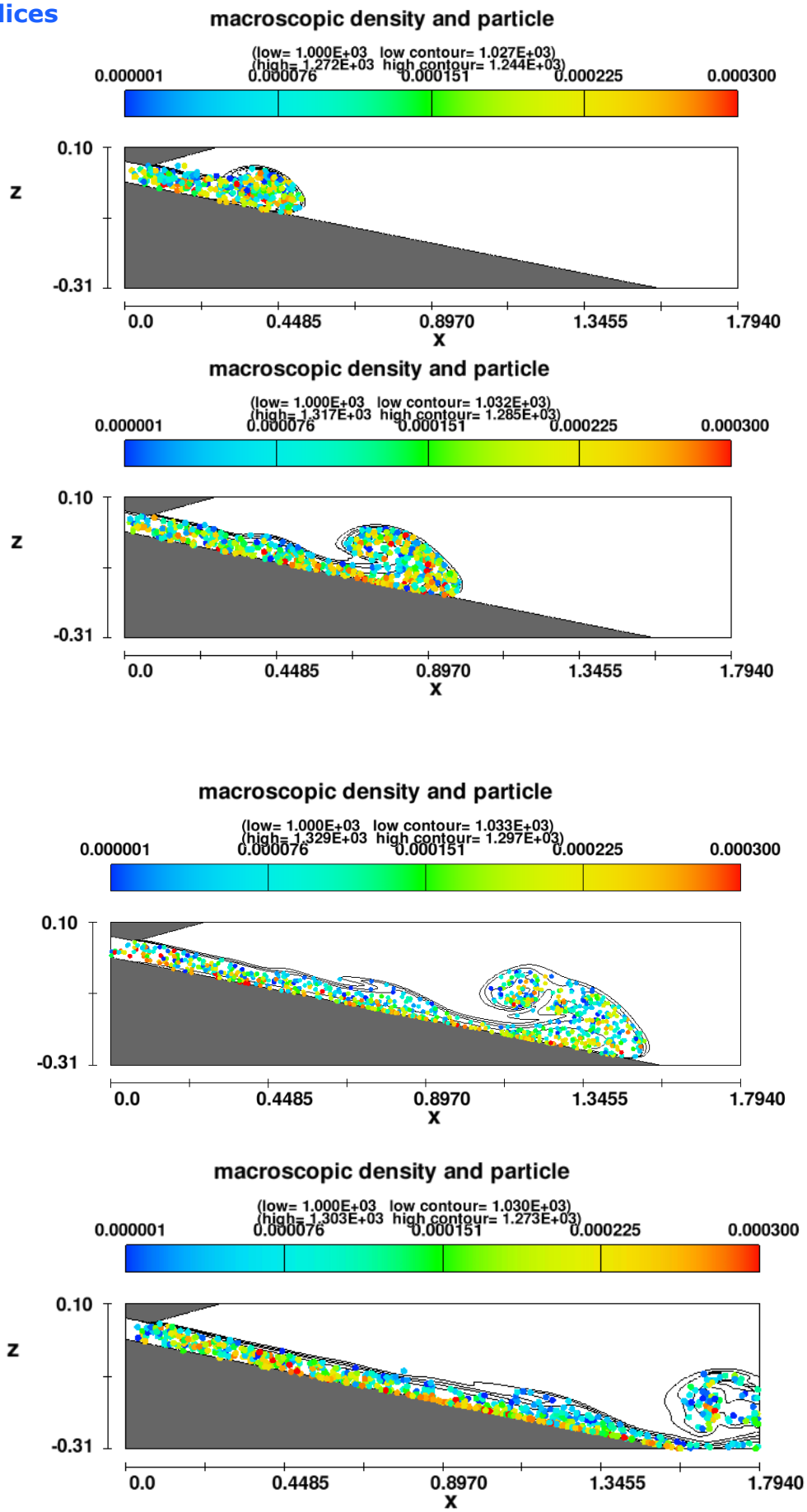

Figure A1 (a-d): Progress of the head of the current showing particles (m) in an example with 11.3deg slope, 13.5v% & 00-100 SF. All particles are generated in equal amount of both fractions varying in grainsize between 1-300mu (independ of the current).

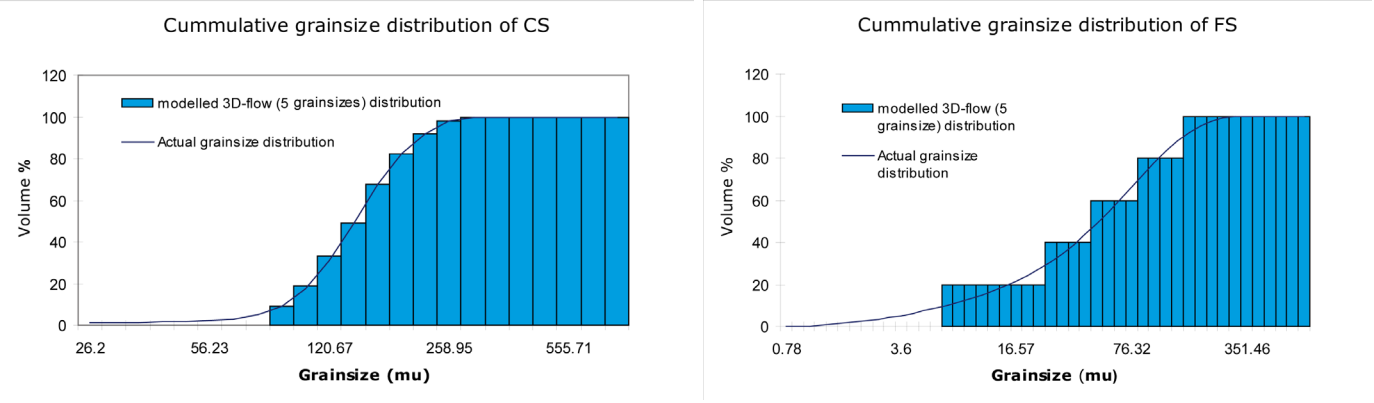

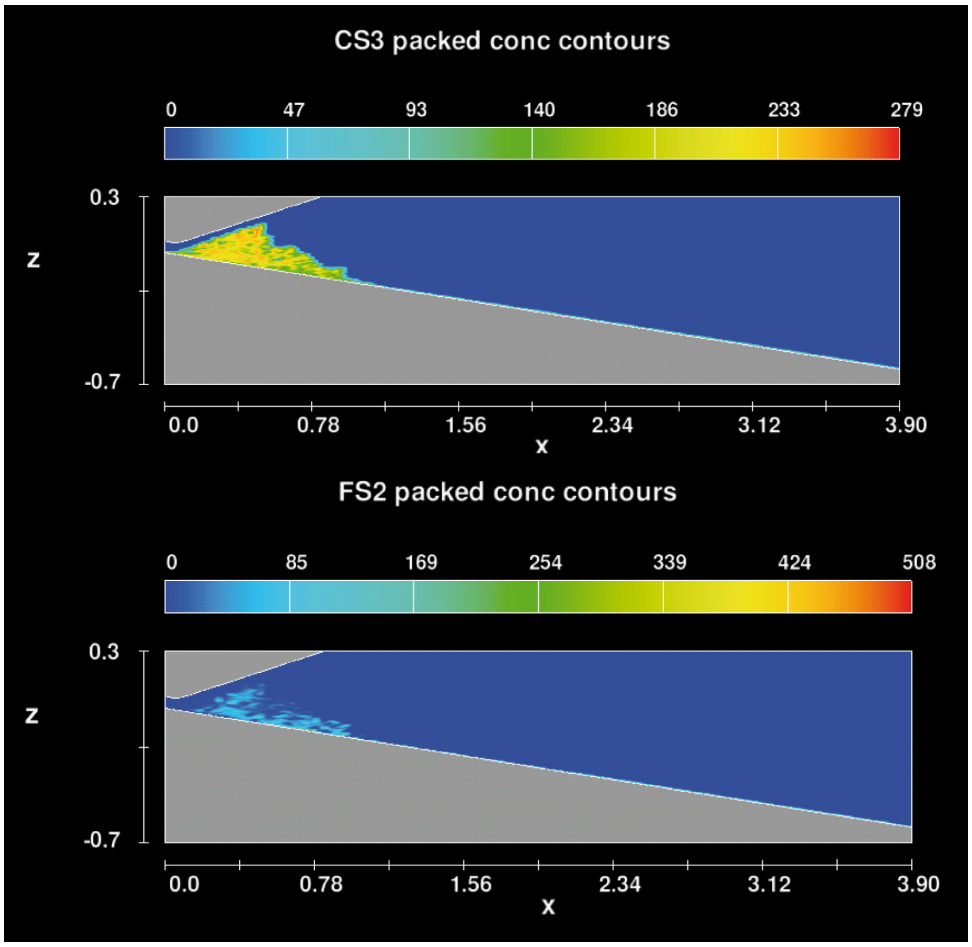

Figure A2 (a-d): Cummulative distribution diagrams of both fractions (a-b) in a 5-grainsize approximation simulation & obstructing deposits due to coarse-grained blockage showing also traces of fine sediments (11.3deg, 13.5v%, 50:50)